4 Recovery against Mechanical Actions

V.C. Li[1], A.R. Sakulich[1], H.W. Reinhardt[2], E. Schlangen[3], K. Van Tittelboom[4], D. Snoeck[4], N. De Belie[4], C. Joseph[5], D.R. Gardner[5], R.J. Lark[5], H. Mihashi[6], and T. Nishiwaki[7]

[1] University of Michigan, MI, USA
{vcli,a.sakulic}@umich.edu
[2] University of Stuttgart, Germany
reinhardt@iwb.uni-stuttgart.de
[3] Microlab, Delft University of Technology, The Netherlands
H.E.J.G.Schlangen@tudelft.nl
[4] Magnel Laboratory for Concrete Research, Ghent University, Belgium
{Kim.VanTittelboom,Didier.Snoeck,Nele.DeBelie}@UGent.be
[5] Cardiff School of Engineering, Cardiff University, United Kingdom
GardnerDR@cf.ac.uk, Lark@cardiff.ac.uk
[6] Tohoku Institute of Technology, Japan
mihashi@timos.str.archi.tohoku.ac.jp
[7] Yamagata University, Japan
ty@archi.tohoku.ac.jp

4.1 Autogenic Self-Healing

Autogenic self-healing has been defined in chapter 1 as a self-healing process where the recovery process uses materials components that could also be present when not specifically designed for self-healing (own generic materials).

4.1.1 Mechanisms of Autogenic Self-Healing

The main mechanism of autogenic self-healing of a crack is the production of calcium silicate hydrate (C-S-H), a hydration product of cement which lends strength to hydrated cement paste (so mechanical properties may be regained) [4.1]. The production of C-S-H occurs when tricalcium silicate (C_3S/alite, Eq.(4.1)) and dicalcium silicate (C_2S/belite, Eq. (4.2)) react with water to form C-S-H and calcium hydroxide (CH/portlandite), the generalized equations for which are:

$$2Ca_3SiO_5 + 6H_2O \rightarrow 3CaO \cdot 2SiO_2 \cdot 3H_2O + 3Ca(OH)_2 \quad (4.1)$$

$$2Ca_2SiO_4 + 4H_2O \rightarrow 3CaO \cdot 2SiO_2 \cdot 3H_2O + Ca(OH)_2 \quad (4.2)$$

As alite contains more reactive calcium, it reacts more rapidly and is responsible for early strength, while belite reacts more slowly and provides strength increases at later ages. During cement hydration, some grains of cement containing alite and belite do not fully react, resulting in unhydrated cores surrounded by hydrated C-S-H and CH material – a natural encapsulation of reactive minerals more or less uniformly dispersed in the concrete. During cracking, these naturally encapsulated

M. de Rooij et al. (Eds.): *Self-Healing Phenomena in Cement-Based Materials*, RILEM 11, pp. 119–215.
DOI: 10.1007/978-94-007-6624-2_4

particles are exposed to the atmosphere and begin to hydrate when exposed to water, which causes a volumetric expansion capable of completely closing microcracks.

The continued hydration of unreacted cement is present in all binders based on Portland cement. For cementitious systems containing significant additions of aluminosilicate materials such as fly ash, blast furnace slag, silica fume, or clay, the pozzolanic reaction may also provide a degree of self-healing capacity. In alkaline environments, silicate species can dissolve from the pozzolanic material to create silicic acid (H_4SiO_4/SH, Eq. (4.3)). Silicic acid can react with dissolved portlandite, the result of which is C-S-H (Eq.(4.4)) and water:

$$3Ca(OH)_2 + 2H_4SiO_4 \rightarrow 3Ca_2 + + 2H_2SiO_4^{2-} + 4H_2O + 2OH^- \quad (4.3)$$

$$3Ca^{2+} + 2H_2SiO_4^{2-} + 4H_2O + 2OH^- \rightarrow 3CaO \cdot 2SiO_2 \cdot 7H_2O \quad (4.4)$$

The C-S-H produced during the pozzolanic reaction can then heal fine cracks in the same manner as the C-S-H produced from the hydration of unreacted cement particles (e.g., volumetric change)

Because the rate of the pozzolanic reaction is coupled to the pH, it is substantially slower than the hydration of unreacted cement. In a cracked specimen, it is likely that the pozzolanic reaction will promote self-healing even on the longest timescales. Since the service life of infrastructure can be on the order of decades, the inclusion of pozzolans may ensure self-healing in structures undergoing repeated damaging even after available unreacted cement has been consumed.

Abd-Elmoaty [4.2] studied the autogenous healing behaviour inside polymer modified concrete (PMC). PMC is made by the dispersion of organic polymers inside the mixing water of concrete. Upon cement hydration, coalescence of the polymers occurs resulting in a co-matrix of hydrated cement and polymer film throughout the concrete. Abd-Emoaty stated that healing occurred in the same way as in traditional concrete. However, healing occurred to a larger extent and was extended over a longer period compared to traditional concrete as more unhydrated cement was available in the matrix because the polymers enclosed the cement particles as a kind of membrane.

4.1.2 Effect of Fibres on Autogenic Self-Healing

Early investigations identified the presence of water and tight crack width as the two most important criteria for autogenic self-healing [4.3-4.5]. Without water, autogenic self-healing chemically cannot occur; without tight crack widths, self-healing products will build up on cracks faces, but fail to fill the crack.

To obtain a "robust" self-healing concrete, Li and Yang [4.6] proposed six requirements: *Pervasiveness* (the ability to heal as soon as, and wherever, a crack appears), *stability* (a healing mechanism that does not become less effective over time), *economic feasibility*, *reliability* (consistency of self-healing), *quality* (recovery of both closing characteristics and mechanical properties) and

repeatability (ability to repair damage from multiple events). Although standard concrete meets some of these requirements, the inability to control crack width hinders development of a fully robust system and largely limits possibilities to only autonomic healing, if at all. It is the brittle nature of normal concrete that makes controlling crack width difficult.

Li and coworkers were the first who proposed the use of a fiber reinforced strain hardening engineered cementitious composite (ECC) in order to restrict the crack width and thus promote autogenous healing. In their early research, polyethylene (PE) fibers were used [4.7], while later on, they started to use poly vinyl alcohol (PVA) fibers [4.6, 4.8-4.11]. A typical composition of ECC consists of 570 kg/m^3 OPC, 455 kg/m^3 silica sand with average grain size of 110 μm, 684 kg/m^3 fly ash, 5 kg/m^3 high range water reducer, poly-vinyl-alcohol fiber and 330 kg/m^3 water. The fiber content is 2 % by volume [4.12]. The tensile strength amounts to 4-5 MPa. The stress-strain diagram is similar to that of a rigid-plastic strain-hardening material.

ECC is micromechanically designed to suppress brittle fracture behavior in favor of distributed microcracking. This behavior is encouraged through the interactions between cement and short fibers, without use of large aggregates, and has found use in a number of applications worldwide [4.13]. Well distributed, tight microcracks are produced even at tensile deformations of up to 4% (Fig. 4.1). In ECC, crack width can be custom tailored to as low as 30 μm; it has been shown that a crack width below 150 μm, and preferably below 50 μm, is critical to the self-healing of any cementitious system [4.6].

The fibers in ECC themselves also encourage the production of healing products. First, bridging fibers lower the cross sectional area of a crack, effectively raising the pH by diminishing flow. Second, for reasons arising purely from fluid dynamics, when water flows around the fiber, a turbulent zone is created on the leeward side. In this zone water velocity can stagnate, encouraging precipitation of healing product and creating a composite fiber/healing product material that bridges the crack

The efficiency of steel cord (SC), polypropylene (PP), PE and PVA fibers was compared by Homma *et al.* [4.14] and Koda *et al.* [4.15]. While SC fibers showed minor crack closing efficiency as the steel started to corrode inside the crack, PVA fibers induced the highest healing efficiency. This was attributed to the fact that PVA fibers promoted the deposition of crystallization products, as hydroxyl groups, attached to the fiber structure, attracted calcium ions.

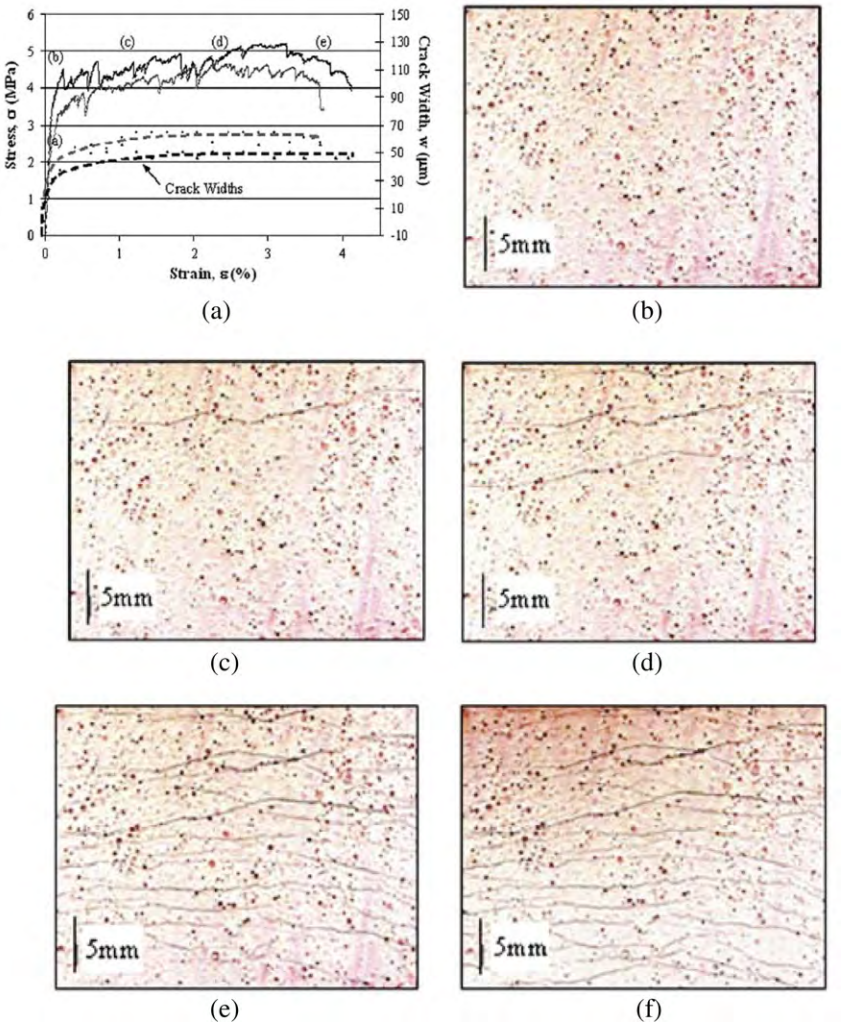

Fig. 4.1 Uniaxial stress/strain curve and crack development in ECC [4.16]

Table 4.1 shows the mix proportions of materials used in a study by Homma *et al.* [4.17]. They studied three types of strain hardening cement-based composites (SHCC), named fibre reinforced cementitious composites (FRCC) by these authors: (1) containing micro polyethylene fibre (ø=12 μm, length=6 mm) (FRCC(PE)), (2) containing steel cord fibre (ø=0.4 mm, length=32 mm) (FRCC(SC)), and (3) containing hybrid composite fibres (i.e. both of PE and SC fibres) (HFRCC).

Table 4.1 Mix proportion of FRCC specimens investigated by Homma *et al.* [4.17]

Types of Mix	Water/Binder	Sand/Binder	Silica fume/Binder	SP/binder	PE fiber (Vol. %)	SC fiber (Vol. %)	Fiber content (no./m^3)
FRCC (SC)	0.45	0.45	0.15	-	-	0.75	187 x 10^4
FRCC (PE)				0.09	1.5	-	221 x 10^8
HFRCC					0.75	0.75	111 x 10^8

Binder = Cement + Silica fume; SP = Superplasticizer (Polycarboxylate)

In all series, four specimens of 25 mm × 75 mm × 75 mm were prepared and cracks were introduced by means of a uni-axial tension test. Fig. 4.2 shows the outline of the tension test. During this test, each specimen was stretched to different strain levels in order to have different maximum crack widths. After the tension test, the crack surface was observed by means of a digital microscope and the crack width was measured (see Table 4.2). The microscopic observation was repeated at 3, 14 and 28 days in order to investigate the effect of the self-healing of cracks.

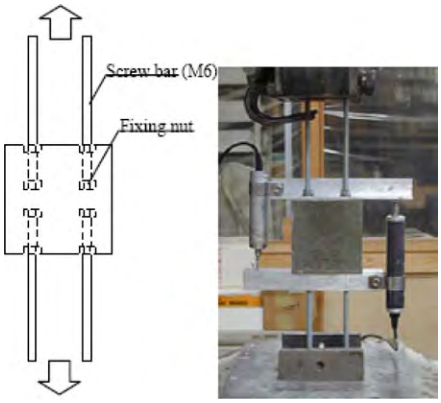

Fig. 4.2 Uni-axial tensile test equipment

Table 4.2 Maximum crack width (mm) evaluated by means of microscope observation

	No. of specimens			
Type of mixes	No. 1	No. 2	No. 3	No. 4
FRCC (SC)	0.035	0.076	0.088	0.757
FRCC (PE)	0.019	0.038	0.119	0.368
HFRCC	0.017	0.081	0.407	0.71

Table 4.3 shows photographs of the crack surface in FRCC(PE), FRCC(SC), and HFRCC. It can clearly be seen in these photographs that the crack surface of all specimens after the tension test is clear and there are no products on the surface. After 3 days the crack surfaces in FRCC(PE) and HFRCC were attached by self-healing products and the crack width decreased as the time advanced. The crack surface in FRCC(SC) was not decreased by the self-healing products. This could be because there were too few fibres that self-healing products could attach to. On the other hand in the place where of a lot of micro PE fibres bridged over the crack, especially in most of FRCC(PE) specimens, there were many attachments of self-healing products. Even in case of FRCC(PE), however, if there were rather a few fibres, the attachment of self-healing products depended on the volume content of PE fibres. Therefore it was concluded that amount of the PE fibre per volume has a great influence on self-healing. After 3 days, it was observed that the steel cords on the crack surface in FRCC(SC) and HFRCC were corroded and the volume expanded.

Table 4.3 Microscopic observation of self-healing products at a crack surface

	Elapsed time (day)			
	0*	3	14	28
FRCC (SC) Steelcord fiber specimen No. 2 (crack width: 1.976mm)				
FRCC (PE) Polyethylene fiber specimen No. 4 (crack width: 0.368mm)		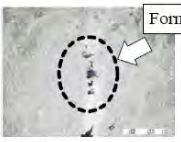		
HFRCC Steel-PE hybrid fiber specimen No. 1 (crack width: 1.532mm)		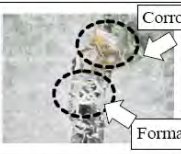		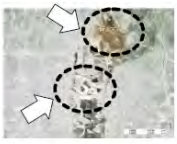

* Immediately after tension test before immersion in water.

Fig. 4.3 shows the time dependence of mean size of self-healing products attached to the crack surface. The increasing rate of the mean size during the first 3 days is higher than that after 3 days. This could be because Ca^{2+} diffusion speed from the inside of FRCC was decreased as the time advanced because of the formation of a self-healing product layer. The order of the amount of the attached products in each FRCC material was FRCC(SC) < HFRCC < FRCC(PE). This order corresponded with that of the number of mixed in fibres per volume fraction

as shown in Table 4.1: FRCC(SC) < HFRCC < FRCC(PE). Therefore it was concluded that the number of mixed in fibres per volume has a dominant influence on the crack self-closing effects.

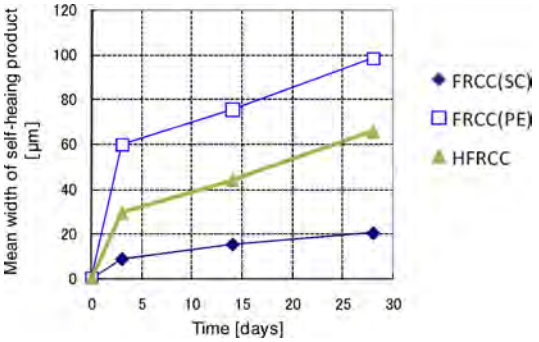

Fig. 4.3 Time dependence of mean size of self-healing products attached at the crack surface

Fig. 4.4 shows the results of the low pressure water permeability test of the cracked and uncracked specimens. As can be seen in this figure, the coefficient of water permeability for all specimens decreased until 3 days except for the uncracked specimens. After 3 days the decreasing rate of the coefficient of water permeability slowed down significantly in all specimens. This corresponds with the microscopic observation results as shown in Fig. 4.3 in which the self-healing products attaching speed is faster until 3 days than after 3 days. It can also be noticed that, in the specimens with a wider crack, the coefficient of water permeability was almost constant after 3 days. This indicates that the formation of calcium carbonate crystals in the wider cracks do not contribute to the self-healing mechanism. On the other hand, in case of specimens with a smaller crack width, the coefficient of water permeability decreased as time advances even after 3 days and in some cases reached to the same values of those obtained in uncracked specimens. This indicates that, in such a small crack width, the formation of calcium carbonate crystals has a great effect on self-healing of cracks.

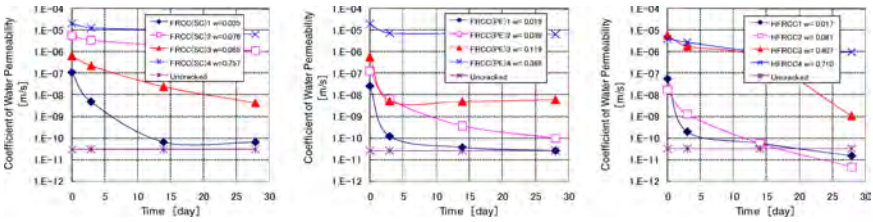

(a) FRCC(SC) (b) FRCC(PE) (c) HFRCC

Fig. 4.4 Time dependence of water permeability coefficient in each FRCC

Fig. 4.5 shows the influence of time dependence of water permeability coefficient due to type of FRCC. The decrease of the water permeability coefficient in FRCC(PE) and HFRCC is more than that in FRCC(SC). This can be explained because the self-healing products could attach to the crack surface more in FRCC(PE) and HFRCC than in FRCC(SC).

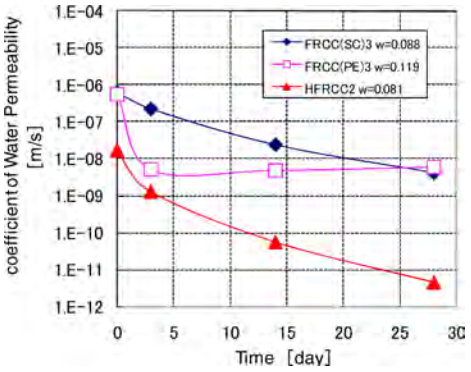

Fig. 4.5 Influence of time dependence of water permeability coefficient due to type of FRCC

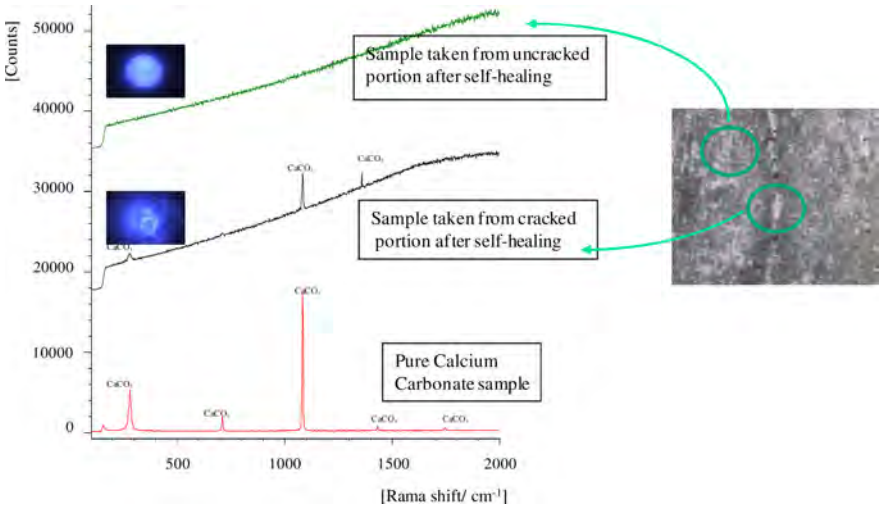

Fig. 4.6 Raman spectroscopy of FRCC(PE) specimens

In order to examine the chemical composition of the self-healing products, FRCC(PE) specimens were analyzed by Raman spectroscopy. Fig. 4.6 shows the Raman spectroscopy of FRCC(PE) samples. In this figure, upper, middle, and lower profiles were taken from uncracked area, cracked area, and pure calcium carbonate crystals, respectively. It can be seen from this figure that the peaks of

the cracked area coincided with those of pure calcium carbonate crystals. On the other hand, in the case of uncracked area, such a peak couldn't be observed. Therefore the formation of self-healing products in FRCC was attributed to calcium carbonates crystals.

In order to evaluate the effect of self-healing on the tensile properties, the self-healed FRCC specimens were tested by uni-axial tension test again. Fig. 4.7 shows the tensile stress-elongation responses before and after the self-healing. Fig. 4.8 shows the schematic of general tensile stress-elongation response of FRCC. In order to compare each FRCC specimen, the strength recovery rate (c) was defined as follows:

$$c = \frac{\sigma_2 - \sigma_0}{\sigma_1 - \sigma_0} \times 100 \tag{4.5}$$

Where σ_0 = the stress at the unloading of the first tension test
σ_1 = the tensile strength at first tension test
σ_2 = the tensile strength after self-healing.

By use of this c, we can judge the curing capability of the strength in each FRCC as follows. If c is over 100, this specimen can be considered to be recovered perfectly. If c is over 0 and under 100, this one was recovered a little. If c is equal to 0, this one was not recovered. If c is under 0, this one was deteriorated. Fig. 4.9 shows the relationship between the strength recovery rate c and residual elongation in each FRCC material.

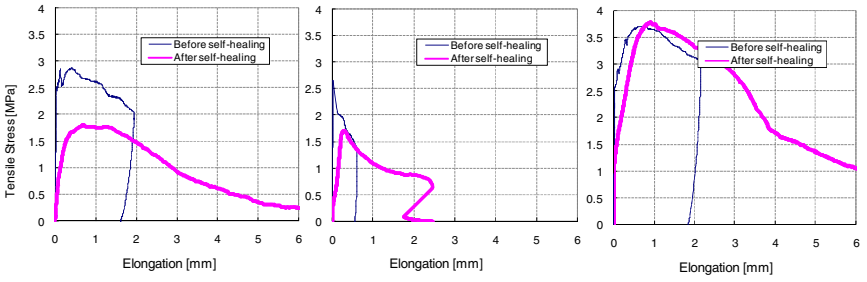

(a) FRCC(SC) (b) FRCC(PE) (c) HFRCC

Fig. 4.7 Comparison of tensile properties of specimens before and after 28 days of self-healing

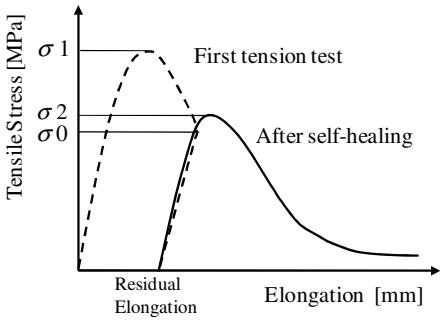

Fig. 4.8 Schematic of the relationship between tensile stress and tensile elongation of FRCC

It can be seen in Fig. 4.9 that after 28 days the recovery rate of the FRCC(SC) was almost zero or even minus. This could be because the self-healing products were not attached to the crack surface and steel cords were corroded during 28 days.

In the case of the FRCC(PE), the recovery rate c is located over 0 and under 100. The tensile strength after self-healing didn't reach the initial tensile strength, but could reach the first unloading stress. This could be because a lot of calcium carbonate crystals attached to many fibres. This indicated that, if the calcium carbonate crystals attaches to the crack surface, the tensile strength after self-healing can be recoverable. Moreover it can also be seen in Fig. 4.9 that the strength recovery rate becomes higher as residual elongation is smaller.

In the case of HFRCC, the recovery rate was higher than 100 when the residual elongation was less than 1.5 mm. It means that the tensile strength after self-healing could reach not only the first unloading stress, but also the first tensile strength. This could be because, similar to FRCC(PE), a lot of calcium carbonate crystals attached to the crack surface with very fine fibres. Moreover the bond property of the steel cord damaged by pull out stress might be recovered by the self-healing products.

By the crack surface observation after the tension test, corrosion of the steel cord in FRCC(SC) was confirmed not only outside, but also inside. However, corrosion of the steel cord in HFRCC was observed on the outside only. This could be because in HFRCC a lot of calcium carbonate crystals attached to the matrix around steel cord fibres. It corresponds with the increase of tensile strength after the self-healing.

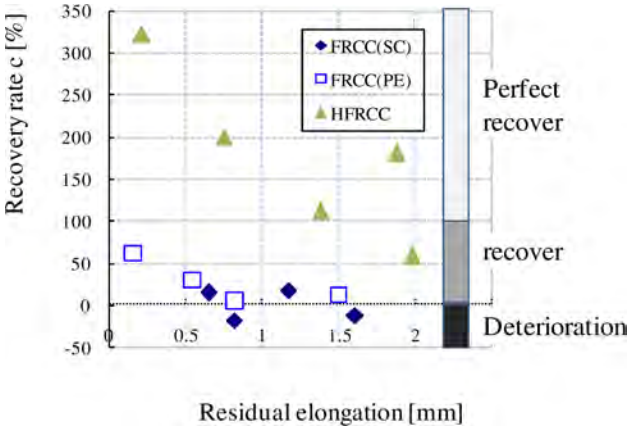

Fig. 4.9 Relationship between recovery rate and residual elongation [4.17]

Due to the low water/binder ratio present in ECC (about 0.26), the presence of notable amounts of unreacted cement, and thus notable self-healing capacity, is almost certain. A specimen that has undergone healing will have a buildup of healing product on crack faces, thus decreasing the cross-sectional area and reducing the flow rate of water through the crack, resulting in a lower permeability coefficient.

In a standard ECC, Lepech and Li [4.16] observed a distribution of 60 μm-wide microcracks after pre-loading in tension up to 3.0%. Compared to a non-ECC reinforced mortar specimen pre-loaded to 1.5%, the permeability of the ECC specimen was six orders of magnitude lower. This was due mainly to the distributed microcracks (as opposed to fewer but larger cracks in the mortar) in the ECC specimen; additionally, substantial self-closing was observed that further reduced permeability.

Homma *et al.* [4.14] found that the water permeability of SHCC specimens with tight crack widths decreased continuously during healing until reaching values similar to those of uncracked specimens. For samples with wider cracks, the water permeability dropped during the first three days of healing, but improvement slowed thereafter. Coupled with microscopic observations, it was concluded that healing product was rapidly produced during the first three days after which healing slowed significantly. In large cracks, this meant a buildup of healing product on crack faces that was insufficient to fill the crack. For similar reasons, Li and Yang [4.6] found that the permeability of samples with crack widths below 150 μm improved after 10 wet/dry cycles; samples with crack widths of 150 μm or above did not improve.

Water permeability tests, however, are complicated by a number of factors. First, the act of carrying out the test itself can cause healing, swelling of C-S-H gel, or continued hydration of semi-hydrated cement to occur as water runs through the cracks. Second, cracks may become blocked by particulate matter that

reduce water flow but do not aid healing. Finally, water permeability accurately describes recovery against environmental action or *self-closing*, in which cracks are blocked to water flow, but does not necessarily describe self-healing in terms of recovery against mechanical action, which implies an improvement in mechanical properties.

Yang *et al.* [4.18] used transverse resonant frequencies to calculate 'Normalized Resonant Frequency,' the resonant frequency of a healed specimen divided by the resonant frequency of a virgin specimen undergoing the same curing regime. In this way, bulk hydration was accounted for, and recovery of properties was attributable solely to self-healing. Specimens with cracks less than 50 μm wide recovered 100% (Fig. 4.10 a). Between widths of 50 and 150 μm recovery diminished, while above 150 μm no recovery was observed. During uniaxial tensile testing after damage and re-healing, tensile strain capacity remained quite high (1.8% - 3.1%) even for samples that had undergone preloading of 2% or 3%. (Fig. 4.10 b) Yang concluded that at least 4-5 cycles were needed to attain the full benefits of self-healing, and noted a substantial recovery of stiffness during the healing cycle. Microscopic observation of failed samples identified both cracks propagating through the healing material as well as fresh cracks in the ECC matrix.

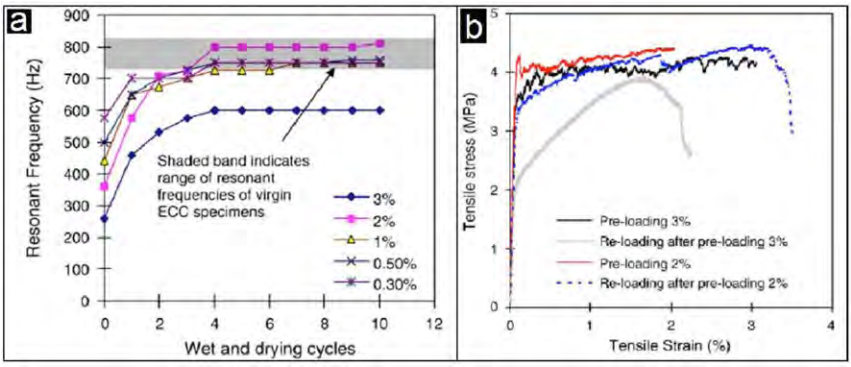

Fig. 4.10 a) Resonant frequency recovery of ECC specimens pre-loaded between 0.30 and 3.0% after 10 wet/dry cycles; b) tensile stress/strain relationships of ECC specimens pre-loaded to 3.0 and 2.0% before and after 10 wet/dry cycles [4.18].

Homma *et al.* [4.14] investigated samples containing both short polyethylene fibers and steel cord which exhibited distributed microcracking behavior. These samples recovered at least 100% of their mechanical properties after 28 days of healing submerged in water after pre-loading. Continued hydration was discounted as a source of this improvement, which was attributed to self-healing products forming on fibers and crack faces. Composites containing only steel cord or short polyethylene fibers did not exhibit distributed microcracking, and thus healing of the ~ 60 μm size cracks was incomplete.

Yamamoto *et al.* [4.19] observed a dramatic increase in longitudinal resonant frequency after as little as one wet/dry cycle. Uniaxial tension tests again confirmed the link between resonant frequency and mechanical properties. Though the stiffness recovered to the same values as an un-healed specimen, at a tensile stress of approximately 2.5 MPa, the stress/strain curves "bent over." It was theorized that this is due either to the formation of mechanically inferior healing products (assumed to be calcite) or to poor adhesion at the healing product/matrix interface. Similarly, Kan *et al.* [4.20] observed significant improvement in RF ratio during the first 4-5 wet/dry cycles, after which improvement leveled off. For samples with 0.3 % and 0.5 % pre-load strain, the RF ratio returned to nearly 100% (indicating almost total healing); for 1.0 % and 2.0 % pre-load strain the RF ratio rose to 95 % and 90 %, respectively. Between 3- and 90-day old samples, the latter had many more cracks of smaller width, which led to slightly better resonant frequency recovery.

In an effort to increase the 'green' nature of ECC, Qian *et al.* [4.21] developed an ECC containing blast furnace slag (BFS) and limestone powder. As the presence of a limited amount of these two additives would lower the amount of unreacted cementitious material in the system after moderate curing times (28 days), it was theorized that the self-healing capacity of the final product would be somewhat reduced. Ultimate deflection capacity, related to flexural strength, was measured. Water-healed specimens had deflection capacities from 65 – 105 % of a virgin sample; air-healed specimens remained between only 40 – 62 %. In total, the mechanical properties seem to indicate that the inclusion of significant amounts of BFS and limestone powder does not negatively affect the self-healing capacity of ECC. Similarly, the incorporation of fly ash has been shown to have little, if any, effect on the healing capabilities of ECC.

In a study on the de-icing salt scaling resistance of both standard ECC and high fly ash ECC, Şahmaran and Li [4.22] observed a substantial recovery of mechanical stiffness in samples that were pre-loaded and then exposed to a de-icing salt solution. The self-healing contributed to the high durability that the ECC samples exhibited during testing, which resulted in their performing inside the limits prescribed by ASTM C672 (Standard Test Method for Scaling Resistance of Concrete Surfaces Exposed to Deicing Chemicals.) That ECC has been shown to undergo self-healing was mentioned by Şahmaran *et al.* [4.23] in a later study on the resistance of ECC to damage from freezing and thawing. Since the standard ASTM test requires relatively rapid cycling of the freezing and thawing cycles, not allowing test material to self-heal, the data obtained from such tests should therefore be considered absolute worst-case scenarios. ECC, incidentally, was shown to have excellent durability in such tests.

ECC specimens have been preloaded to a given strain, immersed in 3 % NaCl solution or cured in air for 30, 60, and 90 days. After the immersion time, the specimens were reloaded. Fig. 4.11 shows typical results. Fig. 4.11 a) is valid for the pre-cracked specimens to 0.5 % tensile strain, whereas Fig. 4.11 b) is valid for the specimens pre-cracked to a tensile strain of 1.5 %. The curves show an almost complete recovery of stiffness when re-loaded in direct tensile tests even after

periods of only one month exposed to NaCl solution. Preloaded ECC specimens with microcracks at 45 μm crack width induced by mechanical loading almost fully recovered their tensile strain. However, both pre-cracked and uncracked ECC specimens exposed to NaCl solution lost more than 10 % of their tensile strength probably due to leaching of calcium hydroxide. Microcracks of ECC specimens that were immersed in NaCl solution appeared completely sealed as a result of self-healing [4.12]. Similar results have been reported in [4.7, 4.8].

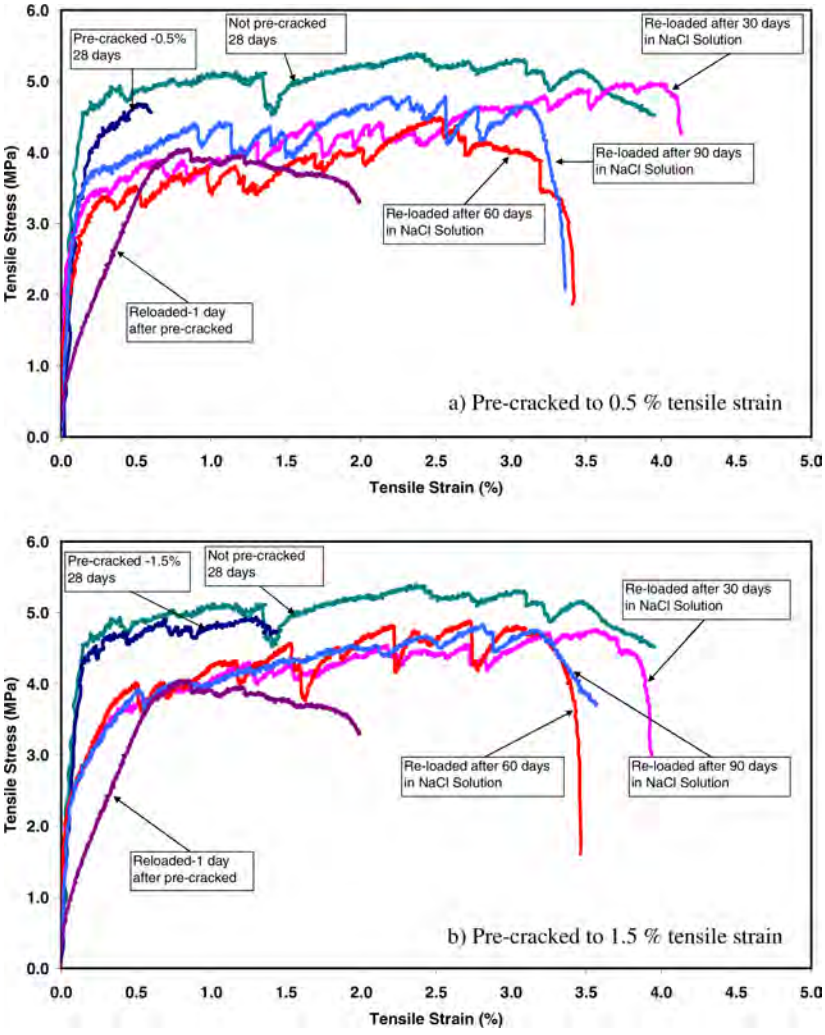

Fig. 4.11 Tensile stress-strain curves of ECC before and after exposure to 3 % NaCl solution [4.12]

For ECC in the presence of water, healing products accumulate on the surface of cracks, and completely fill those with widths less than about 50 μm. The tight crack widths that are an inherent property of ECC require not only less healing product for total rehabilitation, but actively encourage production of healing material by maintenance of pH levels in the incident water. Bridging fibers provide further encouragement for the production of healing product, and are likely to provide sites for the precipitation of these products.

Mechanical testing shows that these products do not just seal the cracks and protect reinforcing steel but heal the cracks, leading to recovery of mechanical performance. Resonant frequency analysis has been shown to be a simple, inexpensive, and non-destructive method to observe the progress of self-healing; previous research has also shown that recovery of resonant frequency can be definitely linked to recovery of mechanical properties.

Little detailed chemical analysis has been performed on the healing products of cements and concretes in general, and ECC in particular. The healing product can be easily identified by optical microscopy (Fig. 4.12 a) or electron microscopy (Fig. 4.12 b), and can usually be observed by eye. Yamamoto [4.19] provided micrographs of the healing product, assuming it to be calcite based on the work by Edvardsen [4.3]; Yang [4.18] and Lepech [4.16] each concluded the healing product to be calcite based on EDS spectra; and Homma [4.14] identified healing product to be calcium carbonate (presumably calcite) based on Raman spectroscopy. It has been shown [4.24], however, that C-S-H can sometimes present a featureless spectrum in Raman analysis.

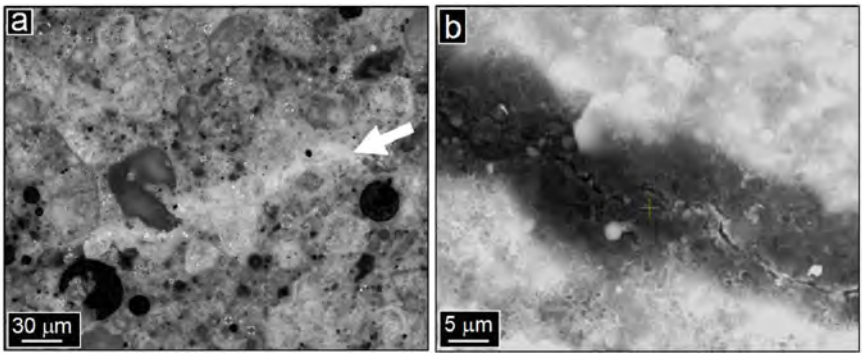

Fig. 4.12 a) optical micrograph of healing product in ECC cement (arrow); b) SEM micrograph of a healed crack.

Kan *et al.* [4.20] observed two distinct healing products in ECC materials through use of scanning electron microscopy (SEM). In very tight cracks, 'fiber-like' C-S-H was identified; only in larger cracks were 'stone like' calcite grains formed. The compositions were confirmed by EDS, however, a large amount (~ 10 at.%) of Mg was also observed. It was speculated that this Mg could take the form of various magnesium carbonates (magnesite or dolomite), hydrates

(barringtonite, etc.) or hydroxides (brucite). The EDS results also indicated that the 'stone like' product, identified as calcite, could be a mixed system with additional C-S-H or portlandite due to an abundance of calcium; the fiber-like phase could also have included portlandite, since there was an abundance of calcium but no carbon. These findings were supplemented with limited TEM observations, which identified several grains of pure calcite. The minute sample sizes used for TEM work, however, mean that clear calcite exists in the healing product, but not how much.

Qian *et al.* [4.21] observed samples of their ECC containing BFS and limestone powder by SEM; EDS identified the healing product to be a calcite "and/or" C-S-H. As with the mechanical properties, it therefore appears that the inclusion of BFS and limestone powder had little, if any, effect on the capacity of the ECC for healing. Whether this C-S-H was produced by the hydration of unreacted cement particles or through the pozzolanic reaction is not discussed. Termkhajornkit *et al.* [4.25] investigated the self-healing properties of ordinary portland cement/fly ash blends at similar ages and found that the degree of healing increased with increasing fly ash content. Therefore, the pozzolanic reaction is likely to be the cause of at least some of the healing.

XRD experiments were used by Kan *et al.* [4.20] to identify calcite in the healing product (calcite produces XRD peaks at 30, 50, and 55 °2θ). XRD analysis only identifies crystalline materials, however; the presence of C-S-H in the healing product could be neither confirmed nor denied. FTIR analysis was also performed. Calcite was specifically identified (sharp peaks at 875 and 714 cm^{-1}) as well as a peak due to the presence of CO_3^{2-} in general (a broad peak at 1460 cm^{-1}). The exact origin of this peak ($CaCO_3$ as opposed to $MgCO_3$, etc.) was indeterminate. Finally, peaks due to silicate bonding were present. Whether these peaks were produced from C-S-H in the healing product or C-S-H scraped from the edges of the healed cracks is uncertain. Slight differences in the peaks led the authors to speculate that CO_2 may be leaching Ca from C-S-H in the bulk, rather than consuming portlandite to form calcite. If true, the Si in the C-S-H in the bulk will become more highly polymerized, thus leading to a more complicated composite material.

4.1.3 Experimental Evidence in Ultra High-Performance Concrete

Ultra High-Performance Concrete (UHPC) is a cementitious material with very low water-cement ratio. Granger *et al.* [4.26] used for their experiments a water-cement ratio of 0.2 and additionally silica fume. After 2 days water curing, the specimens were heat-cured at 90 °C and 100 % RH for 48 h. In a three-point bending test, the prismatic specimens with a center notch were loaded in a displacement controlled manner till reaching the peak load and further until a CMOD of about 30 μm. The unloading yielded a CMOD between 5 and 15 μm. Thereafter, the specimens were stored in water for a certain time.

Fig. 4.13 illustrates the deflection-softening behaviour of UHPC. The peak bending stress is about 7.3 MPa at a CMOD of 15 µm. Unloading took place at a load level of 2 kN which corresponds to a bending stress of 3.75 MPa. Reloading follows the original force-CMOD curve.

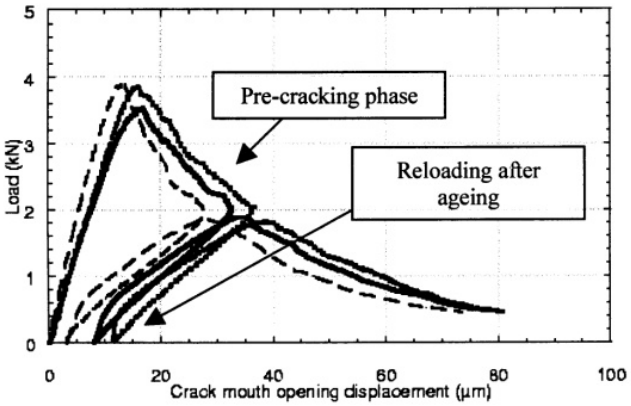

Fig. 4.13 Load-CMOD behaviour of virgin specimen (Pre-cracking phase) and reloading after 3 weeks in air [4.26]

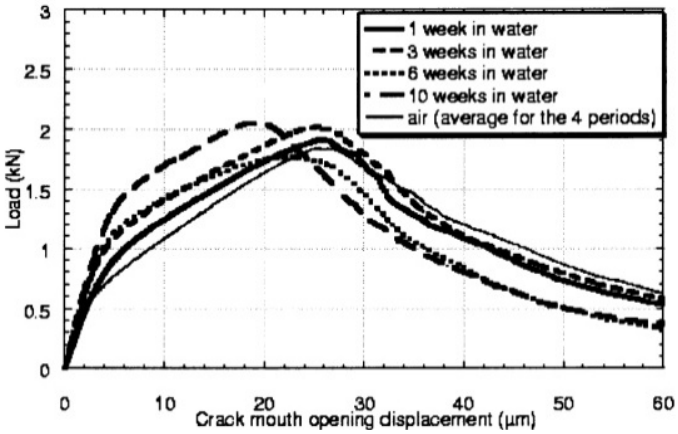

Fig. 4.14 Load-CMOD behaviour of cured specimens and non-cured ones [4.26]

The storage in water led to slightly different behaviour as shown in Fig. 4.14. Prolonged water curing resulted in an increase of bending stress compared to non-cured specimens. The initial stiffness of cracked specimens (reloading stiffness) after 10 weeks storage in water is almost the same as the one of the virgin specimens. CMOD decreases with time of water storage. Resonance frequency and acoustic emission measurements let the authors conclude that a self-healing effect was present. The cause of self-healing is seen in the formation of new

products in the crack due to continued hydration of fractured unhydrated cement grains [4.27].

Morimoto *et al.* [4.28] developed a new type of strain hardening cementitious composite; ultra high performance strain hardening cementitious composites (UHP-SHCC). This material combines excellent protective performance, which is similar to that of ultra high performance fiber reinforced concrete (UHPFRC), with a significantly higher tensile strength and strain hardening at peak strength. Especially, the material has controlled fine cracks (less than 20 μm) and low water-to-binder ratio with unhydrated cement. In addition, silica fume, that causes pozzolanic reaction, was mixed in UHP-SHCC. These characteristic gave the advantages for self-healing after initial cracking.

Table 4.4 shows the mix proportions of UHP-SHCC used in this study. Two kinds of fiber volume (V_f), 1.25% and 1.5%, were used. To examine the effect of the expansion agent on recovery of resistance against permeation, 20 kg/m^3 expansion agent (ettringite/lime composite type) was mixed in the case of the mix proportions with 1.25%. fiber volume. 15% of the cement was replaced by silica fume. High strength polyethylene (PE) fibers were used with a diameter and length of 0.012 mm and 6 mm, respectively.

Table 4.4 Mix proportions of UHP-SHCC

Mix proportion	W/B	Water (kg/m^3)	Cement (kg/m^3)	Silica fume (kg/m^3)	Sand (kg/m^3)	Super-plasticizer (kg/m^3)	Air reducing agent (kg/m^3)	Expansion agent (kg/m^3)	Fiber (kg/m^3)
V_f=1.25%	0.22	341	1316	232	155	15.5	0.062	0	12.1
V_f=1.25%+EX	0.22	340	1294	232	155	15.5	0.062	20	12.1
V_f=1.50%	0.22	340	1313	232	155	15.4	0.062	0	14.6

Plate-shaped specimens with a cross section of 150 mm×30 mm were prepared. There were two rebars of D6 in the specimen to improve the crack formation. Rebars of D10 were also embedded in both specimen ends to hold the specimen by a testing machine (see Fig. 4.15a). The specimens were demoulded one day after casting and cured in water in a constant temperature room (20°C). Then air permeability tests and water permeability tests were conducted at the age of 32~35 days after the specimens were dried in air for a couple of days. And at the age of 36~37 days, cracks were induced by uni-axial tensile test, as shown in Fig. 4.15b. Loading was controlled by LVDT fixed on both specimen surfaces (gauge length: 150 mm). Each specimen was loaded until the tensile strain of either 0.1% or 0.2%, and then unloaded. After the tensile tests, the air and water permeability test were conducted again. Afterwards, specimens were cured under air or in water at a constant temperature of 20°C for 20 days. Table 4.5 summarizes specimen series, unloading strain and re-curing conditions

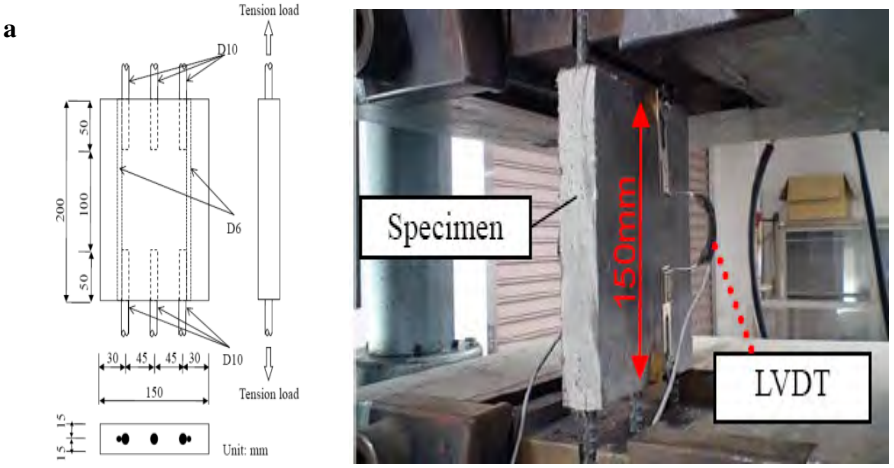

Fig. 4.15 Shape of specimens used (a) and performance of uniaxial tensile test (b)

Table 4.5 Types of specimens

Series	Fiber volume	Unloading strain (%)	Re-curing condition
1.25-0W	Vf=1.25%	0	Water
1.25-0A			Air
1.25-0.1W		0.1	Water
1.25-0.1A			Air
1.25-0.2W		0.2	Water
1.25-0.2A			Air
1.25EX-0W	Vf=1.25% +EX	0	Water
1.25EX-0A			Air
1.25EX-0.1W		0.1	Water
1.25EX-0.1A			Air
1.25EX-0.2W		0.2	Water
1.25EX-0.2A			Air
1.5-0W	Vf=1.5%	0	Water
1.5-0A			Air
1.5-0.1W		0.1	Water
1.5-0.1A			Air
1.5-0.2W		0.2	Water
1.5-0.2A			Air

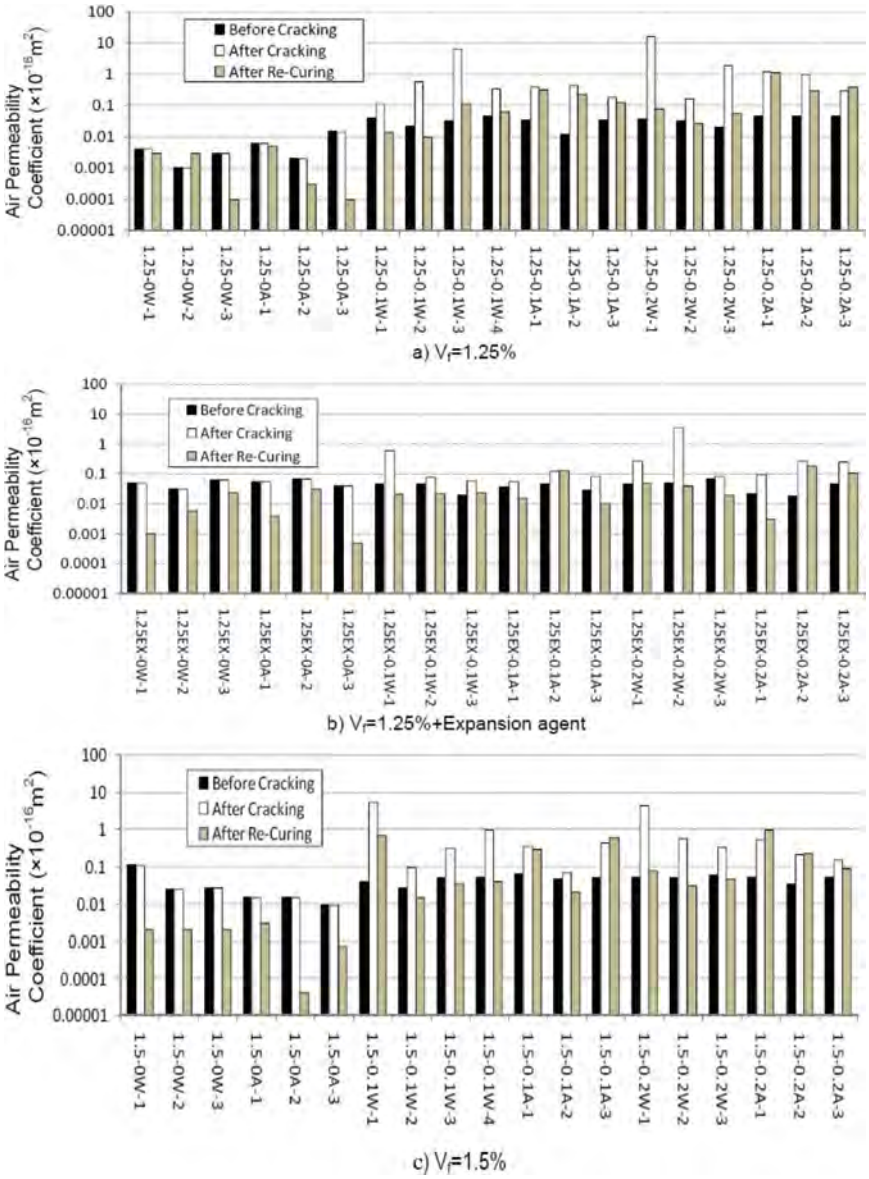

Fig. 4.16 Recovery of air permeability coefficient for specimens containing 1.25% (without (a) and with (b) expansion agent) and 1.5% fibers (c)

In control specimens, air permeability coefficients became smaller with increase of time (Fig. 4.16). The authors [4.28] supposed that this decrease was due to densification of the matrix with increase of age. Air permeability coefficients of cracked specimens became dramatically larger just after loading. After re-curing, however, the air permeability coefficients of all cracked specimens, especially cured in water, became smaller. Regarding the different curing conditions, a difference in air permeability was observed. Curing in water was more effective for self-healing, compared to air-curing. When the results, obtained from the water permeability tests were examined (results not shown), the same conclusions were drawn. The authors stated that the main cause for recovery of the resistance against air and water permeability is both; densification of the matrix in UHP-SHCC and formation of re-hydration products along the induced cracks. Besides, the effect of the added expansion agent was not significant in this test.

4.1.4 Experimental Evidence in Early-Age Concrete

Tests on early-age concrete have been performed at Delft University of Technology [4.29-4.31]. In the experiments several parameters are varied. The parameters that are discussed in this chapter are:

- the amount of compressive force applied during healing. The variation of this parameter is 0.0, 0.5, 1.0 and 2.0 MPa.
- the type of cement in the concrete mix, both a Blast Furnace Slag Cement (BFSC) and an Ordinary Portland Cement (OPC) is tested.
- the moment of creating the first crack in the specimen through a controlled 3-point bending test. The cracks are made at an age of 20, 27.5 (further named 1 day), 48 and 72 hours. The age at loading has some variation, since the specimens are cast at the same time, but for testing only one machine is available. Each test, including preparation, takes about 45 minutes.
- the crack (mouth) opening of the crack. Initial crack openings of 20, 50, 100 and 150 μm are discussed in this chapter.
- the influence of the Relative Humidity (RH) during healing. Specimens are stored under water and in a climate chamber with 95% and 60 % RH respectively.

In all cases only one parameter is varied at any one time. The default parameters in the tests are 1.0 MPa compressive stress, concrete made with BFSC, crack made at age of 1 day, crack opening of 50 μm and healing under water. All the tests are performed at least three times. In Table 4.6 the mix composition of the concrete is given. Where the concrete mix is changed the CEM III (BFSC) is replaced by the same amount of CEM I 52.5 R (OPC).

Table 4.6 Mixture composition of self-healing concrete specimens

Component	Type	Amount kg/m^3
Cement	CEM III/b 42,5 LH HS	375
Water		187.5
River gravel	8 - 4 mm	540
	2 - 4 mm	363
	1 - 2 mm	272
	0.5 - 1 mm	272
	0.25 - 0.5 mm	234
	0.125 - 0.25 mm	127

The healing process took place either in a stress-free state or with an applied compressive stress. In the latter case the specimen is placed in a compression loading device which applies a compressive force to close the crack. This force is measured by means of the deformation of a calibrated steel spring. The amount of compressive force is varied in the tests. In Fig. 4.17 the compressive loading devices are shown with specimens subjected to 0.5, 1 and 2 MPa compressive stresses. The specimens are then stored for a specific period at a certain temperature and relative humidity (or under water) to undergo crack healing. In addition to healing of the crack the concrete will also undergo further hydration. This means that the mechanical properties of the material itself will also improve.

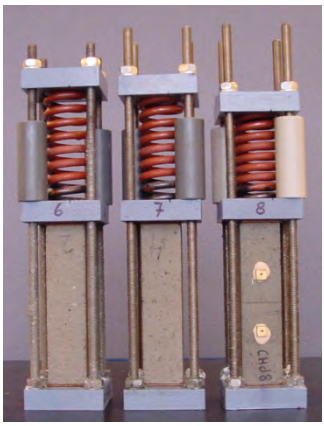

Fig. 4.17 Compressive loading devices

A question which emanates from this work is whether the crack has the same length in a specimen tested at an age of 1 day as at 2 weeks, when in both cases the crack opening has reached a value of 50 µm. To be able to answer this, the

specimens have been vacuum impregnated with a fluorescence epoxy after the test. The cracks are then visualized under UV-light. The scatter in the crack length that is observed is rather large, but it turned out that in all the situations at a crack width of 50 µm, the crack tip had reached about half way up the height of the specimen.

The following figures show some results. The healing effect is expressed in terms of recovered bending strength and stiffness.

In Fig. 4.18 the flexural stress is plotted versus displacement for the reloading test after 2 weeks healing for a specimen with (1 MPa) and without (0 MPa) applied compressive stress. Furthermore, the graph is shown of the specimen without healing. The latter is obtained after reloading a specimen tested at an age of 2 weeks. The graph shows that when the crack is not closed (the compressive stress is 0 N/mm^2) the recovery of strength is minor. The same observations were done recently for similar tests on HPC [4.26]. However, with a compressive stress of 1 MPa both the stiffness and the strength of the specimen are recovered and show values close to the reference specimen.

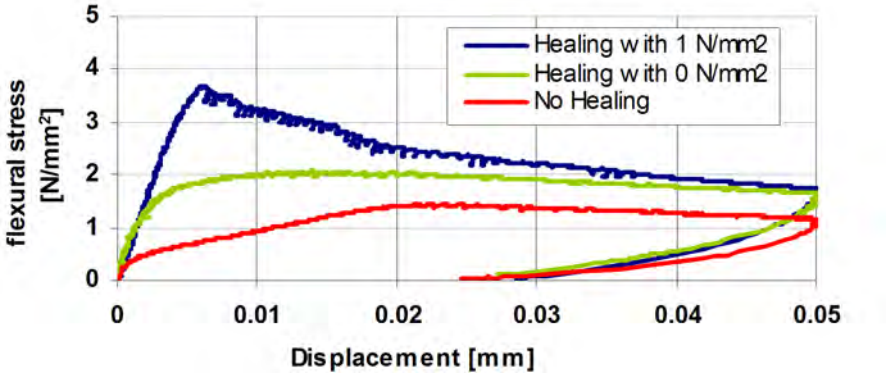

Fig. 4.18 Bending stress vs. displacement diagram of specimens with and without healing [4.31]

Fig. 4.19 gives the relative strength of the specimen after healing for different amounts of compressive stress applied during healing. The relative strength is given as a percentage of the strength of the un-cracked virgin specimen tested at an age of 2 weeks (see Fig. 4.19, peak in first loading part). In the figure a line is also shown (with vertical bars showing the scatter) which represents the strength of the material of the unhealed specimen. The figure shows clearly that almost no increase in strength is obtained when the specimen is not loaded in compression (0 N/mm^2). Furthermore, it can be seen that when compressive loading is applied to close the crack, the amount of compressive stress does not significantly influence the strength gain.

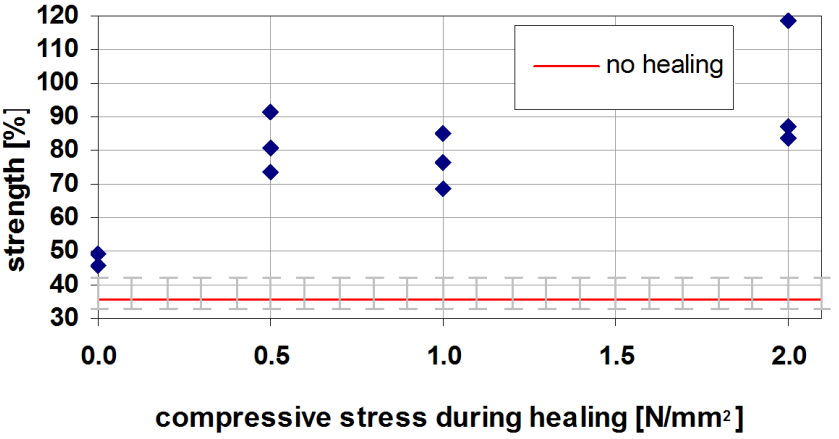

Fig. 4.19 Relative strength of specimens after healing

(a)

(b)

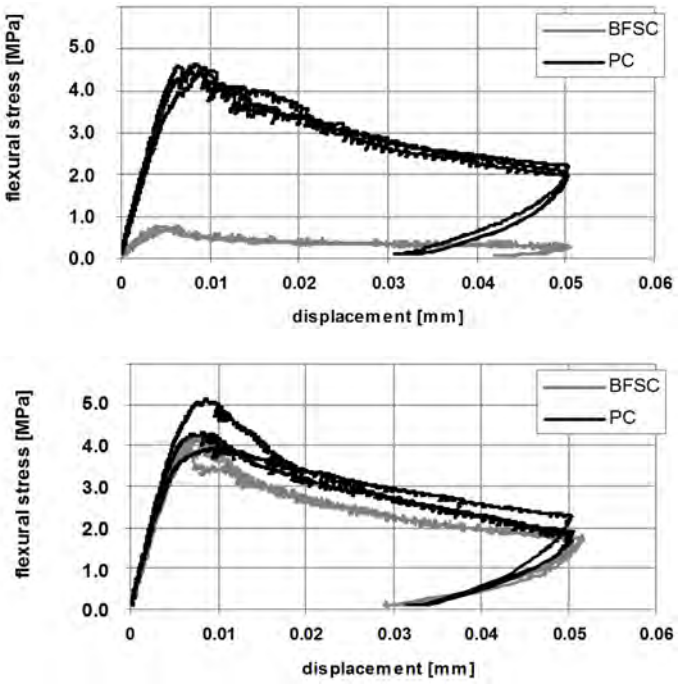

Fig. 4.20 Flexural stress versus crack opening for tests (a) after 1 day and (b) after healing with compression for BFSC and PC concrete

The influence of the cement type in the concrete mix is presented in Fig. 4.20 and Fig. 4.21. In Fig. 4.20a the flexural stress is plotted versus the crack opening displacement for the test performed on a 1 day old specimen. It can be seen that the specimens containing the faster reacting PC have a much higher strength. The

concrete with PC is further matured. In Fig. 4.20b the result is plotted for the tests after healing on both materials. Now the strength for both materials is almost equal. Also, for the specimen tested for the first time after 15 days (Fig. 4.21a) it can be seen that the strength of both materials is almost equal. Fig. 4.21b gives the plots for the reloading test, which represents the strength of the unhealed specimens. From these tests it is clear that in the BFSC-concrete the strength gain after 1 day is minimal. Healing of the crack can then take place more readily because there is still a large amount of hydration of the cement which has not yet taken place. However, in the PC-concrete the result that is obtained is remarkable, since here also the strength is almost fully recovered. Probably this concrete has after hydration a large amount of unhydrated cement left. Thus, the potential for early-age crack healing is much higher in PC-concrete.

(a)

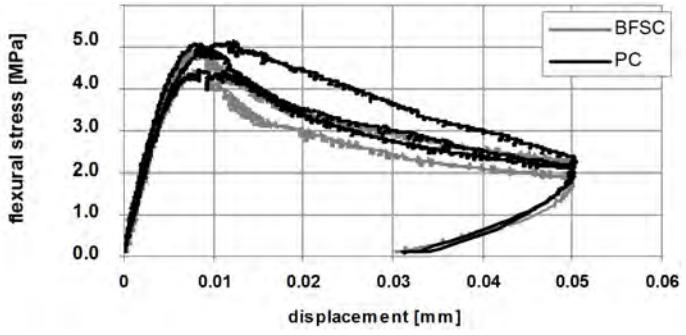

(b)

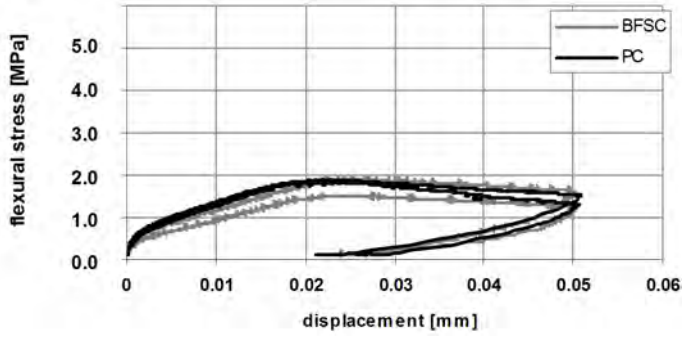

Fig. 4.21 Flexural stress versus crack opening for reference during first test (a) and reloading after 15 days (b) for BFSC and PC concrete

The third parameter that is investigated is the moment of cracking or the age of the specimen when the first crack is produced. In Fig. 4.22 the stress-displacement curves are shown for specimens at different ages when the first crack was introduced. In these tests the crack is opened up to a crack mouth opening of 50 μm. Subsequently, the specimens are loaded in compression with a compressive

stress of 1 MPa and stored under water for 2 weeks. The strength after healing (relative to the strength of the virgin specimen) is plotted in Fig. 4.22 for the various ages at which the first crack is made. The reference test for each series is always performed at the same age. So this means that for instance the strength of the specimen tested for the first time at 72 hours and subsequently healed for 2 weeks is compared with the strength of a specimen loaded for the first time at an age of 17 days. The difference in strength of the virgin material between the ages of 14 and 17 days is, however, very small. A clear decrease in strength recovery is observed with increasing age of the specimen when the first crack is made.

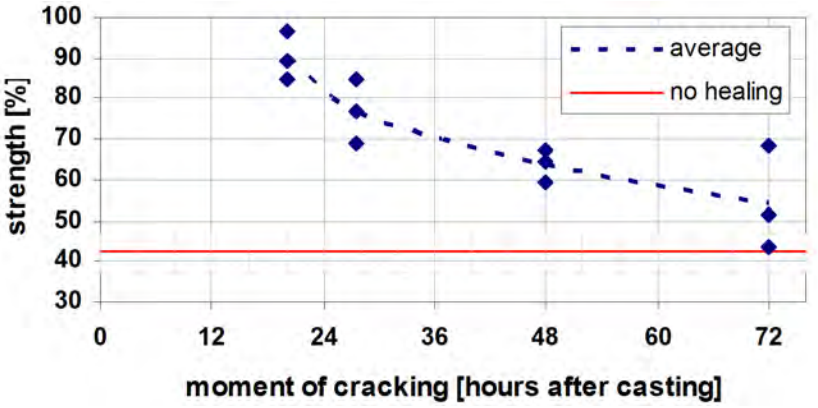

Fig. 4.22 Influence of age at pre-cracking on recovered bending strength [4.31]. Compressive stress 1 MPa, storage 2 weeks.

The fourth parameter discussed in this section is the influence of the width of the crack that is made in the specimen on the strength recovery. In these tests the specimens are loaded at an age of 1 day and the compressive stress during healing is equal to 1.0 MPa. A larger crack mouth opening will result in a longer crack which has propagated further into the specimen. The load that can be carried at a larger crack opening will be smaller. The results show a significant amount of scatter, but there seems to be no influence of crack opening on the strength recovery after healing.

The last parameter studied is the influence of the relative humidity on crack healing. It turned out that only for the case when the specimens were stored under water during the healing period, recovery of strength was possible. For the cases when the specimens were stored in an environment of 95% or 60% RH almost no increase in strength was observed. For the case of 95% RH the specimens were even stored for a period of 3 months, however, even under these conditions no crack healing was observed.

From the experimental results it can be concluded that:

- Cracks do heal when the conditions are such that the cracks are made at an early age and the cracks are closed again (a compressive stress is applied) and the specimens are stored under water.
- The amount of compressive stress does not seem to influence the strength recovery. The results indicate that a compressive stress is needed to close the crack, but once the two crack faces touch each other again, or the distance between the crack faces is small enough, crack healing can occur.
- Both for concrete made with BFSC and OPC crack healing takes place. Most probably in the case of OPC there is a lot of unhydrated cement left in the crack. Storing the specimens in water probably opens the way to further hydrate this cement in the crack. In the bulk material water cannot reach these unhydrated particles. This means that concrete with OPC probably has additional capacity for crack healing at a later stage when compared to BFSC-concrete.
- With increasing age of the specimen at the moment the first crack is made, a decrease in strength recovery is found. The age of the specimen when the first crack is made indicates the degree of hydration that has already occurred. The amount of hydration that can still take place is therefore fixed. The amount of potential strength recovery is therefore limited when the concrete has already reached a high degree of hydration when the crack is made.
- The width of the crack does not seem to influence the strength recovery due to healing. The tests with different crack mouth openings all show similar amounts of strength recovery.
- Crack healing is only observed when the cracked specimens are stored under water.

Ter Heide and Schlangen believe that ongoing hydration is the mechanism for crack healing that leads to the strength recovery in this investigation. This mechanism only works when the crack is closed again. It has been shown that crack healing does take place when enough humidity is present. The simulations that have been performed strengthen this hypothesis. It has been shown through simulation that the increase in strength in the crack due to further hydration could be sufficient to explain the observed recovery in flexural strength found in the experiments. The simulations also showed that higher strengths can be obtained in the crack compared to the bulk material when it is assumed that due to the water in the crack the final degree of hydration is reached faster in this zone.

For the practical situation of early age surface cracks in (massive) concrete structures, which are a concern from a durability point of view, this investigation shows some promising results. It indicates that these surface cracks can disappear again, at least under the right conditions as discussed above.

4.1.5 Self-Healing in Self-Compacting Concrete

Self-compacting concrete (SCC) has almost the same composition as conventional compacted concrete, however, due to adjustment of the aggregate content, especially the fine part, and the addition of chemicals and mineral admixtures, a concrete type is obtained which doesn't need to be compacted. One of the main advantages of using SCC is the reduction in construction time, however, this may result in situations where the concrete is subjected to early overloading. Therefore, Abdel-Jawad and Dehn [4.32] decided to investigate the ability of self-healing in self-compacting concrete.

Concrete specimens (100 mm x 100 mm x 100 mm) from three self-compacting concrete mixes with different water to cement ratios (0.45, 0.5 and 0.55) were prepared and loaded to different stress levels, namely; 40%, 60% and 80% of its maximum strength at the ages of 1 day and 3 days. These specimens were wet-cured in companion with control specimens up to the age of 28 days. At 28 days, the previously loaded specimens, along with the control specimens, were tested by measuring the compressive strength and the ultrasonic pulse velocity through the specimens in the direction perpendicular to the loading direction.

Fig. 4.23 a and b present the compressive strength obtained at 28 days for previously loaded specimens at stress levels of 40%, 60% and 80% of their obtained strength at the age of 1 day and 3 days, respectively. The compressive strength of the control specimens (not subjected to previous loading) is shown along. It is obvious that the previously loaded specimens achieved almost the same strength as that of the control specimens, especially for the 0.45 w/c ratio concrete. The same conclusion can be stated for the specimens preloaded at the age of one day, or at the age of three days.

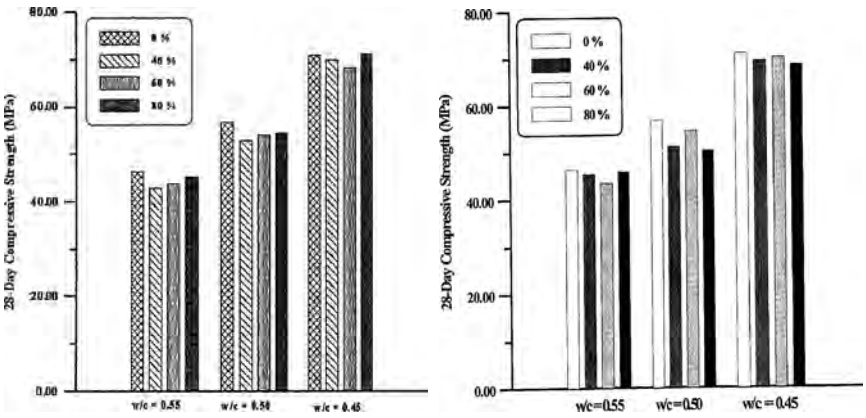

Fig. 4.23 Compressive strength at 28 days for previously loaded specimens at the age of one day (a) and three days (b) [4.32]

It is well known that the velocity of ultrasonic pulses through any solid material is affected by the existence of cracks in the material. Abdel-Jawad and Dehn [4.32] employed this technique to evaluate the potential of crack healing. From Fig. 4.24 it is seen that the ultrasonic pulse velocity of the previously loaded specimens is the same or even sometimes higher than that obtained for the control specimens. This means that all the cracks produced due to the earlier loading have been healed as a result of the subsequent hydration of the cement, as the concrete was cured in water up to 28 days. The same behaviour was obtained when analyzing the date for the concretes exposed to the different loading levels at the age of three days (data not shown).

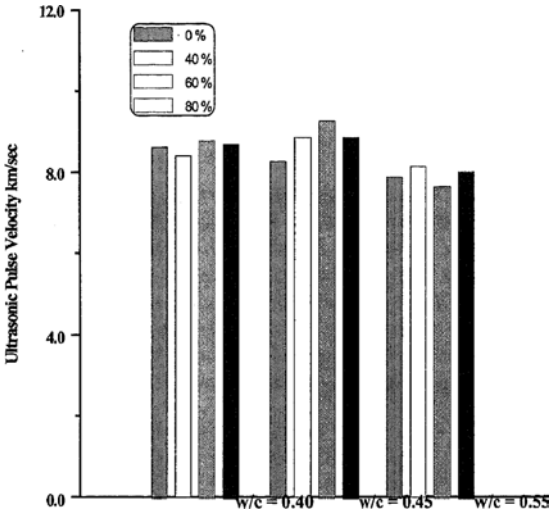

Fig. 4.24 Ultrasonic pulse velocity at 28-days for previously loaded specimens at the age of one day [4.32]

4.2 Autonomic Self-Healing

Autonomic self-healing has been defined in chapter 1 as a self-healing process where the the recovery process uses materials components that would otherwise not be found in the material (engineered additions).

4.2.1 Autonomic Crack Closure

Studies on crack healing of cementitious materials have shown that the degree of healing is a function of crack opening, with little likelihood of healing in cracks wider than 0.1 mm. [4.5]. Furthermore, it has been demonstrated that autogenic crack healing is significantly enhanced if a crack is subjected to compression. [4.30].

In the approach suggested by Sakai *et al.* [4.33] and Kuang and Ou [4.34, 4.35], cracks develop until normal width but at the time of unloading, cracks are closed due to the super elastic behaviour of embedded shape memory alloys (SMA). In addition, SMA exhibit a shape memory effect, where upon the system of the research group of Cardiff University is relying [4.36-4.40]. This research group tries to develop a cementitious material system in which shrinkable polymer tendons are activated by heating so as to generate a low level of pre-stress capable of autonomic crack closure and thus enhancing autogenic self-healing. Details of this system (Fig. 4.25), have been discussed by Lark *et al.* [4.41] and Jefferson *et al.* [4.42] and a recent experimental study has sought to identify what the combined activation method and curing regime should be to maximize the degree of autogenic self-healing [4.43].

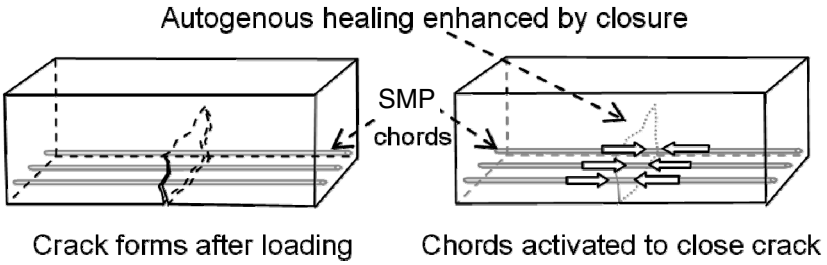

Fig. 4.25 Schematic illustration of autogenic crack healing enhanced by autonomic crack closure [4.36].

In this study small scale hollow prismatic mortar beams that were tested in a series of 3-point bending experiments were used. Fig. 4.26 illustrates the specimen configuration.

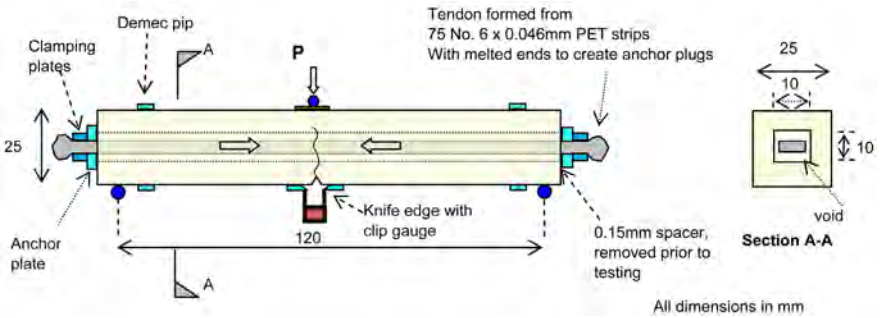

Fig. 4.26 Specimen configuration [4.36]

All mortar specimens were cast using a water:cement:sand mix ratio of 0.6 : 1 : 3 by weight. The cement used was ordinary Portland-fly ash cement, designation CEM II/V-V32.5 R, and the sand was 0/4 mm, EN12610 compliant sea dredged

sand. Prior to mixing, the sand particles were passed through a 1 mm sieve to give a maximum aggregate size of 1 mm.

To ensure that the polymer tendons did not bond with the cementitious matrix, the specimens were manufactured as hollow beams. The hollow void through the specimens was produced by inserting polystyrene rectangular formers prior to casting. The polystyrene rectangular formers were removed on day 3 and a central 3mm notch was cut, as shown in Fig. 4.26, to predetermine the location of the crack.

The shrinkable polymer tendons comprised 75 individual Polyethylene terephthalate (PET) strips, each measuring 6 mm x 0.046 mm. The tendons had a cross-sectional area of approximately 4% of the un-notched specimen. The ends of the tendons were bonded together using a soldering iron and were inserted into the hollow voids of the specimens. An end plate and clamp system were securely attached to one end of the tendon to act as an anchorage. The specimens were then held vertically with the tightened clamp end at the top so that a 1 kg weight could be hung from the clamp to be attached at the bottom end of the tendon and a 0.15 mm spacer inserted between the beam and the end plate. With the spacer in place, the lower clamping system was securely tightened. The spacers were removed prior to testing, their thickness having been calculated so that the tendons would not provide any pre-stress to the specimens prior to heat activation. This ensured that the tendons remained completely loose within the specimens during stage 1 testing.

Table 4.7 Stages of experimental procedure

Stage	Description
1	Casting (day 1)
	Curing under sealed conditions (days 1 to 4)
	Initial cracking at day 4
2	(a) heat activation (Starting on day 4 for 18 hours)
	(b) 'healing' (for 48 hours)
3	Loading to failure at day 8

N.B. The curing regime during the 'healing' phase is referred to as the healing regime.

The experimental procedure was divided into three stages as shown in Table 4.7.

In stage 1, specimens were loaded under 3-point bending at a rate of 0.001 mm/s to a crack mouth opening displacement (CMOD) of 0.30 mm and then unloaded. This CMOD was measured by a light crack mouth opening displacement gauge ($CMOD_{CG}$), which was inserted between two knife edges that

were glued either side of the notch on the underside of the specimens. Load was controlled via feedback from a linear variable displacement transducer (LVDT) which measured the displacement of the loading platen, as illustrated in Fig. 4.27.

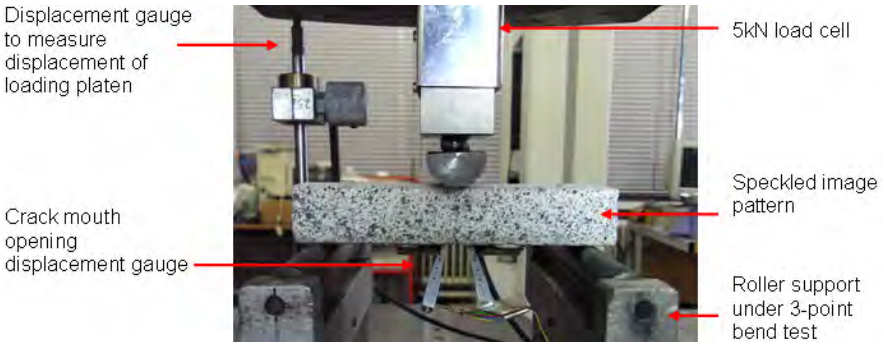

Fig. 4.27 Three-point bend test setup [4.43]

In stage 2a, the specimens were subjected to heat treatment at 90°C for 18 hours in order to activate the polymer tendons. This generated a pre-stress in the specimens of which was anticipated that it would close the crack formed in stage 1. Then, in stage 2b, the specimens were self-healed for a further 48 hours. At the end of this 'healing' stage (2b), the specimens were tested to failure in stage 3 in order to identify the success of the tendons in closing the pre-formed crack and to examine whether any autogenic self-healing had taken place. Three activation-healing (AH) regimes were investigated for stages 2a and 2b as shown in Table 4.8.

Twelve 145 mm x 25 mm x 25 mm specimens were cast for each of the procedures. For each procedure, the twelve specimens were divided into four groups of three beams. Three of the beams had the polymer tendon left inside the beam for all stages (PET specimens); three of the beams had the tendon left in place for stages 1 and 2, but removed before stage 3, (PETr specimens) and six control beams were tested to failure with no tendons, three of which were tested at stage 1 (Ctrl1 specimens) and three tested at stage 3 (Ctrl2 specimens). Material tests were also carried out using six small scale 25 mm x 25 mm x 25 mm cubes to determine the compressive strength and six 160 mm x 40 mm x 40 mm prismatic mortar beams, three of which were used for fracture energy tests and three for elastic modulus tests.

Table 4.8 Heat activation methods and healing regimes

AH regime	Heat activation method			Healing regime	
	Description	Temp. (°C)	Time (Hrs)	Description	Time (Hrs)
1	Dry heat activation	90	18	Cured in water at ambient temperature	48
2	Steam heat activation	90*	18	Specimens left in the steam chamber with the steam production turned off and the chamber allowed to return to ambient conditions	48
3	Water heat activation	90	18	Specimens left in the water tank with the temperature allowed to return to ambient conditions	48

N.B. *the atmospheric temperature was measured at 90 ^{o}C and the water in the tank was heated to 100 ^{o}C in order to produce steam conditions

One side face of each specimen was sprayed with a black and white speckled pattern to enable Digital Image Correlation (DIC) [4.44] to be used to monitor the displacements of the specimen. Two cameras were set up that tracked the speckled pattern every 5 seconds throughout the test enabling displacements and strains to be measured in 2D. The selection of two points either side of the notch allowed a second measurement of the CMOD which is denoted $CMOD_{DIC}$ and applies to a level 1.75mm above the lower surface of the specimens.

The results of this work are to be published in a paper by Isaacs *et al.* [4.43, 4.44] and from this work it was concluded that crack closure and autogenic self-healing can be achieved on small scale hollow prismatic mortar beams post tensioned with shrinkable polymer tendons. It was demonstrated that autonomic self-closure was achieved as a result of the shrinkage stress developed by the activated tendons and in two of the regimes adopted for activating and healing the specimens it was clear that effective autogenic self-healing had been achieved, i.e.:

- Dry heat activation and water based healing (AH1)
- Steam activation and healing (AH2)

In the former, the initial mechanical stiffness was recovered and strength recoveries of approximately 80 % (PETr) and 125 % (PET) were achieved. In the latter, the initial mechanical stiffness was again recovered and load recoveries of approximately 80 % (PETr) and 200 % (PET) were achieved. It was concluded that both dry heat activation followed by water curing, and steam activation and curing are both effective heating/healing regimes, with the latter providing the highest prestress force.

Only 16% of the initial strength was recovered in specimens activated and healed in water at 90 °C although the regime did activate the tendons and produced sufficient prestress to achieve autonomic self-closure. It is possible that the reduced level of autogenic self-healing in this case was related to the formation of bubbles in the crack which may have impeded the healing process but this requires further investigation.

4.2.2 Tubular Encapsulation of Liquid Healing Agents

4.2.2.1 Mechanical Activation

4.2.2.1.1 Internal Supply of Healing Agent

Carolyn Dry [4.45-4.47] already proposed the use of encapsulated liquid healing agents to repair cracks in concrete autonomously, in the early 1990's. In her experiments she used hollow brittle glass fibers which contained air-curing cyanoacrylate as healing agent. Cement prisms contained 2 metal reinforcing fibers and 16 adhesive filled 150 ml glass pipettes which were embedded inside the matrix. A second set of samples had the same composition lacking the adhesive. A schematic representation of the sample setup is shown in Fig. 4.28.

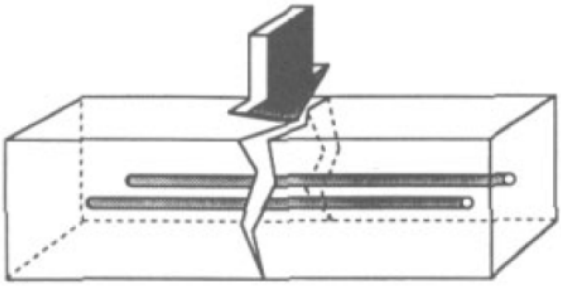

Fig. 4.28 Timed release of chemicals occurs when the brittle fiber breaks under load [4.46]

Each sample was loaded in three-point-bending, causing the repair fibers to break and release their chemicals into the cement matrix. Auditory confirmation of glass pipette breakage was accomplished. After two weeks of drying of the repair agent, the samples were reloaded in three-point bending. Fig. 4.29 represents a record of the load displacement for those two loading events on the samples.

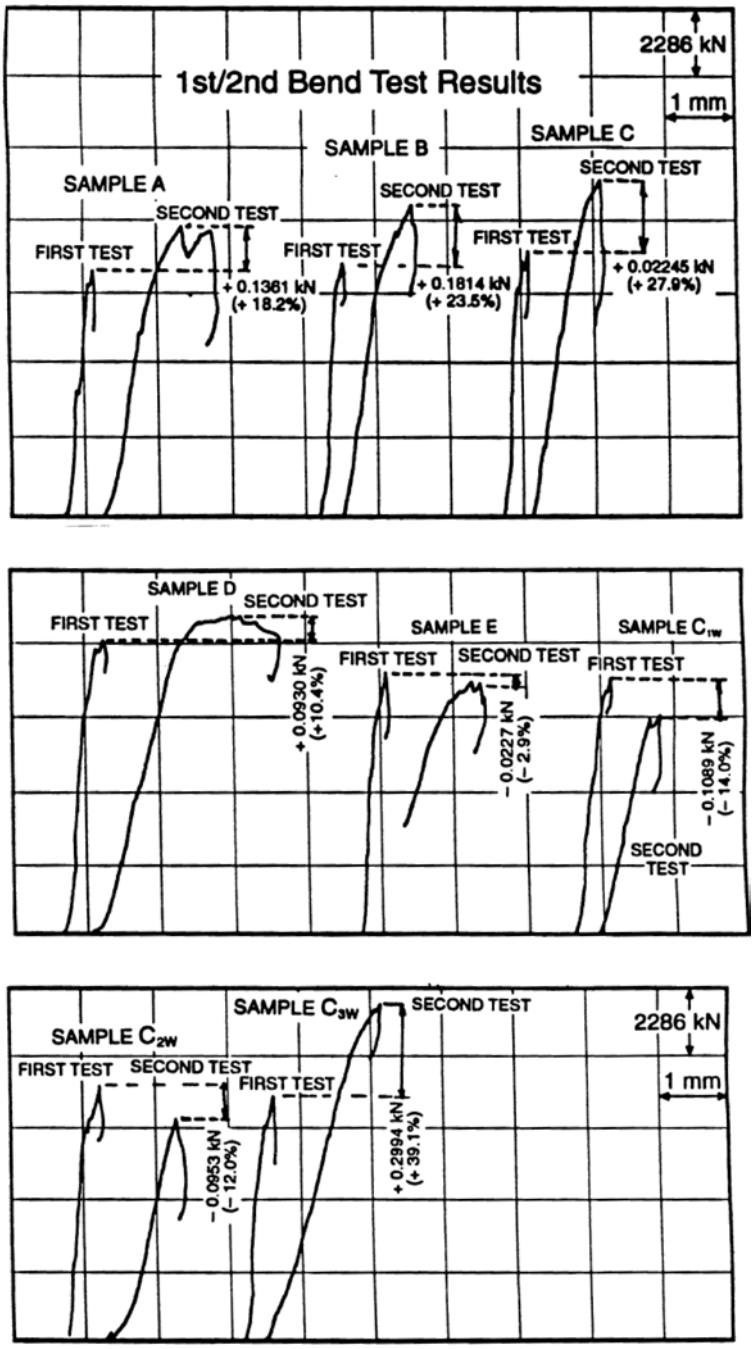

Fig. 4.29 Load displacement diagram obtained for different test series during first and the second 3-point bending test [4.47, 4.48]

A comparison of the records obtained during the first loading in flexure (before release of the chemical) and the second bend test loading (after release of the adhesive into the matrix) revealed several important facts. Most of the adhesive-loaded samples carried more of the load on the second bend than on the first bend, while in general, that was not the case for the controls. The inference made from this is that the crack opening displacement curve for the controls follows the normal reduction in load resistance, while the adhesive filled samples reverse it, in that crack opening displacement is reduced with the next loading and the fitted samples carry more load in the second test than controls. Also ductility as measured by deflection was improved for the samples containing released adhesive.

In a second series of experiments, Carolyn Dry [4.45] investigated the possible rebonding of fibers after debonding of the fibers occurred. In order to test this, mortar samples were made, containing adhesive filled glass pipettes proximate to a metal fiber and a second set of samples containing pipettes with no adhesive. In each of these samples, the metal fiber was pulled in tension until debonding occurred. The load displacement curve revealed a debond release typical of a bond with a brittle material in all cases (Fig. 4.30). The samples were then loaded under three-point bending in order to break the adhesive filled glass pipettes. After two weeks of curing, the metal wire was pulled again. The load displacement curve for the samples with adhesive revealed a bond release that was typical of an elastic-bonded material, while the samples without adhesives exhibited no rebonding to release. The authors concluded that these results were positive and suggested that fibers could be rebonded with adhesive released upon loading.

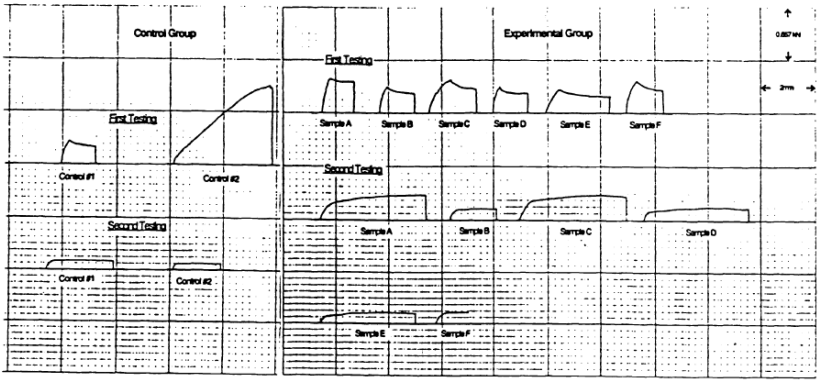

Fig. 4.30 Comparison of load displacement diagrams for control versus experimental group during first and second pull of metal fibers [4.45]

Tran Diep Phuoc Thao *et al.* [4.49, 4.50] proposed the use of an air-curing epoxy resin as healing agent. Perspex tubes and glass tubes were tested as possible encapsulation materials. It was found that Perspex tubes showed visible cracks on

the surface due to a chemical reaction between the healing agent and the tubes. As Perspex tubes are stronger and more ductile in comparison with glass tubes, the rupture of the tubes would be delayed and therefore glass tubes were chosen as encapsulation material. Tubes with an inner diameter of 4 mm and a length of 250 mm were used in the experiments as this size seemed most suitable according to the preliminary tests.

Concrete specimens 300 mm x 80 mm x 50 mm were cast using a mortar mix of 0.8:1:1 (water, cement, sand). In each beam two glass tubes were embedded. The tubes were filled with epoxy (POR-15) and aquastick was used to seal both ends. The tubes were placed at 10 mm from the bottom of the specimen whereas the steel wire mesh (ø1.3 mm) was placed at 20 mm from the bottom of the specimens. A similar set of specimens but without glass tubes was cast to serve as control specimens. All specimens were compacted using a vibrating table, demoulded after 24 hours and air-cured for 3 days before test were carried out (Fig. 4.31).

Specimens were subjected to a 3-point bending test. The control specimens were loaded till failure, in order to determine the load displacement curve. Each specimen with self-healing properties was tested beyond the point where an audible 'pop' sound was heard, which indicated fracturing of the glass tubes. The load was held until leakage of epoxy was observed on the bottom surface of the specimen. The specimen was then unloaded and left unloaded for 4 days before being loaded again. The second test was terminated soon after more leakage of epoxy was observed. The load was then removed and the specimen was left to heal again for 3 days before being loaded again and tested to failure in the third loading test.

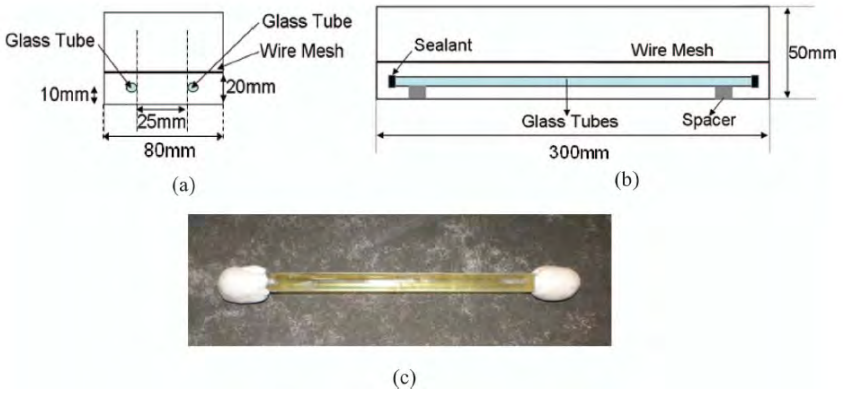

Fig. 4.31 Self-healing system, (a) front elevation, (b) side view, (c) epoxy filled glass tube with aquastick as sealant [4.49]

The presence of the self-healing system decreased the overall elastic modulus of the beam as the epoxy filled glass tubes were less stiff than the concrete that was replaced. During the first loading cycle, the strength of the beam with

self-healing properties, represented by the first peak at a load of 2.23 kN, was similar to the strength of the control beam (see Fig. 4.32). A second peak was observed which was caused by breakage of the glass tubes, typically occurring within 10 seconds after the crack in the mortar beam was initiated. Once the tubes were broken, gravity and capillary forces acted as the driving force for the epoxy to flow towards the gaps formed by the crack.

During the second loading cycle, an initial peak of 1.44 kN was noticed, which corresponded to the initiation of a second crack. However, the specimens could be further loaded up to a higher load of 2.31 kN. The newly formed crack initiated from a point at the bottom surface of the beam that was very close to the first crack and they bridged together when the second crack propagated further into the specimen. From these findings the authors suggested that the first crack had been partially healed. The epoxy in the vicinity of the crack mouth cured fully having been in contact with air for four days. However, in regions close to the crack tip, which is depleted of air for curing, curing may not have completed with some epoxy still in its liquid state. This weak zone attracted nearby propagating cracks. Next, the smaller damage initiation load of 1.44 kN may be due to softening of the beam caused by the formation of micro cracks in the vicinity of the first crack zone during the first loading, Although, the specimens were partially healed after three days, the recovered strength equaled the strength of the control specimen.

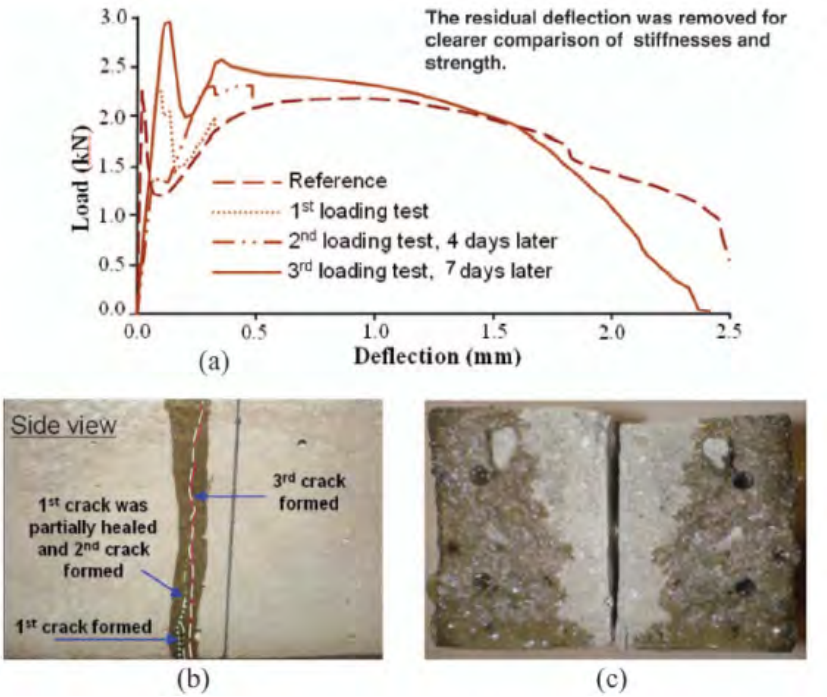

Fig. 4.32 Experimental results of self-healed specimen, (a) load-deflection curve, (b) order of crack formation, and (c) dissected specimen after healing thrice [4.49]

During the third loading cycle, a new crack was formed but this time it did not merge with the previous crack suggesting that the damage has been fully healed. As cracking only starts from the weakest point in a specimen, complete healing strengthened this zone and it is not surprising that a new crack initiated at a location corresponding to the next weakest zone in the specimen. This is confirmed by the result of the experiment showing the strength of the specimen has increased to 2.95 kN, which is 32% higher than that of the reference specimen.

In their later research, Pang *et al.* [4.51] embedded their encapsulated healing agent inside bigger sized structural concrete members namely a beam (125 mm x 200 mm x 2000 mm, Fig. 4.33a), a column (Ø 200 mm x 800 mm, Fig. 4.33b) and a slab (100 mm x 1000 mm x 1000 mm, Fig. 4.33c). Here, the glass tubes were coiled with spiral wire followed by a 3.5 mm thick mortar layer to protect them from premature damage during casting. The self-healing efficiency was qualified as the stiffness recovery of the members after repeated loading and unloading cycles.

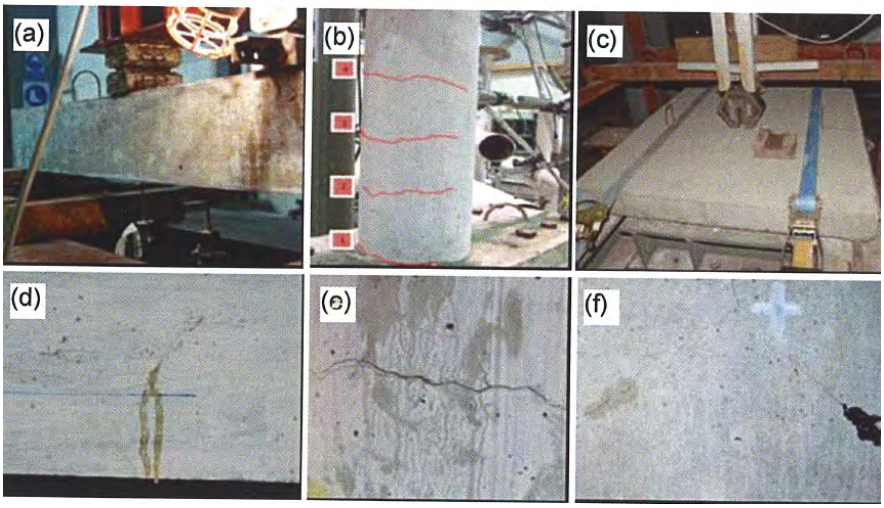

Fig. 4.33 Evaluation of the self-healing efficiency of a beam (a), a column (b) and a slab (c). Self-healing of a crack inside a beam (d), a column (e) and a slab (f)

The beam element exhibited multiple crack healing capabilities with 84% of the initial flexural stiffness being recovered. The column element showed a stiffness recovery of up to 70%. This high healing efficiency was not expected as in this case, the crack planes developed in a direction normal to the direction of the gravity flow (Fig. 4.33b). The slab was assessed for its healing capability when subjected to multiple drop weight impacts. Again, multiple crack healing was observed, with the maximum healing efficiency, in terms of stiffness recovery, found to be 99%.

In both studies mentioned before one-component, air curing healing agents were used. Mostly, single-component agents are preferred above multi-component healing agents because incomplete mixing of the different compounds is feared. However, air-curing may be limited as limited air is available inside the crack. In the study of Tran Diep Phuoc Thao *et al.* [4.49, 4.50] it was already mentioned that incomplete curing of the agent inside the crack was noticed. Therefore, Carolyn Dry [4.52], proposed in her later research to make use of a multi-component healing agent. Multi-components agents have more stability than a single component adhesive because they are activated at a later date i.e. in situ. She proposed the use of methyl methacrylate (MMA) as healing agent. This agent consisted of three compounds: the MMA monomer, cumene hydroperoxide and cobalt neodecanoate, the latter two components being the initiator and activator, respectively. The cobalt neodecanoate solution and MMA solution were mixed together, being the first compound while the second compound was cumene hydroperoxide.

In previous experiments of Dry, glass tubes were used as delivery system [4.45, 4.46]. However, in this study she proposed the use of hollow tunnels which were coated with a brittle sealer [4.52]. In order to obtain these hollow tunnels, rounded steel rods were cast in concrete beam samples and pulled out after 24 hours of curing. They left small tunnels through the length of the samples. The inside of the tunnels was coated with a thin layer of Thompson's water seal and capped using brass pipe fittings set in the concrete at the ends of the beam. The larger tunnels were loaded with the cobalt/MMA solution while a single small tunnel was made and loaded with the cumene hydroperoxide initiator. The beam samples had a 1.8" triangular notch, set in the middle underside of the beam. The concrete beam samples were $15^{1/4}$" long, 3" deep and $2^{3/4}$" wide. The concrete was reinforced by three pair of 0.2 gauge piano wires (see Fig. 4.34).

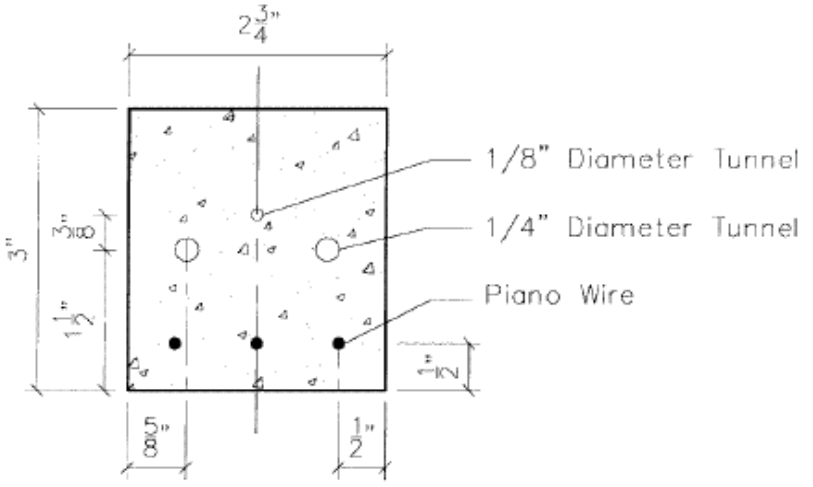

Fig. 4.34 Beam sample section [4.52]

Cracks were created by performance of three-point bending tests. During the bending test, the two liquids leaked out into the cracks and entirely filled them with a solid plexiglass like matrix within 24 hours. When standardized for 0.5 mm of deflection, the adhesive repaired beams (1, 2 and 3 in Table 4.9) carried more load in the second test (+130%), while the two controls (C1 and C2 in Table 4.9) carried 117% and 65%. When standardized to 1 mm of deflection, the results show even more strength gain from the adhesive repaired specimens. This means that at specific points of deflection (0.5 mm and 1 mm) after failure, the beams proved to be more ductile and continued to resist more load in the second test. As shown in Table 4.10, the adhesive repaired samples had also greater deflection at failure (100%-800%), while the controls did not (-77% - 135%). The authors concluded that the MMA adhesive bond restored strength and made the beam more flexible.

Table 4.9 Three-point bending strength test results when standardized to specific points of deflections [4.52]. Resistance (kN) given at points of deflection beyond failure.

	0.5 mm deflection			1.0 mm deflection		
Sample no.	Test 1 (kN)	Test 2 (kN)	Test 2 (%)	Test 1 (kN)	Test 2 (kN)	Test 2 (%)
1	0.8	1.1	137.5	0.5	1.2	240
2	0.9	1.2	133.3	0.6	1.1	183.3
3	0.4	1.25	312.5	0.3	1.1	366.6
C1	1.5	1.75	117	2.375	2	84
C2	1.375	0.9	65	1.75	1.8	103

Table 4.10 Three-point bending test deflection results [4.52]

Sample no.		First test (max. mm at failure)	Second test (max. mm at failure)
1	Test sample	0.2	1.6 (+ 800% of first test)
2	Test sample	0.25	0.025 (+ 100% of first test)
3	Test sample	0.175	0.35 (+ 200% of first test)
C1	Control sample	0.35	0.27 (-77% of first test)
C2	Control sample	0.24	0.325 (+ 135% of first test)

In their research, Van Tittelboom and De Belie [4.53, 4.54] compared the efficiency of different types of healing agents. Both, single-component and multi-component healing agents were tested on their suitability. Selection of the healing agents was based upon several requirements, such as: viscosity, reaction time, shelf life. In Table 4.11 an overview of the healing agents used and their most important properties is given.

Glass tubes with an internal diameter between 1 mm and 2 mm and a length ranging from 100 mm – 150 mm were used as encapsulation material. In case 2-component healing agents were used, 2 glass tubes were glued next to each other, so tubes with two compartments were obtained. One compartment was filled with the first component while the other compartment was filled with the second component. When a crack appears, both tubes break and both components flow into the crack. Upon contact of both components, the healing agent reacts inside the crack which is then healed. For 1-component, air-curing healing agents, singular tubes were used. Breakage of these tubes brings the healing agent into contact with the air inside the crack which causes hardening of the glue and crack repair.

Table 4.11 Overview of the different types of healing agents used and of their most important properties [4.53]

Healing agent	Type	Code	Number of compounds	Viscosity of most viscous compound at 20°C	Reaction time
			[-]	[cPs]	[sec]
Rite Lok EC5	Cyanoacrylate	CA	1	5	5 - 15
Prime Rez 1100 HM	Epoxy	EP1	2	150	1.740
Prime Rez 1200 LM	Epoxy	EP2	2	80	1.800
Concresive EP 2055	Epoxy	EP3	2	360	2.400
Meyco MP 355 1K	Polyurethane	PUR1	2 (or 1)	600	50 - 300(*)
Icema R 145/31	Polyurethane	PUR2	1	7.200	2.400 - 10.800

(*) when 10% accelerator is added

Specimens with internal glass tubes were prepared as shown in Fig. 4.35. When the mortar matrix had hardened, the prisms were cracked, and thus the healing mechanism was triggered, by means of a crack width controlled three-point-bending test.

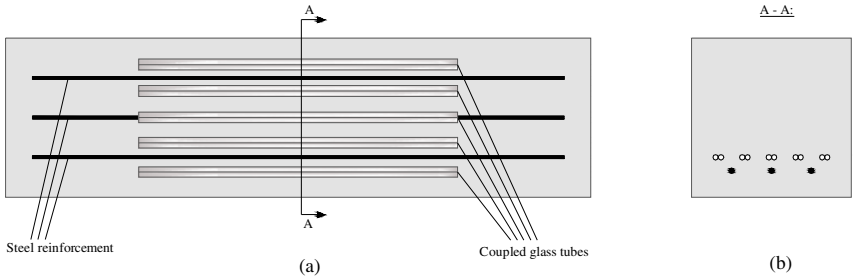

Fig. 4.35 Top view (a) and cross section (b) of the mortar prisms in the case coupled tubes are used [4.53]

The self-healing efficiency of the different types of healing agents was evaluated by comparing the regain in mechanical strength. One day after performance of the bending test, when the healing agent inside the cracks of the autonomic self-healed specimens was thought to be hardened, samples were loaded again in three-point-bending. From the obtained loading curves, the peak load was determined and this value was used as an indication of the strength. The strength of the beams after self-healing was compared with the original strength for each type of healing agent used. After performance of both loading cycles samples were completely broken and cross sections were examined to evaluate the amount of glue that came out of the tubes and to verify if the glue had hardened inside the crack.

In Fig. 4.36, regain in strength is shown for all test series in terms of percentage. For the reference sample (REF), containing empty glass tubes, no strength regain was observed upon reloading.

Samples containing encapsulated cyanoacrylate (CA) showed some regain in strength, however, during crack formation, no glue migration was seen at the crack faces. Even when specimens were completely broken and cross sections were examined, no leakage of the glue was seen. It is thought that the glue already hardened inside the glass tubes, before crack formation, and that due to this fact the glue did not come out of the tubes. Presence of small air bubbles inside the tubes is sufficient to cure the glue before tube breakage. The regain in strength, which was observed during reloading, may then be attributed to the fact that the 'hardened glue bars' acted as a kind of reinforcement, bridging the two crack faces. This is similar to the mechanism, examined by Sakai *et al.* [4.33] and Isaacs *et al.* [4.36], to obtain self-healing properties in concrete.

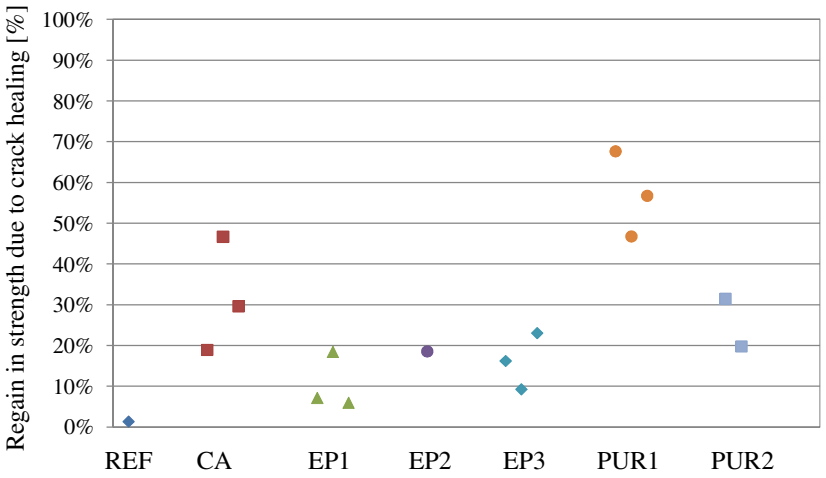

Fig. 4.36 Regain in strength in terms of percentage for the different types of healing agent used [4.53]

When epoxy (EP1, EP2 and EP3) was used as healing agent, regain in strength was rather low. Again, during crack formation no glue migration was seen at the crack faces. When the beams were completely broken, it was seen that the glue partly came out of the tubes. However, the migration front was limited and moreover it was seen that the glue was still liquid at the moment the beams were broken. Minor mixing of both components, leading to imprecise stoichiometry may be the reason. These results prove the dependence of epoxy resins to the precise mix ratio which makes this type of glue unsuitable as healing agent in self-healing concrete.

When polyurethane was used to heal the cracks, good results were obtained. Two types of polyurethane were used here. PUR2 is a quite viscous, 1-component healing agent, consequently cracks were only partly filled with this type of glue. During examination of the cross sections, it was also seen that part of the glue was still liquid. Therefore, only 20-30% of regain in strength was obtained with this agent. The other type of polyurethane, PUR1, gave better results. PUR1 is a low viscous, 1-component polyurethane that starts foaming upon contact with water or air. However as the reaction time of this product may be shortened by addition of an accelerator, double glass tubes were used, like in the case of 2-component healing agents. One compartment was filled with polyurethane while the other compartment was filled with a mixture of accelerator and water. When PUR1 was used, 45-70% of strength regain was observed. It was already seen during the first loading cycle, when cracks were created, that the glue leaked out of the tubes, into the cracks. In Fig. 4.37, one of the specimens is shown during the bending test and migration of the glue at the crack faces is visible. When examining the cross sections it was seen that almost half of the surface was covered with healing agent when PUR1 was used.

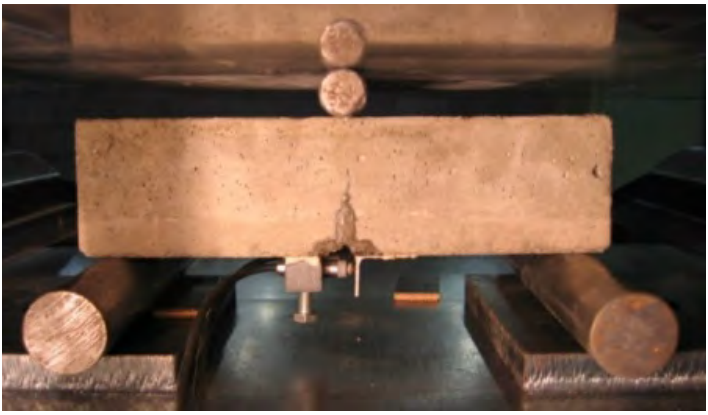

Fig. 4.37 Migration of polyurethane (PUR1) to the crack faces observed during the bending test [4.53]

From the experiments described above it may be concluded that the type of healing agent used is very important when striving for self-healing properties in concrete. 1-component, air curing healing agents have the drawback that the glue may already start hardening inside the tubes when air bubbles are enclosed; 2-component epoxy resins are very sensitive to the mix ratio and no polymerization reaction will occur when the compounds are mixed randomly.

As best results were obtained when the polyurethane *Meyco MP 355 1K* was used, more experiments were performed with this type of healing agent [4.55, 4.56]. Glass tubes with an internal diameter of 2 mm and 3 mm with a varying length (so the internal volume was the same for both types of tubes) were filled with the polyurethane. Mortar beams and mortar cylinders with internal tubes were prepared and regain in mechanical properties and decrease in water permeability due to self-healing were tested.

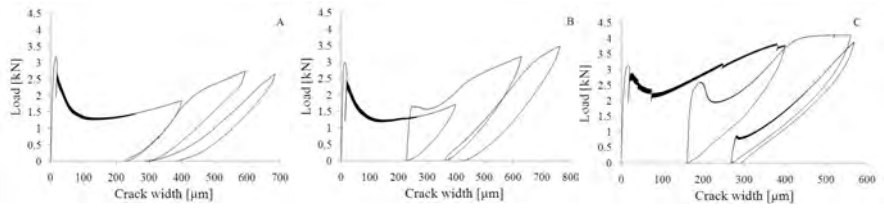

Fig. 4.38 Load [kN] versus crack width [µm] during crack formation (first curve) and first (second curve) and second (third curve) reloading cycle for a reference sample (A), a sample with a manually healed (B) and autonomic self-healed (C) crack [4.55]

Regain in mechanical strength was compared against reference samples, from which cracks were not healed. Samples were compared with manually healed cracks and samples with autonomic self-healing properties. First, cracks were

created in all samples during a first loading cycle. After this loading cycle, cracks of the specimens for manual healing were treated. Specimens with glass tubes inside were autonomously healed during loading due to release of glue out of the tubes. One day later all beams were reloaded and regain in mechanical properties was tested. Again one day later a second reloading cycle was performed. In Fig. 4.38 the loading curves are drawn for three specimens, one of each group.

When cracks are not healed, no regain in mechanical strength is observed during reloading. For the manually healed specimens only during the first reloading cycle regain in strength is observed while for the specimens with autonomic self-healing properties strength regain is obtained during the first and the second reloading cycle. From these loading curves, the strength and the stiffness of the beams was calculated and the mechanical properties after (self-)healing were compared with the original values. The peak load F_c was used as an indication of the strength while the slope of the curve, joining the points 0 F_c and 0.4 F_c, was used to indicate the stiffness.

In Fig. 4.39A regain in strength is shown for all test series in terms of percentage. It is seen that for the reference samples no regain in strength was obtained nor during the first, nor during the second reloading cycle. In the case cracks were manually healed 56 till 71 % of the original strength was regained, during the first reloading cycle. However, when the samples were reloaded again no regain in strength was obtained. If encapsulated healing agents were present inside the mortar matrix, it is shown that during the first reloading cycle 33 till 83 % of strength regain is obtained due to leakage of the glue out of the tubes. When those specimens were loaded again, some additional glue leaked out of the tubes and during the second reloading cycle again 11 till 28 % of regain in strength is observed.

In Fig. 4.39B regain in stiffness is shown. It is seen that for the reference samples no regain in stiffness was obtained. In the case cracks were manually healed 21 till 59 % of the original stiffness was regained. However when these samples were reloaded again no additional regain in stiffness was observed. If encapsulated healing agents were present inside the mortar matrix, it is shown that during the first reloading cycle 29 till 62 % stiffness regain is obtained. When those specimens are loaded again, 20 till 38 % regain in stiffness is observed.

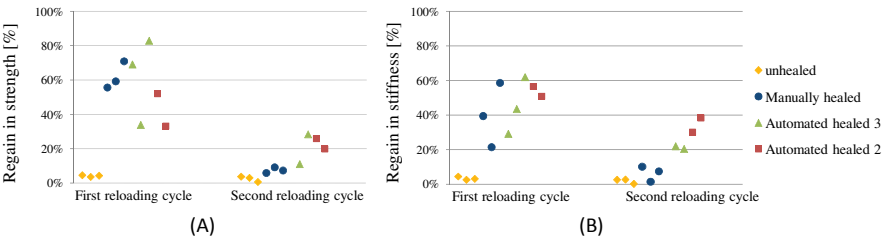

Fig. 4.39 Regain in strength (A) and regain in stiffness (B) in terms of percentage during the first and the second reloading cycle for unhealed samples, samples of which the cracks are manually healed and samples with self-healing properties obtained by means of embedded glass tubes with an internal diameter of 2 mm and 3 mm which are filled with glue [4.55]

Normally, the efficiency of emptying of the tubes is dependent on the capillary forces inside the tubes, which are reduced when the tube diameter increases. However, an alteration in the diameter of the glass tubes from 2 mm to 3 mm does not seem to give significant differences in outcome, as it can be seen in Fig. 4.39A and B. Release of the glue seems to be more influenced by coincidental effects.

Besides regain in mechanical properties, it is also aimed that the autonomic self-healing leads to crack closing, so aggressive liquids and gasses cannot longer enter the concrete matrix through cracks. Therefore, water permeability measurements were performed (with the test setup shown in Fig. 2.19) onto unhealed, manually healed and autonomously healed specimens. The permeability coefficient of those specimens was compared with the one obtained for uncracked specimens.

In Fig. 4.40 it is seen that even in the case of uncracked specimens, some water leakage appears, however, the amount is very low. When created cracks were manually treated with polyurethane, the water permeability still remains low and the results are comparable with those obtained for uncracked specimens. When samples with self-healing properties were cracked and subjected to a water permeability test, it is seen that the water permeability coefficient k is higher than in the case cracks were manually healed, however, the water leakage is 100 times till 10000 times less than in the case cracks are left untreated. In this graph it is also seen that there is no difference between the efficiency of tubes with an internal diameter of 2 mm or 3 mm.

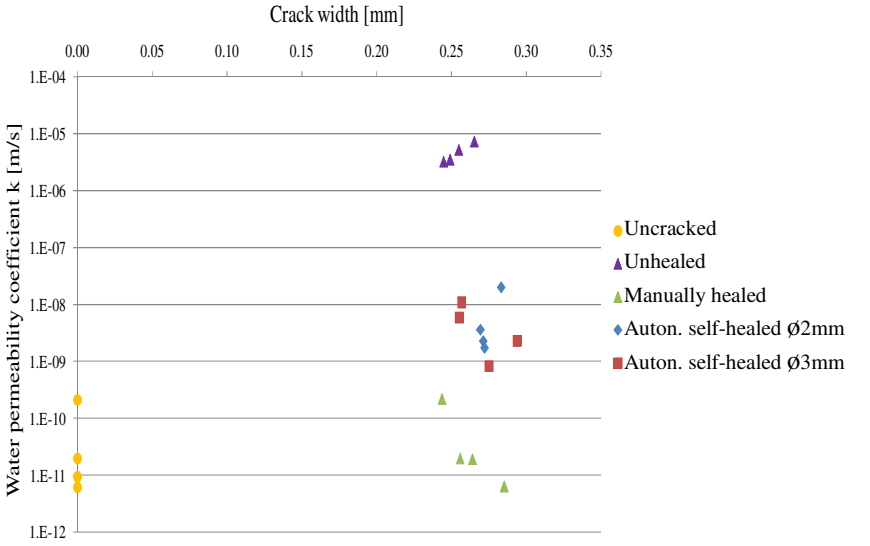

Fig. 4.40 Water permeability coefficient k [m/s] obtained for uncracked and unhealed samples, samples of which the cracks are manually healed and samples with self-healing properties obtained by means of embedded tubes with an inner diameter of 2 and 3 mm [4.55]

The experiments described before were laboratory experiments, proving the concept of self-healing concrete. However, Carolyn Dry [4.57, 4.58] already incorporated the proposed self-healing mechanism into real scale structures. In 1997, the research group of Dry casted continuous bridge deck slabs containing encapsulated healing agent. Part of the capsules were used as delivery system to heal shrinkage cracks while other capsules were used to repair internal shear cracks.

In order to heal shrinkage cracks, scored hollow glass fibers were embedded in the top surface of the bridge decks (Fig. 4.41 A). Due to drying shrinkage, stresses occur which causes cracking near the surface and so fibers are pulled apart at the scored line. Subsequently the adhesive flows out from the broken tubes and fills the control joint crack, as seen in Fig. 4.41 B. The used repair adhesives had a low modulus of elasticity and allowed future movement to resist stresses and strains in the deck without additional cracks extending from the shrinkage micro cracks.

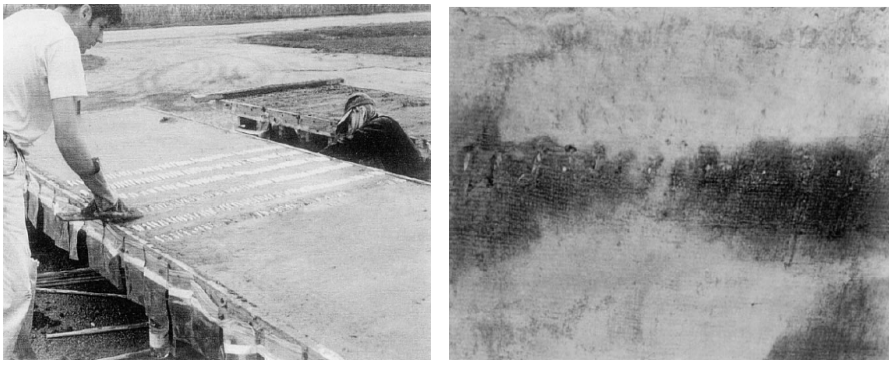

(a) (b)

Fig. 4.41 (a) Photo of the tubes embedded in the top surface of the deck; (b) Photo of the control joint line created by the release of sealant from embedded tubes or fibers [4.58].

Visual assessment was the primary means used for assessing behaviour of the sealant-filled tubes. The sealant, VOC, changed color, first to light blue and then orange, when released into contact with concrete. It was noticed that tubes which were partly or fully embedded, broke and released their content, as shown in Fig. 4.41 B. Repair tubes which were not covered did not break, although these were more exposed to the environment and freezing and thawing weather cycles than the fully embedded tubes (Fig. 4.42). From this it was concluded that the environmental forces did not cause breakage of the tubes, but tubes were broken due to shrinkage stresses. During these experiments the authors also attempted corrosion monitoring, but no conclusive data were obtained. Therefore, the authors concluded to pond salt water onto the surface and due to leakage through the cracks change on voltage potential can be measured. Later, they also want to measure the reduction in water permeability due to shrinkage crack repair.

In order to repair internal shear cracks, tubular capsules containing stronger, high modulus adhesives were placed below the surface in areas of tension caused by bending. All four decks were tested three times each, in bending. Deck 1 had VOC embedded at its surface and cyanoacrylate repair capsules through its section. Deck 2 was the control deck, and contained no repair adhesives. Deck 3 had several hundred Tripp-adhesive-filled capsules embedded randomly through the section at mid-span of the deck length. It also had a transverse row of longitudinally aligned capsules with VOC just beneath the top surface of the decks. These are within the tensile zone during load-induced bending. Deck 4 had Trip on its surface and nothing through its section. The structural cracks, which were induced by loading (Fig. 4.43), were successfully repaired as evidenced by higher strength than a tested control deck without adhesives and by the creation of new cracks in some places where the old repaired cracks had not re-opened (Table 4.12).

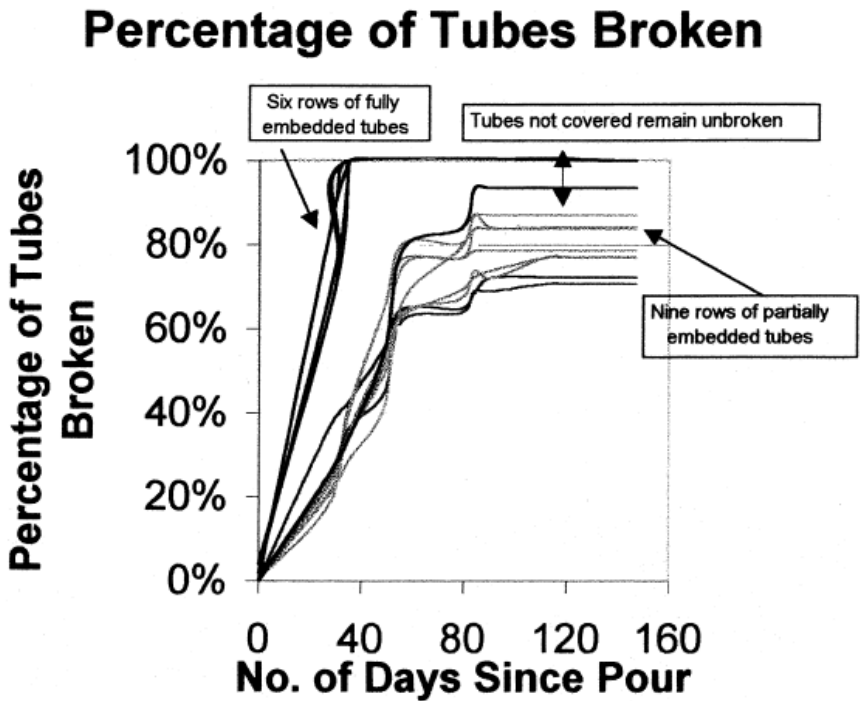

Fig. 4.42 Chart of the percentage of tubes, which released sealant over time [4.58]

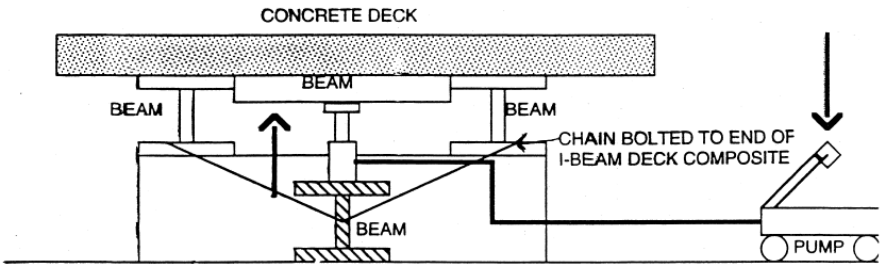

Fig. 4.43 A diagram of the testing method setup used to induce structural shear cracking [4.58].

Table 4.12 A listing of loads carried at failure point by the four bridges in three bending tests [4.58]

	Strength increase				
Deck no.	1st Load (kips)	2nd Load (kips)	% change	3rd Load (kips)	% change
1	1250	1250	0%	1100	-12%
2	1200	800	-33%	800	-33%
3	1500	1500	0%	1200	-20%
4	1500	1800	20%	1700	13%

To reduce the suction effect exerted by the sealed ends of cylindrical capsules, de Rooij and coworkers [4.59, 4.60] proposed to encapsulate the healing agent inside coated hollow plant fibers. When cracks propagate in the concrete matrix, the fiber bundles tend to delaminate and subsequently the healing agent is released from the splintered fiber bundles into the damaged areas where it subsequently reacts.

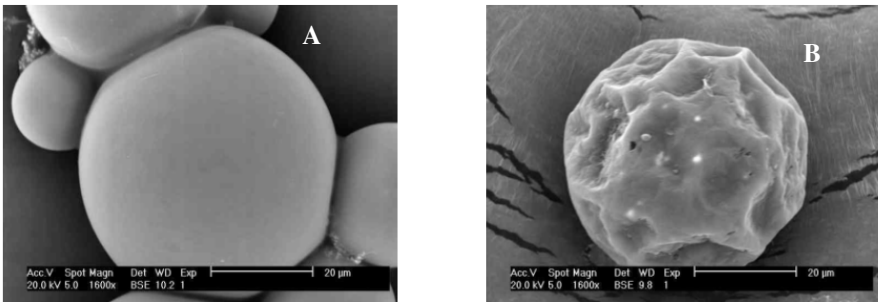

Fig. 4.44 Microcapsule filled with tung oil (A) and microcapsule filled with $Ca(OH)_2$ (B) [4.61]

In all studies listed before, capsules had a tubular shape. Although, it is less commonly investigated, in some studies capsules with a spherical shape are incorporated in the matrix to provide cementitious materials with self-healing properties. For example in the study of Cailleux and Pollet [61], where it was aimed to provide repair mortars with self-healing properties, tung oil, $Ca(OH)_2$ or bisphenol-F epoxy were encapsulated by spherical gelatin microcapsules (Fig. 4.44).

When the encapsulated healing agent was mixed into the repair mortar, it was shown that some capsules were destroyed during mixing, resulting in release of the encapsulated agent (Fig. 4.45A). Capsules which survived the mixing process (Fig. 4.45B) only ruptured upon crack appearance. At that time, tung oil hardened upon contact with air. The other proposed healing agent, being $Ca(OH)_2$, formed $CaCO_3$ crystals upon reaction with carbon dioxide (CO_2). For the epoxy, a hardener was dispersed through the mortar and hardening of the epoxy resin was obtained when the resin came into contact with the hardener.

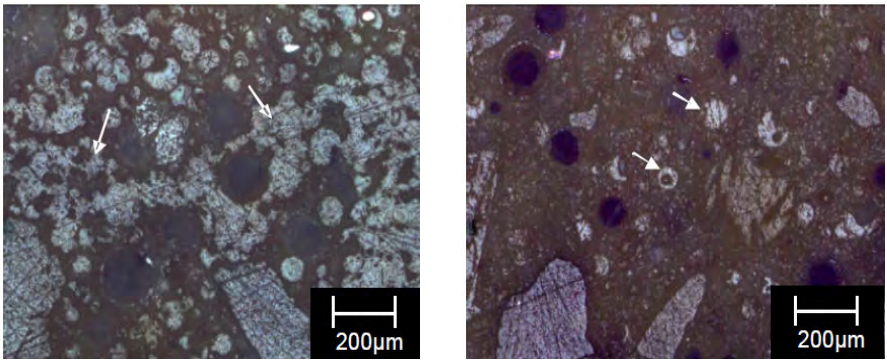

Fig. 4.45 Polished cross-section of mortar matrix containing damaged microcapsules filled with tung oil (A) and mortar matrix containing intact microcapsules filled with epoxy (B) [4.61]

To evaluate the self-healing efficiency, specimens with dimensions of 150 mm x 150 mm x 30 mm were cast and subjected to a three-point bending test in order to create cracks with a width of 40 µm. For samples containing encapsulated epoxy resin, the two fractured surfaces adhered again after some time, proving that self-healing of the introduced damage had occurred.

Huang and Ye [4.62] and Pelletier *et al.* [4.63] encapsulated a sodium silicate (Na_2SiO_3) solution by spherical capsules. Huang and Ye encapsulated the solution through storage in sponge pieces with a diameter of 5 mm which were afterwards sealed with wax (Fig. 4.46A). In the study of Pelletier *et al.*, the solution was encapsulated by polyurethane microcapsules with sizes ranging from 40 – 800 µm (Fig. 4.46B). While in the study of Huang and Ye, mixing in of the capsules by

hand was necessary to survive the process, the capsules used by Pelletier *et al.* seemed to survive the mixing process. Moreover, the latter capsules did not seem to affect the compressive strength while those used by Huang and Ye did have a negative effect on the mechanical properties.

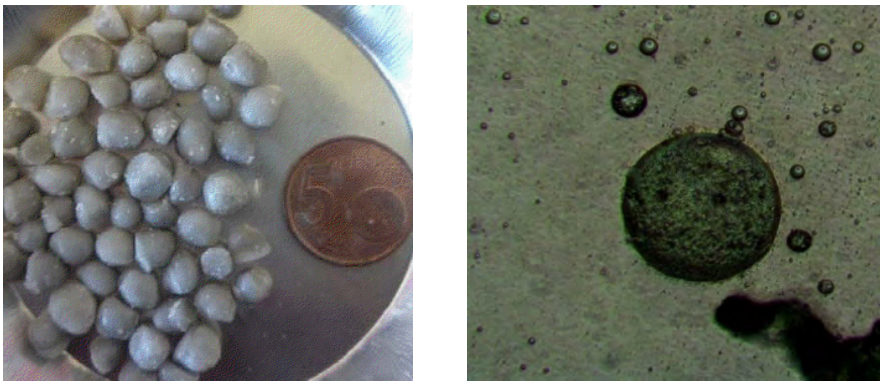

(A) **(B)**

Fig. 4.46 Image of the encapsulated sodium silicate solution as it was done by Huang and Ye (A) [4.62] and light microscopy image of a polyurethane microcapsule used by Pelletier (B) [4.63]

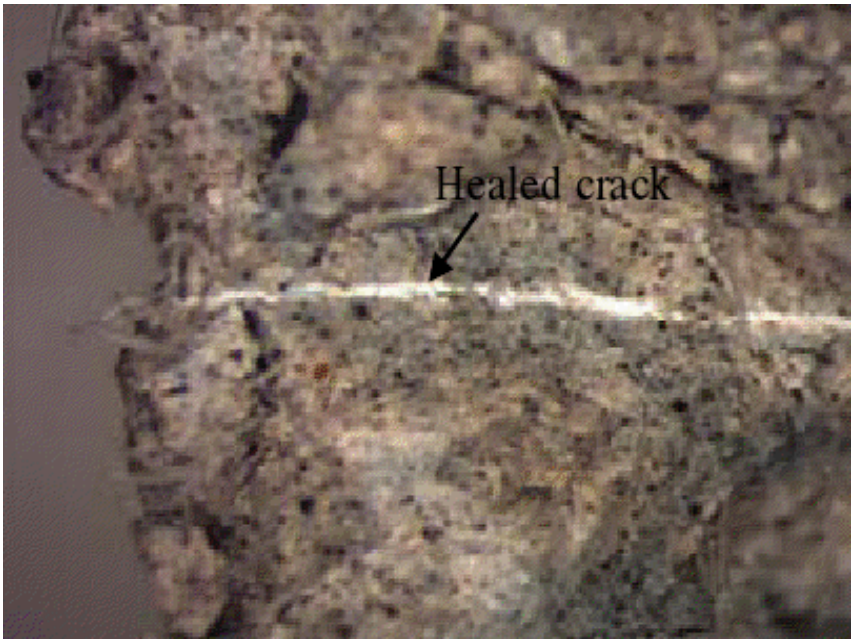

Fig. 4.47 Cracked sample after healing occurred [4.62]

Both authors [4.62, 4.63] mentioned that at the moment of crack appearance, the capsules broke and the Na_2SiO_3 solution was released. The latter will reacted with the $Ca(OH)_2$, naturally present in concrete, to form a calcium silicate hydrate (CSH) product that healed the crack (Fig. 4.47). By means of EDS analysis, the formation of CSH inside the cracks was proven by Huang and Ye [4.62].

In their study, Pelletier *et al.* [4.63] evaluated the healing efficiency as the possibility to recover some of its strength after acquiring some minor micro scale damage. Therefore, samples were loaded to incipient failure, indicated by a sharp decrease in the load displacement curve. After the samples were left to heal for one week, they were reloaded. Pelletier noticed that the load at failure of the capsule-containing samples was 26 % (Fig. 4.48A) of the original value while the samples without capsules displayed only a recovery of 10% (Fig. 4.48B).

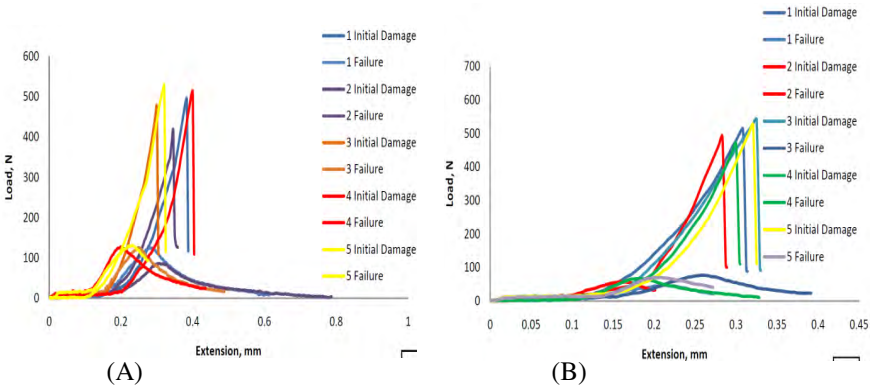

Fig. 4.48 Load versus displacement (extension) for flexural strength characterization of capsule-containing (A) and control samples (B) [4.63]

In the studies mentioned before, all embedded capsules had the same content and the healing agent was able to cure upon contact with the air, the cementitious matrix or a hardener which was dispersed through the matrix. In addition to the single-capsule approach, multi-capsule systems exist. This means that two or more different types of capsules which sequester separate components of the healing agent are embedded in the matrix. In the latter case, healing occurs upon rupture of both types of capsules and release of both components which then contact each other.

An example of this approach, is the system proposed by Mihashi *et al.* [4.64]. They used spherical capsules with a urea formaldehyde formalin (UFF) shell containing a two-component epoxy resin. The researchers, however, noticed that it was difficult for the two-component epoxy to harden, due to insufficient mixing of both components in the crack. Feng *et al.* [4.65] also used spherical microcapsules with a urea formaldehyde (UF) shell filled with a two-component epoxy resin. However, these researchers modified the epoxy resin with a diluant chemical to adjust the viscosity, with the aim of obtaining superior mixing of both

components. Although reaction of this epoxy resin may occur at room temperature upon contact with the curing agent, crosslinking of the structure and beneficial properties are obtained when a thermal curing process at 120°C is provided during 1 h. This additional heat treatment makes this technique less convenient. Kaltzakorta and Erkizia [4.66] encapsulated a two-component epoxy resin by silica microcapsules, instead of their polymeric counterparts. This research is still in its initial phase and up to now researchers have only proven the possibility to mix in this type of capsules in cement paste, so no statements can be made about the healing efficiency.

Yang *et al.* [4.67, 4.68] used silica gel shell microcapsules with a diameter of around 4.15 µm which were prepared through an interfacial self-assembly process and sol-gel reaction. In Fig. 4.49 a schematic overview of the capsule preparation is depicted. While part of the microcapsules were filled with MMA oil, the rest was filled with triethylborane (TEB) oil which was used as initiator.

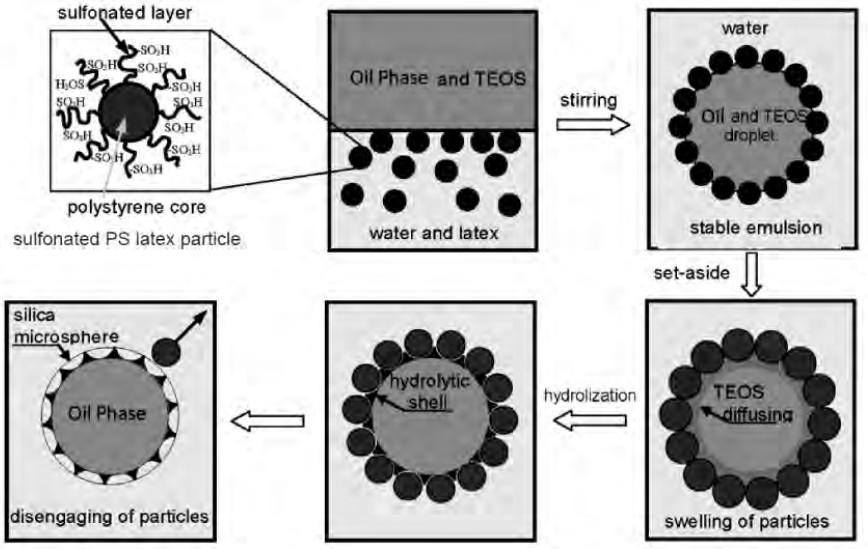

Fig. 4.49 Schematic illustration of the capsule formation [4.67, 4.68]

It was possible to mix both types of microcapsules into a mortar matrix containing carbon microfibers which were added to mitigate cracking at the micro scale. As both MMA and TEB have a viscosity similar to that of water, they can easily migrate into micro cracks through capillary action after rupture of the capsules. Polymerization of the healing agent is then initiated by contact of both components, bonding the crack faces together.

In order to evaluate the healing efficiency, electrochemical impedance measurements were performed at 28 days, just after being loaded under 80% of the compressive strength and 24 hours and 7 days after being loaded. From these

measurements it was shown that at least part of the artificially induced micro cracks could be healed. In addition, the gas permeability was measured for samples after being loaded till 80% of the ultimate compressive strength and set aside for 24 hours to allow the released healing agent to polymerize. Relative to the control, the highest decrease in permeability coefficient, measured for the samples with encapsulated healing agent was 66.8% (Fig. 4.50A). Also the fatigue behaviour of these samples was tested and it was shown that the samples with encapsulated healing agent showed a significant prolonged second stage and their strain increment curves were less steep (Fig. 4.50B). This clearly demonstrates the beneficial role of the embedment of encapsulated healing agent to inhibit the initiation and propagation of cracks.

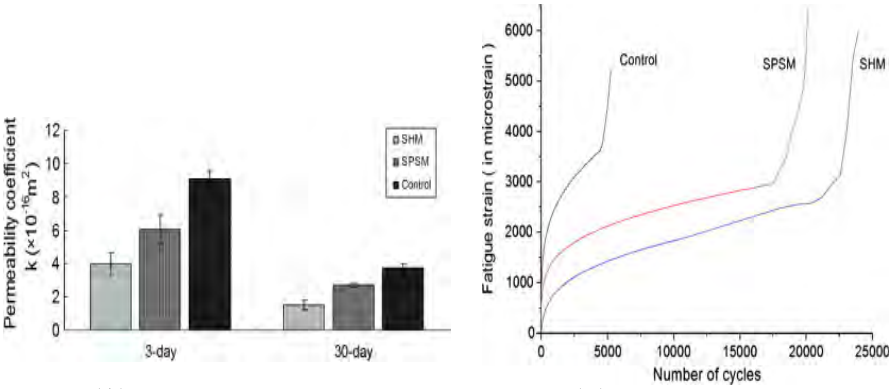

Fig. 4.50 Permeability coefficient of cement mortar composite at 3-day and 30-day curing ages, after being loaded under 80% of ultimate compressive strength and set aside for 24 hours (A) and relationship between the fatigue strain and the number of cycles under uniaxial compression cyclic loading for SHM (with microcapsules filled with MMA and TEB admixed), SPSM (with sulfonated polystyrene particles admixed), and control mortar specimens respectively (B) [4.68]

4.2.2.1.2 External Supply of Healing Agent

Preliminary investigations by Joseph *et al.* [4.39, 4.69] revealed difficulties in achieving the release of a cyanoacrylate healing agent from glass tubes embedded completely within the mortar beams. It was believed that the negative pressure forces created by the wax plugs at the ends of the borosilicate glass capillary tubes were the cause of this. Future experiments revised the encapsulation system to longer capillary tubes which extended outside of the mortar specimens and thereby removed the issue created by the wax plugs [4.39, 4.69].

Joseph *et al.* [4.39, 4.69, 4.70] subsequently undertook a substantial parametric study on adhesive based self-healing of mortar beams. The parameters examined by the authors were the effect of loading rate, reinforcement level and specimen age on self-healing. A summary of the specimen configuration can be seen in Table 4.13.

Table 4.13 Specimen configuration

	Set 1. Notched, lightly reinforced	Set 2. Notched, lightly reinforced	Set 3. Notched, moderately reinforced	Set 4. Notched, heavily reinforced	Set 5. Notched, lightly reinforced, varied loading rate
No. of Beams	2 Ctrl	2 Ctrl	2 Ctrl	2 Ctrl	1 Ctrl
Ctrl=Control	4 SH	4 SH	4 SH	4 SH	3 SH at each loading rate
SH = Self-Healing					
Age at first test	28 days	28 days	28 days	70 days	70 days
Mix ratio by weight	0.55:1:3.5	0.6:1:3.5	0.6:1:3.5	0.6:1:3.5	0.6:1:3.5
(water : OPC : sand)					
Reinforcement	1No. 3.15mm	1No. 3.15mm	2No. 3.15mm	1 No. 6.7mm	1No. 3.15mm
	ϕ high yield steel bar	ϕ high yield steel bar	ϕ high yield steel bar	ϕ high yield steel bar	ϕ high yield steel bar
5mm deep notch	Yes	Yes	Yes	Yes	Yes
Stroke loading rate (mm/s)	0.003	0.003	0.003	0.003	0.00075, 0.003 and 0.012

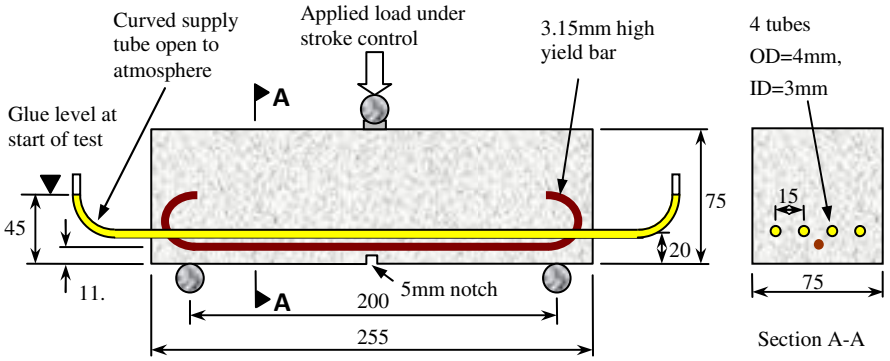

Fig. 4.51 Testing arrangement for self-healing experiments on notched beams [4.71]

The experimental setup in each of the tests comprised 4 hollow capillary tubes of inner diameter 3 mm, open to the atmosphere, filled with a low viscosity cyanoacrylate, encased within mortar beams, as illustrated in Fig. 4.51.

The capillary tubes in the SH beams were filled with cyanoacrylate and the control beams were filled with ink, or left empty, prior to 3-point bend testing. All tests were conducted in two stages, whereby a predefined amount of damage (crack mouth opening displacement (CMOD)) was produced during the first 3-point bend test, followed by unloading and then reloading to failure after a curing period of 24 hours. The experimental set up is shown in Fig. 4.52.

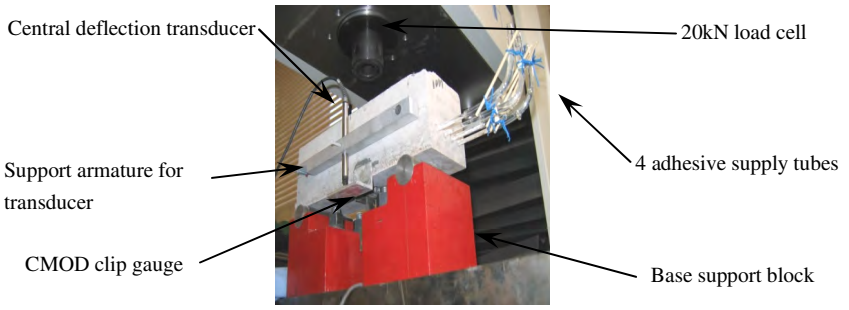

Fig. 4.52 Experimental set up for first and second stage loading [4.71]

Fig. 4.53 shows a typical load-CMOD response for a notched autonomic self-healed beam during the first and second (denoted SH beam (healed)) 3-point bend tests, compared to that of a control beam. The glass capillary tubes, once broken, released cyanoacrylate into the crack plane which flowed rapidly under the influence of attractive capillary forces across the two crack faces. The cyanoacrylate experienced extremely rapid curing due to the moist alkaline environment of the mortar. This resulted in what can be considered as an instantaneous 'primary' autonomic self-healing effect and is characterised by the change in gradient of the autonomic self-healed beam compared to the control beam after the fracture of the glass tubes.

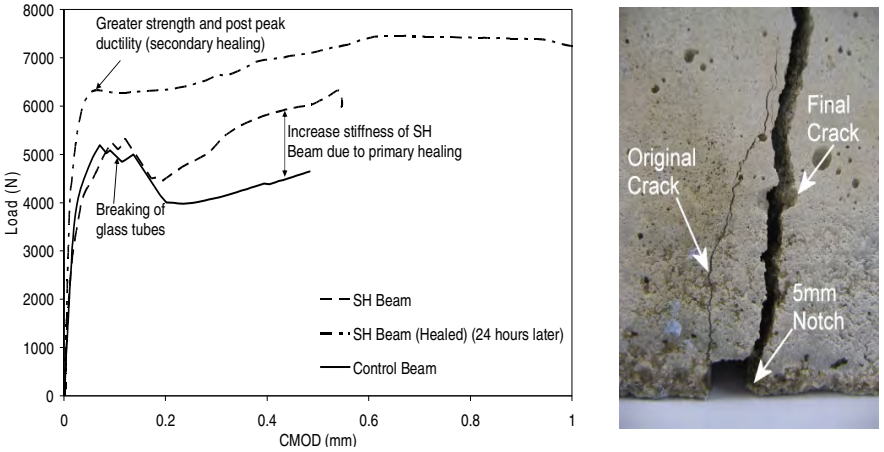

Fig. 4.53 Typical Load-CMOD response for a notched self-healed (with cyanoacrylate) and control beam

Secondary autonomic self-healing was also apparent in all experimental sets, whereby in the second loading stage the specimens exhibited increased stiffness, higher peak load and a more ductile post peak response. The authors concluded that this could be attributed to the ability of the low viscosity cyanoacrylate to permeate into an extended zone around the crack face. This created a modified

"polymer-cementitious composite" zone around the crack face which better resisted the final crack that was forced to propagate through this zone as a result of the loading arrangement.

The authors noted that when the reinforcement level was increased the stiffness of the primary autonomic self-healing response also increased. This was attributed to the slower growth of macro cracks with the higher levels of reinforcement, which resulted in the cyanoacrylate being loaded at a slower rate, thereby allowing more bonds to form to heal the specimen. Moreover similar results were observed when considering the effect of loading rate on the primary autonomic self-healing response, with slower loading rates affording the cyanoacrylate greater time to form bonds, resulting in increased primary autonomic self-healing stiffness [4.39].

With regards to the effect of specimen age on autonomic self-healing Joseph *et al.* [4.39] reported that there was no apparent effect on healing ability with increasing specimen age. Unlike autogenic self-healing, which is highly dependent on specimen age as shown by Schlangen *et al.* [4.29], autonomic self-healing is primarily dependent on the efficacy of the healing agent, in terms of its viscosity and curing abilities within the mortar, and the delivery system and therefore it is not unexpected that specimen age is not an important parameter in autonomic self-healing experiments.

Qualitative evidence was also provided by Joseph *et al.* [4.39, 4.70, 4.71] to support their quantitative results. They noted the distinct sound of the glass tubes breaking in the first loading stage together with evidence of ink staining on the surface and the presence of glue on the underside of the crack. They reported that the cyanoacrylate in the supply tubes was still in liquid form during the second loading stage and thereby could contribute to a tertiary autonomic self-healing response as it is released over the duration of the second loading stage, however, this particular effect was not measured. The authors also reported proof of glue flow into the crack plane demonstrated by staining patterns above and below the glass tubes, as shown in Fig. 4.54. Moreover, Joseph *et al.* [4.39] reported evidence of new crack formation between the first and second loading stages as seen previously in Fig. 4.53. This work is being developed further to enhance the delivery system, making it more robust for its application in reinforced concrete structures.

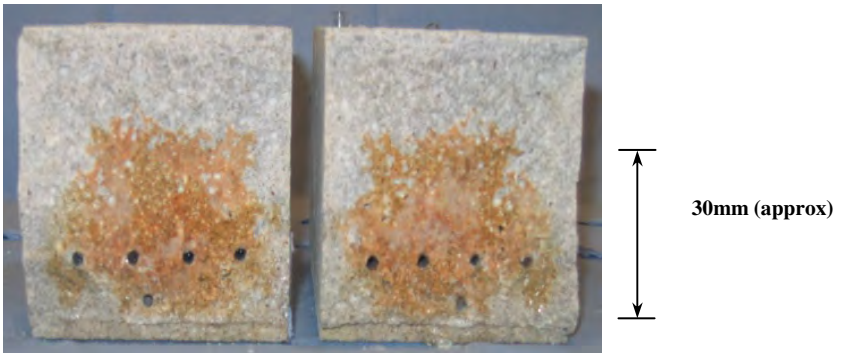

Fig.4.54 Typical glue migration and effective zone of healing for self-healed beams

Mihashi *et al.* [4.72] carried out three-point bending tests onto single notched (20 mm) specimens with dimensions of 40 mm x 40 mm x 130 mm (Fig. 4.55). Into the specimens glass pipes were embedded which were connected with the outer side of the specimen. In addition two more test series were prepared; specimens without glass pipes from which cracks were not repaired and specimens without glass pipes from which cracks were repaired manually. Each test series consisted of three specimens.

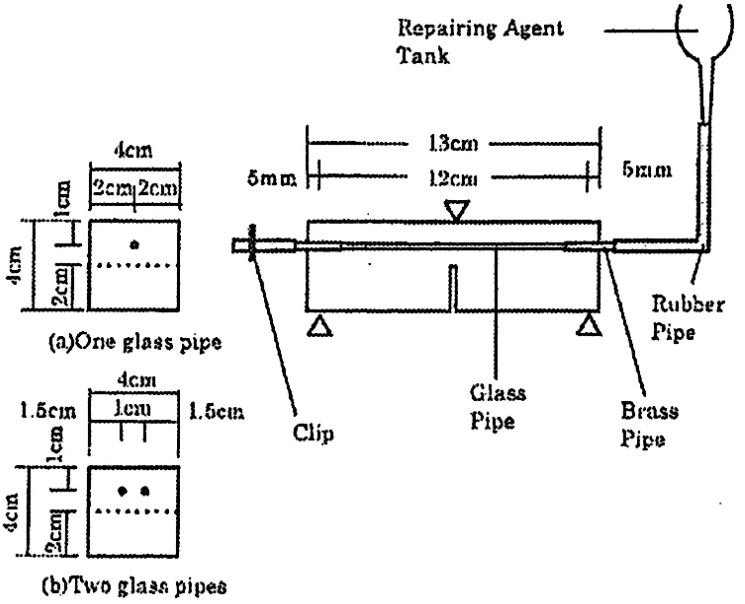

Fig. 4.55 Test setup and specimen [4.72]

Three different healing agents were used; stereochromy with alkali-silica as major element (27% diluted solution, indicated with B in Table 4.14), stereochromy with alkali-silica as major element (main solution, indicated with B' in Table 4.14) and epoxy resin (two fluid blend, indicated with C in Table 4.14). For the test series in which epoxy was used as healing agent, two glass pipes were embedded (Fig. 4.55b), one for the principal agent and one for the hardener; for the other test series, only one glass pipe was used (Fig. 4.55a).

Table 4.14 Overview of the performed experiments [4.72].

Sample	W/B (%)	SF/BI (%)	V_a:V_m	V_f (%)	Repairing agent	Second curing duration (days)	Use of repairing agent
P1	*All:*	*All:*	*All:*	*All:*	-	7	None
P4	40	10	1:1	0.5		28	
B1	(38+2)				Agent B	7	Injection by hand
B4						28	
B'1					Agent B'	7	
B'4						28	
C1					Agent C	7	
C4						28	
g-B1					Agent B	7	Glass pipe
g-B4						28	
g-B'1					Agent B'	7	
g-B'4						28	
g-C1					Agent C	7	
g-C4						28	

Cracks were created in the specimens by means of a three point bending test. The specimens were unloaded when penetration of the repair agent was observed at the surface of the concrete after the maximum load has been reached. These specimens were then cured for 7 or 28 days (see Table 4.14) before they were loaded again in a similar bending test.

Fig. 4.56. shows schematically the relation between the load and the CMOD in the bending test. The specimens were unloaded at the load level P1 after the maximum load, and the maximum load after reloading is defined Pr. Pr/P1 is defined as strength recovery ratio. In Fig. 4.57. the strength recovery ratio is shown for the different crack treatment techniques. From the relation between the residual CMOD and the strength recovery ratio for every 'P' and 'g' test series, it is clearly observed that the repaired specimens in the zone indicated by '*1' in Fig. 4.57 show an extremely high strength recovery ratio for the repairing agent of both B and B'. Thus, the restraint of crack propagation may be effective for repair. On the other hand the repaired specimens with larger residual CMOD than this zone give a relatively constant strength recovery ratio with asymptotic convergence. From these finding the authors concluded that the strength recovery may not be achieved by the repairing agent used in this paper beyond a certain level of crack width.

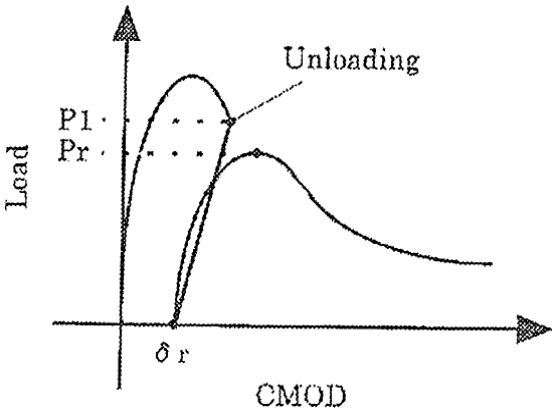

Fig. 4.56 Load versus CMOD relation [4.72]

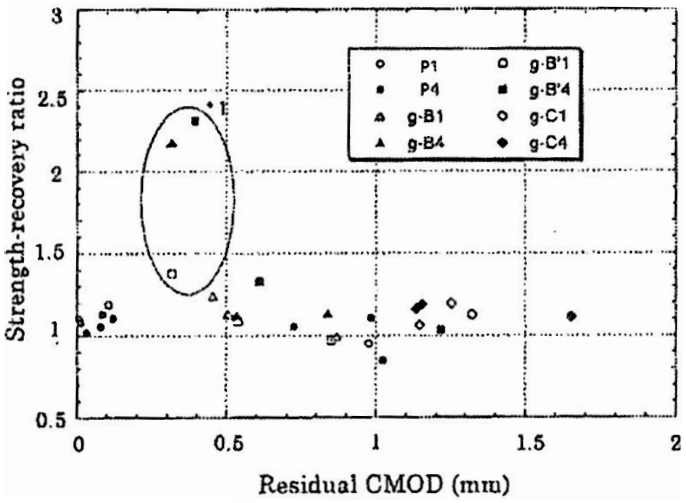

Fig. 4.57 Residual CMOD versus strength recovery ratio [4.72]

The method by which healing agents are embedded in a cementitious material is of utmost importance, as the ability to release the healing agent from the system will govern the degree of autonomic self-healing that is achieved. The volume of required healing agent depends upon the aggressiveness of the environment and the ability of the chemical to move into the matrix. In instances in which a very large volume of chemical is required or where fibers have been depleted of their chemical over many years, vehicles for outside replenishment would be useful.

Dry [4.73] tested the efficiency of filling the glass tubes before or after crack appearance. She concluded that it is better to provide an external reservoir with healing agent which is released after cracks appear. Thus, enough quantity of agent to fill the generated crack can be supplied. Therefore, in her later

experiments glass capillaries were connected with the outside of the concrete structure (Fig. 4.58) [4.73]. A large volume of chemical was delivered by vacuum pressure, drawing it through hollow fibers into the matrix interior. When the vacuum is released, the chemicals flow through the fibers porous walls into the matrix.

Fig. 4.58 Demonstration of the pressure release concept. Adhesive in the fiber and a balloon is under pressure. When the specimen cracks, the pressure differential causes the adhesive to flow rapidly into the crack site.

Carolyn Dry [4.47, 4.48, 4.74-4.76] also made use of frame structures as test specimen (see Fig. 4.59a). These frames represent in a general form, buildings and bridges or components thereof. Glass pipettes were situated throughout the beam and into the moment connections at the columns (Fig. 4.59b). Glass pipettes can be seen extending from the frame for filling (Fig. 4.59a).

In these experiments, the authors tried to control the locations of structural damage by the strategic release of appropriate internal repair adhesives. High modulus, stiff adhesives released at the structural joints allow damaged joints to regain stiffness, thus preventing future damage at joints and insuring the translation of forces elsewhere. Low modulus adhesives released within the structural members close or seal cracks, but do not increase member stiffness. Thus, these sealed cracks are allowed some movement before additional cracking occurs. The combination of these adhesives into a single system allows forces in members to be safely transferred through connections to the more flexible members where failure should occur at ultimate loading. Furthermore dynamic

load energy is dissipated within these structural members while maintaining the critical structural integrity of the connections. Such systems, intelligently react in the event of excessive damaging forces – by driving forces through the structure to adequate members during the process of structural self-repair.

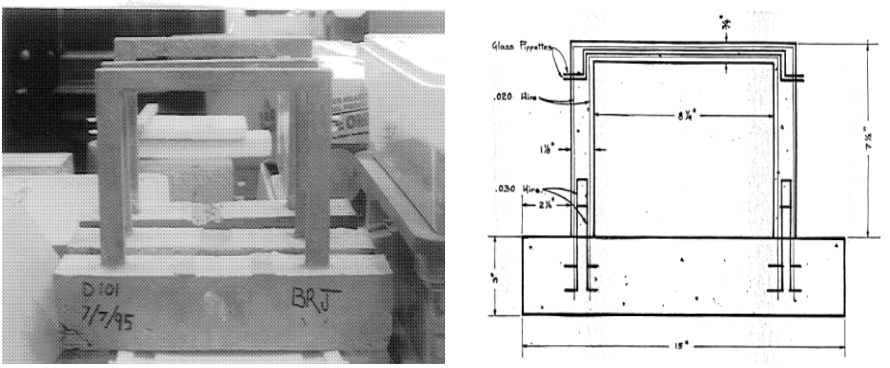

(a) (b)

Fig. 4.59 (a) Photo of test frame, glass pipettes can be seen extending to the exterior for filling with adhesive; (b) Drawing of a concrete test frame [4.48].

During this experiment, three different adhesives were tested, each of them separately, within a generic concrete structural model. One stiff adhesive, cyanoacrylate, and two non-stiff adhesives, epoxy and silicon, were encapsulated. The crack healing efficiency was compared to control specimens which contained empty glass tubes.

The samples were poured, allowed to cure for 24 hours inside the forms, then removed and placed inside a water bath and allowed to continue curing for an additional 28 days. When the samples were removed from the bath, water was forced out of the pipettes with compressed air. The samples were then allowed to dry for 2 weeks before any tests were run.

The tests were performed through the use of a universal testing machine subjecting the frames to a constant in plane compressive force applied at the beam column joint and in a direction parallel to the base. During the first of two tests, each sample was loaded to a deflection of 5 mm in order to induce minor cracking in the frame. The corresponding resistant force in the frame was recorded and cracks were clearly marked. Load was applied in the same manner during the second test, two weeks later, this time until the sample reached failure. Load and deflection were recorded and the number of cracks located within the area of the adhesive's coverage were observed and identified as either "re-opened" or "new" (see Table 4.15).

Table 4.15 Re-opened versus new cracks

Sample	Avg. Old	Avg. Reopen	Avg. New	Ratio (new/reopen)
Control	3.33	3.67	2.0	0.55
Cyanoacrylate –	2	1.67	3.0	1.80
stiff adhesive	3	0.67	1.67	2.50
	3	1.67	1.33	0.80
	4	1.67	1.33	0.80
	2	1.67	1.33	0.80
Epoxy –	2	2.33	0.33	0.14
Non-stiff adhesive	4	2.33	0.33	0.14
	4	2.33	0.33	0.14
	4	3.0	0.67	0.22
	4	3.0	0.67	0.22
	3	3.0	0.67	0.22
Silicon –	3	3.0	0.67	0.22
Non-stiff adhesive	3	3.0	0.67	0.22
	4	3.0	0.67	0.22

The cyanoacrylate, stiff adhesive, samples had the highest ratio of new cracks to re-opened cracks. This indicated that old cracks sealed by the cyanoacrylate in the first test provided increased strength in the second test, causing redistribution of stress to the uncracked section, where new cracks were formed. All of the other samples had an average new/reopened crack ratio of less than 1.0, indicating that the cracks sealed by the epoxy and silicon, non-stiff adhesives, experienced reopening without transferring stress to the uncracked region.

Instead of providing the healing agent by long glass tubes, which are very prone to cracking during casting of the beam, Pareek and Oohira [4.77] provided holes inside the concrete (Fig. 4.60). These were filled with epoxy, before or after crack formation, by means of a syringe which was connected to the open end.

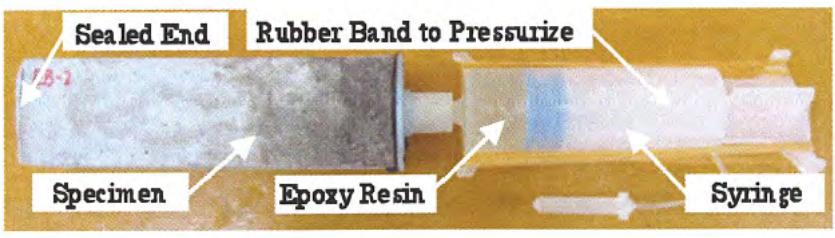

Fig. 4.60 View of crack injection system [4.77]

As the hollow core will result in strength reduction, Sangadji and Schlangen [4.78, 4.79] proposed to use a hollow network which consisted of porous concrete. Their approach was inspired by the structure of human bones, consisting of an outer compact part and an inner spongy part. Sangadji and Schlangen casted porous concrete cylinders surrounded by a PVA film inside concrete beams. When the dense concrete matrix is casted around the porous part, the PVA film will dissolve and thus exchange becomes possible between the inner and the outer layer. They plan damage to be detected by sensors, which switch on a pump that injects the epoxy healing agent available in a reservoir through the porous network concrete layer to make it dense and seal the cracks (Fig. 4.61).

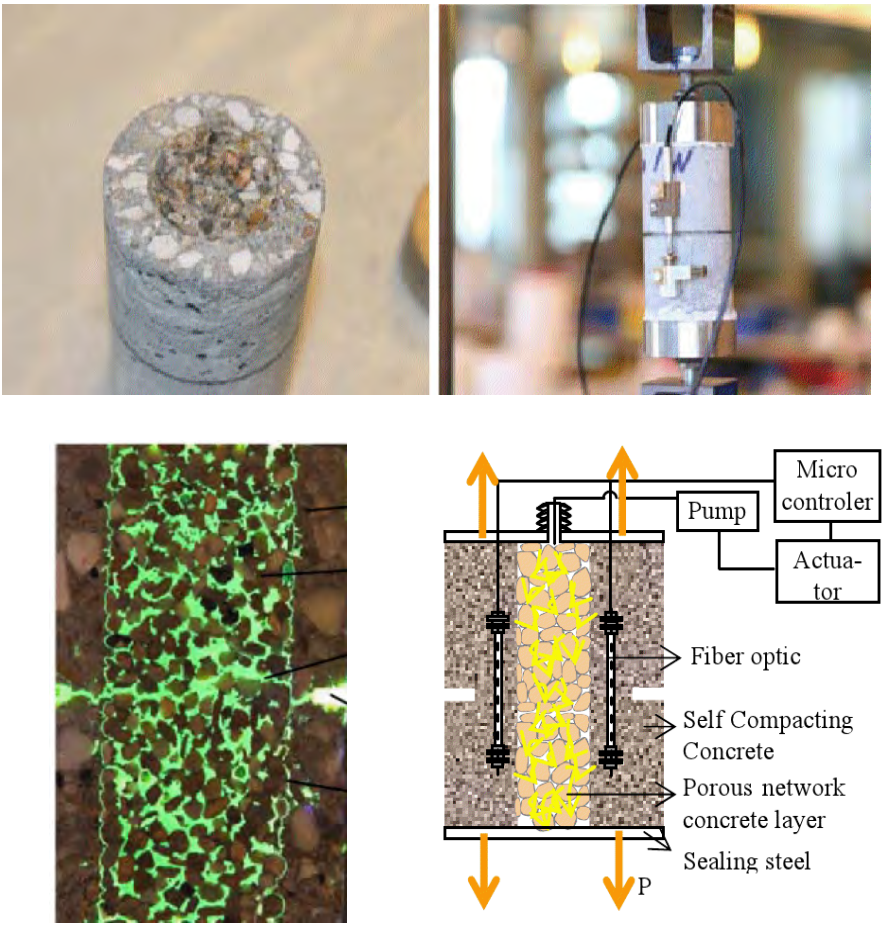

Fig. 4.61 Porous concrete as reservoir for healing agent

4.2.2.2 Physical Activation

4.2.2.2.1 Internal Supply of Healing Agent

The healing mechanisms described in the previous section were activated through mechanical impact. Crack appearance caused breakage of the brittle encapsulation materials. However, the trigger mechanism may also be a physical action such as release of heat. This way of activation has been used by several researchers in order to release the healing agent.

In one of her studies, Carolyn Dry [4.46, 4.58] used hollow, porous-walled, polypropylene fibers, filled with liquid methyl methacrylate and coated with wax. These fibers were positioned inside concrete beams, as shown in Fig. 4.62 a. At the moment cracks are noticed, the concrete matrix needs to be heated. Due to this heating, the wax coating on the porous fibers will melt and the methyl methacrylate will move out into the cracked matrix (Fig. 4.62 b). Afterwards the heat is raised and the methylmethacrylate will polymerize inside the crack (Fig. 4.62 c).

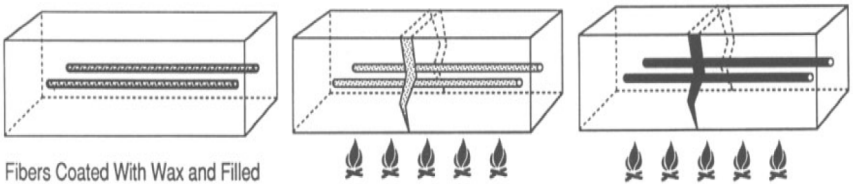

a) Fibers coated with wax and filled with methylmethacrylate

b) Wax coating melted with initial heating, methylmethacrylate released from fibers into cracks

c) Methylmethacrylate polymerized during second heating, closing previous cracks

Fig. 4.62 Schematic diagram of the active repair system proposed by Dry [4.46]

As shown in Fig. 4.63, research results showed that after the methyl methacrylate polymerizes in the pores and cracks of the concrete, permeability is reduced. Permeability tests were done in accordance with the method described in [4.80].

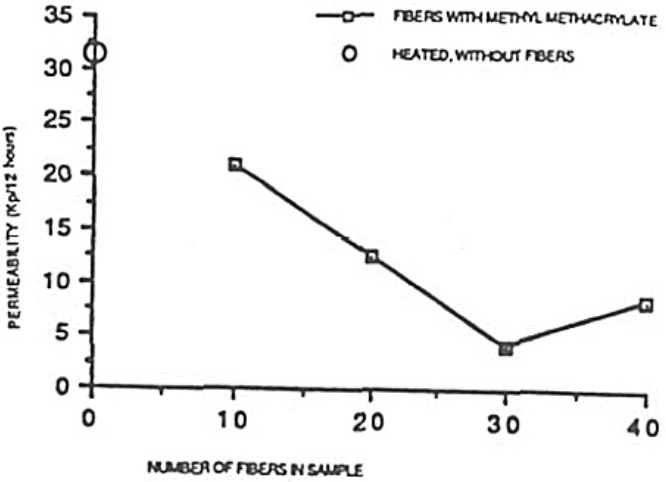

Fig. 4.63 Permeability of Portland cement containing methyl methacrylate and wax released from polypropylene fibers (samples cured for 7 days, heated to 212 °F for 30 min [4.46]

A comparison of internal release versus exterior application with gravity feed was made (Fig. 4.64). The results showed samples with internally released chemicals had better compressive strength and less permeability than those using conventional surface application of methyl methacrylate and heating. Research has shown that this interior chemical delivery system works in the sense of delivering chemicals inside the matrix.

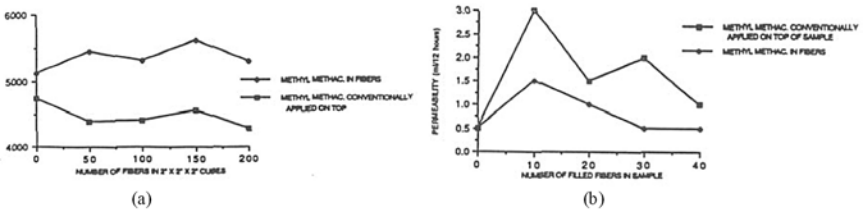

Fig. 4.64 Effect of internal release of methyl methacrylate and wax from porous polypropylene fibers and internal polymerization against conventional application from the exterior top surface on compressive strength (a) and permeability (b) (samples heated to 212°F for 30 min.) [4.46]

4.2.2.2.2 External Supply of Healing Agent

Nishiwaki *et al.* [4.81-4.83] suggested a smart autonomic self-healing system for concrete which is composed of a self-diagnosis composite and a heat-plasticity

organic film pipe. The self-diagnosis composite is functionalized as heating device that can selectively heat around a generated crack by electrification. The heat-plasticity organic film pipe containing repair agent is embedded in concrete beside the heating device and is melted only in the heated zone. Next, repair agent is released from the melted surface of the pipe and fills the crack.

A concept of the proposed smart autonomic self-healing system is schematically shown in Fig. 4.65. A strain monitoring sensor fabricated using a specific fiber type and conductive matrix functions as the heating device. This sensor is not only a strain gauge but also both structural material and functional material for measuring the damaged area, recording damage history and so on. In this study, a smart autonomic self-healing composite fabricated using fiber-reinforced composites and conductive particles was employed as a heating device. Fig. 4.66 shows a schematic diagram of the structure of this sensor.

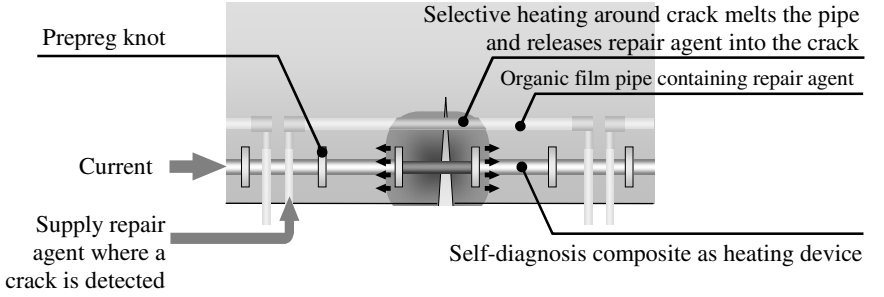

Fig. 4.65 Schematic diagram of proposed self-healing concrete system [4.82]

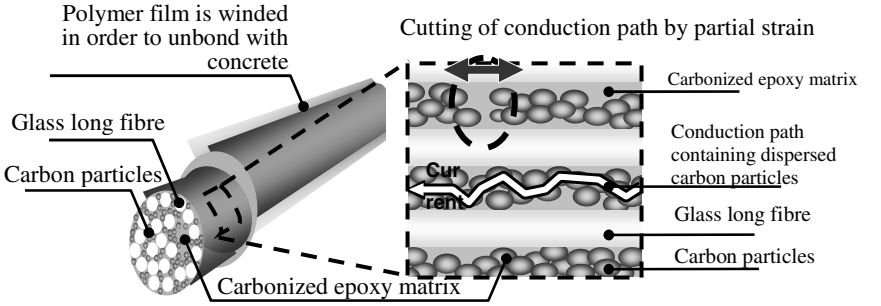

Fig. 4.66 Schematic diagram of dispersed conductive particles in strain monitoring sensor [4.82]

The proposed self-healing system is implemented with a suitable arrangement of heating devices and thermal-plastic pipes containing repair agent in concrete. To decide on a proper arrangement, a three-dimensional thermal analysis was

carried out to simulate the temperature distribution in concrete with embedded heating devices. After this analysis, experimental studies were carried out to prove the effectiveness of the proposed self-healing system. Fig. 4.67 shows the geometry of the employed specimen.

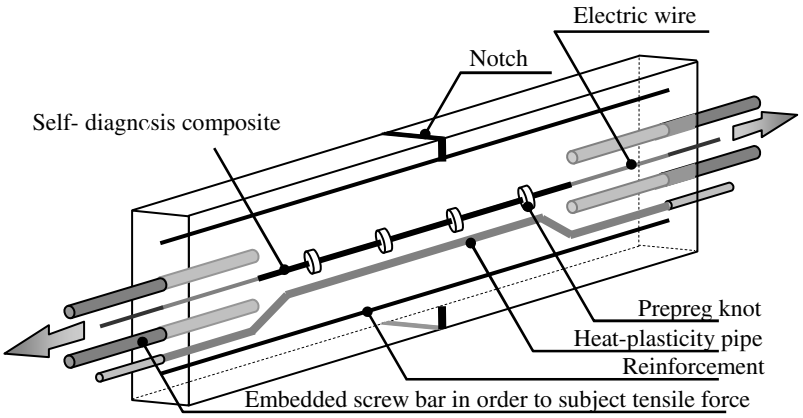

Fig. 4.67 Geometry of employed specimen [4.82]

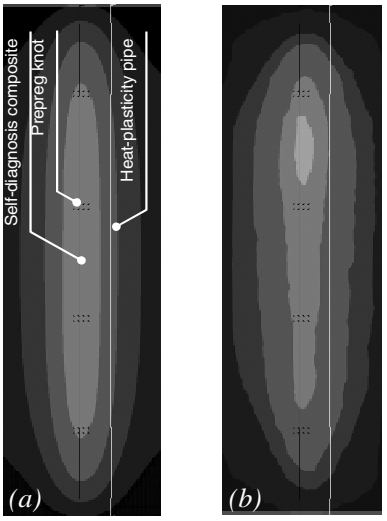

Fig. 4.68 Temperature distribution before cracking: (a) analyzed, (b) experiment [4.82].

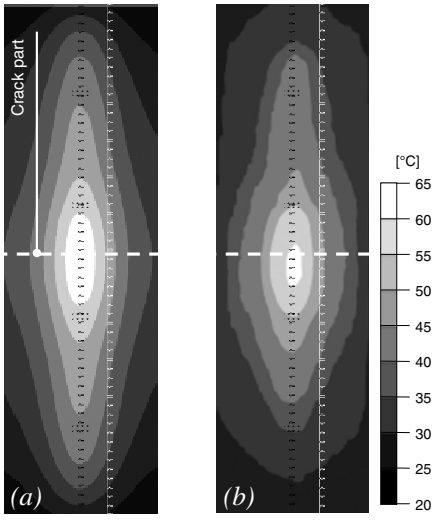

Fig. 4.69 Temperature distribution before cracking: (a) analyzed, (b) experiment [4.82].

Fig. 4.68 (a) shows the temperature distribution at the surface of the model without any cracking as obtained through thermal analysis after 30 min from the start. Fig. 4.68 (b) is an experimental result corresponding to Fig. 4.68 (a).

Fig. 4.69 (a) shows the result of the analysis on the specimen with cracking that leads to a partial increase in electric resistance. Fig. 4.69 (b) is an experimental result corresponding to Fig. 4.69 (a). These figures clearly show that the high temperature part is concentrated between two prepreg knots including the generated crack part where the electrical resistance partially increases. Thus, the selective heating around generated crack is expected to be able to melt the embedded pipe selectively and to perform the proposed self-healing system effectively.

To confirm the effect of self-closing a permeability test was carried out [4.33]. Fig. 4.70 shows the relationship between the generated crack width and the quantity of water leakage through the crack. This graph shows that cracks in the specimen repaired with the self-healing system let in a much smaller amount of water than cracks in specimens without repair.

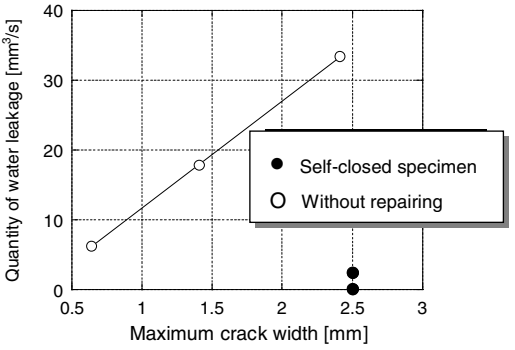

Fig. 4.70 Relationship between generated maximum crack width versus quantity of water leakage [81].

In their latest work, Nishiwaki *et al.* [4.84] embedded their self-repairing device (SRD), composed of a self-diagnosis composite (SDC), a heat-sensitive pipe (HSP) and a copper plate which connects both of them, inside a layer of fiber reinforced concrete which was provided at the bottom of a beam (Fig. 4.71).

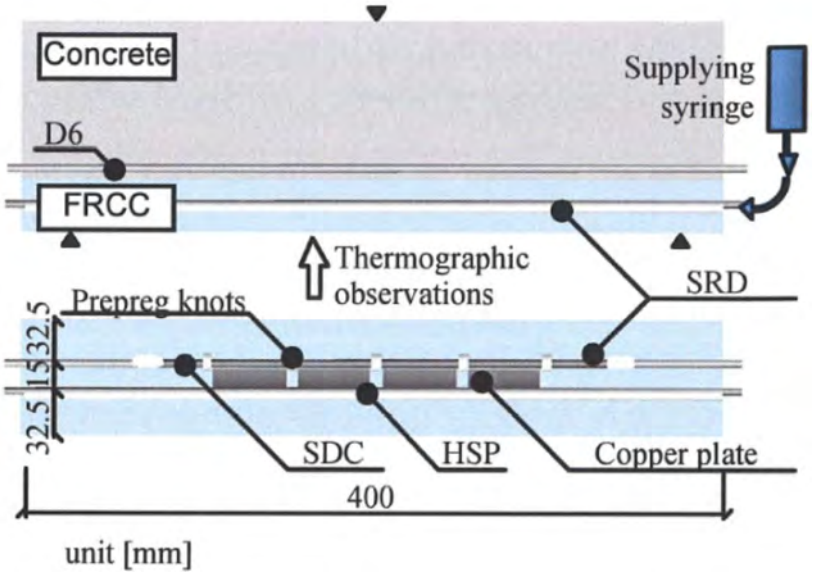

Fig. 4.71 Geometry of the specimen [4.84]

4.2.2.3 Recovery of Water Tightness and Mechanical Properties

When tubular vials with healing agents are applied to normal concrete, the amount of chemical available for crack closure and autonomic self-healing is rapidly exhausted, especially in case of wide cracks. Li *et al.* [4.7] therefore suggested an autonomic self-healing concept called: Passive Smart Self-healing Engineered Cementitious Composite (PSS-ECC) which has regaining water tightness and mechanical properties. ECC is used because it can control the width of the tensile crack to be narrow. So called SAC fibres (Self-healing Agent Carrying fibres) are embedded in ECC matrix.

Self-healing mechanism of PSS–ECC is demonstrated by regain in material stiffness after damage is imposed by a mechanical load in a 3-point bending test. Fig. 4.72 shows the arrangement of the embedded pipes in the cross section of two series (M1 and M2).

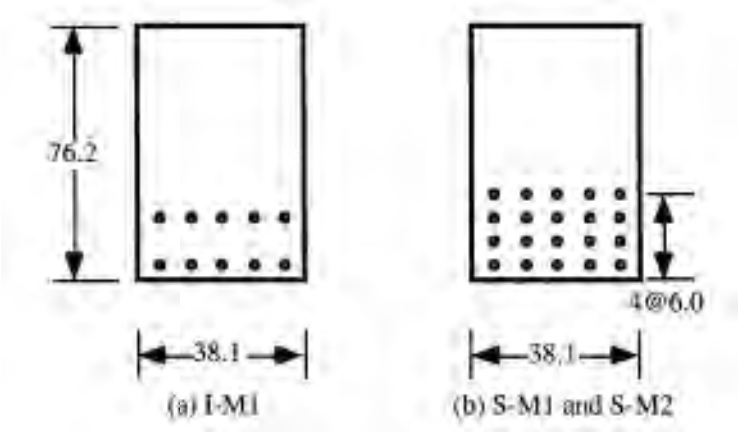

Fig. 4.72 Cross-section of flexural specimen, showing position of glass fibers (units: mm)

The stiffness changes are reported in Fig. 4.73 a and b for materials M1 and M2, respectively. Each stiffness is normalized by the initial stiffness (uncracked) of each specimen. Solid symbols represent PSS–ECC systems. Six out of nine specimens showed higher regained stiffness on first reloading than the initial stiffness, and two specimens were close to the initial stiffness. As a result, eight out of nine PSS–ECC specimens indicated recovery of stiffness. In contrast, specimens having no SAC fibers all suffered stiffness degradation from 10% to 40%. The self-healing effect is validated by regaining of flexural stiffness in beams reloaded after an initial cycle of loading to beyond first cracking followed by unloading.

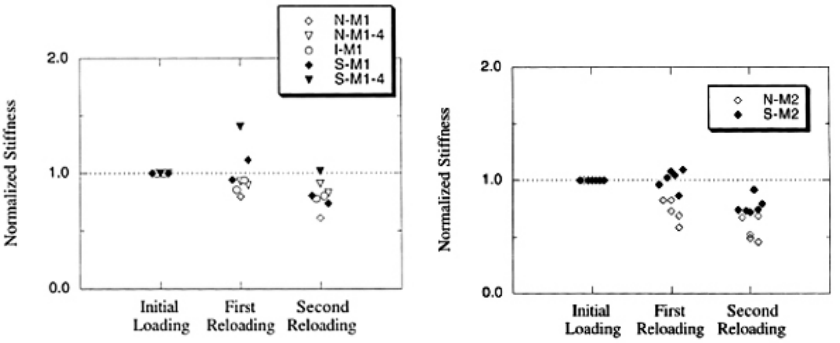

(a) Material M1 (b) Material M2

Fig. 4.73 Normalized stiffness in flexural beam

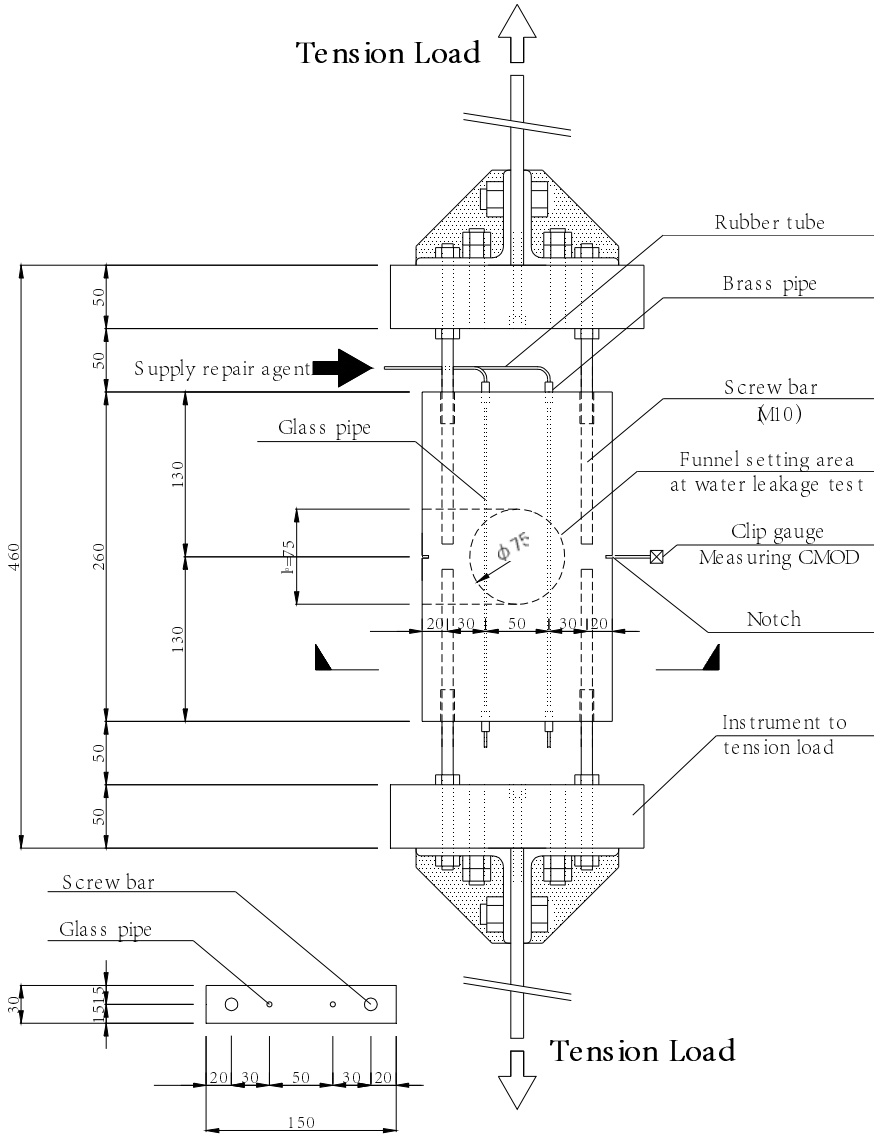

Fig. 4.74 Specimen and test method [4.85]

Nishiwaki *et al.* [4.85] suggested an autonomic self-closing system with glass pipes embedded in HPFRCC (High-Performance Fibre Reinforced Cement Composites) which shows multiple cracking and strain hardening in tension as well as in bending, see Fig. 4.74. A fluid repair agent, which when in contact with concrete material chemically reacts forming solid crystals, is injected to the embedded glass pipes. The testing procedure was carried out in two separate steps.

In the first step the test specimen was subjected to uniaxial tensile load until desired damage (cracking) level. Thereafter, the specimens were unloaded and a permeability test was carried out using the cracked specimen.

Fig. 4.75 shows the relation between maximum crack width and the calculated coefficient of water permeability. The results show that the self-closing system was effective in HPFRCC specimens with maximum crack width above 0.2 mm, but not often effective when the maximum crack width was below this value. However, in mortar specimens the self-closing system was ineffective. For mortar specimens whose maximum crack width was from 2.5 to 4.5 mm, the permeability test could not be performed, since discharge was instantly.

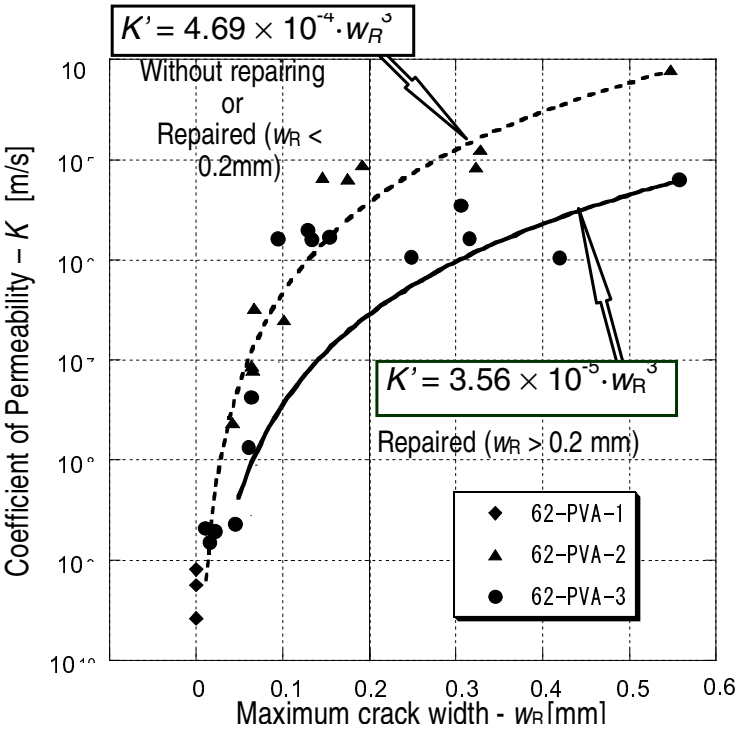

Fig. 4.75 Relationship water permeability coefficient (K) and maximum crack width (w_R) [4.85]

4.2.3 Particles Mixed into the Mortar

4.2.3.1 Self-encapsulation

The Japanese research group of Ohama and Demura proposed the use of polymer modified mortars containing epoxy resins without hardeners to repair cracks

autonomously [4.86]. When epoxy resins are added to the concrete matrix without addition of hardeners, the outer layer of epoxy will harden due to the presence of alkalis or hydroxide ions in the matrix [4.87]. Due to this, the outer epoxy layer will be solid while the inner layer is still liquid. This means that the epoxy resin phases exist as self-capsuled epoxy resins. By preloading, the mortar matrix is cracked, and the self-caspuled epoxy resins are partially broken. The unhardened epoxy resin flows out of the capsules into the micro-cracks, and the unhardened epoxy resins filling the micro cracks may be hardened by alkalis of hydroxide ions in the mortars. Due to this, autonomic self-repair of cracks is obtained (see Fig. 4.76).

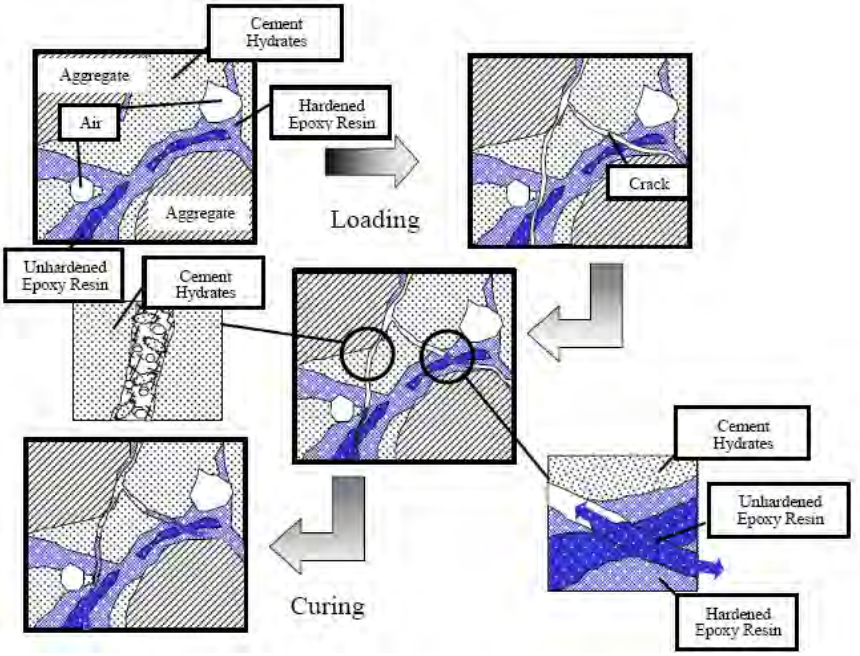

Fig. 4.76 Simplified model for self-repair mechanism for microcracks by self-capsuled epoxy resin in epoxy modified mortar.

In their experiments, the authors [4.86] used diglycidyl ethers of bisphenols A and F as epoxy resins. The epoxy modified mortars were mixed with a mass ratio of cement to fine aggregate of 1:3. The polymer-cement ratios amounted 0%, 5%, 10%, 15% and 20% and the flow was adjusted to be constant at 170±5 in the water cement ratio range of 73 to 78%. Prismatic specimens of 40 mm x 40 mm x 160 mm were molded and subjected to combined wet/dry curing. Then, half of the specimens were cut down to make cubic specimens of 40 x 40 x 40 mm. Afterwards, compressive loads of 0% and 85% of the maximum compressive load were applied to the longitudinal direction of the specimens for preloading (Fig. 4.77). After

loading, the specimens were dry-cured again at 20°C and 50% relative humidity. After 28 days the prismatic and cubic specimens were tested for flexural and compressive strength and compressive strength, respectively.

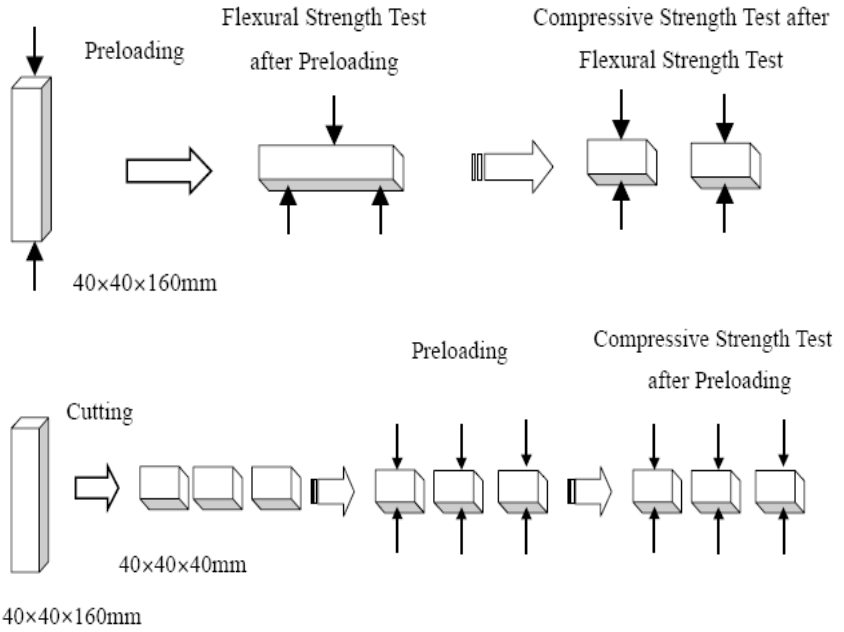

Fig. 4.77 Methods for preloading and strength test for prismatic and cubic specimens

It was found that the 56 days flexural and compressive strengths of the preloaded epoxy-modified mortars were almost the same as those of the unpreloaded epoxy-modified mortars and were higher than the 28 days flexural and compressive strengths of the unpreloaded epoxy-modified mortars. Similar results were found for the cubic specimens. From these findings the authors concluded that strength developed after pre-loading. According to the authors this strength development was caused by the combined effect of acceleration of cement hydration and self-repair of microcracks with epoxy resins.

4.2.3.2 Expansive Chemical Agents

Ahn *et al.* [4.88-4.90] propose to obtain self-healing properties in concrete by using a combination of expansive agent, geo-materials and chemical agent. Self-healing concrete cylinders (10 cm x 20 cm) were prepared by mixing in the three mentioned compounds. Specimens were cured for 1 month and then artificially cracked. Crack width was controlled between 0.1 mm and 0.3 mm according to the maximum allowable crack widths dictated by the construction codes. Subsequently the specimens were water cured for 1 month.

In Fig. 4.78 the healing process of one of the cracked specimens is shown. In this case, the crack with an initial width of 0.2 mm was almost completely healed after 28 days. Rehydration products were clearly observed after 14 days, and the crack self-healed perfectly even though there were small cracks between the rehydration products after 200 days as shown in Fig. 4.78f.

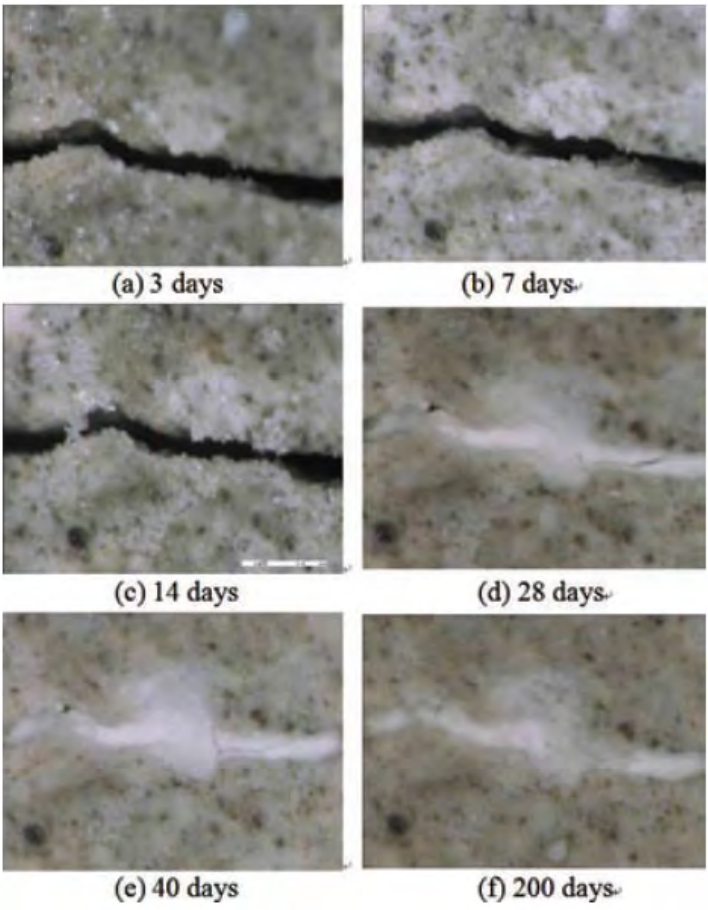

Fig. 4.78 Process of self-healing on [OPC90%+CSA5%+Geo-materials5%] pastes at normal water/binder ratio of 0.45 [4.88]

Fig. 4.79a shows the entire self-healed shape of one of the cracked specimens by top, side, bottom and cross-section. It was noticed that there was a difference between the phases of the original matrix and the self-healing zone. Therefore, microscopy and SEM analysis with EDS detector were carried out to investigate the morphology, shape and size of rehydration products and to clarify re-hydration.

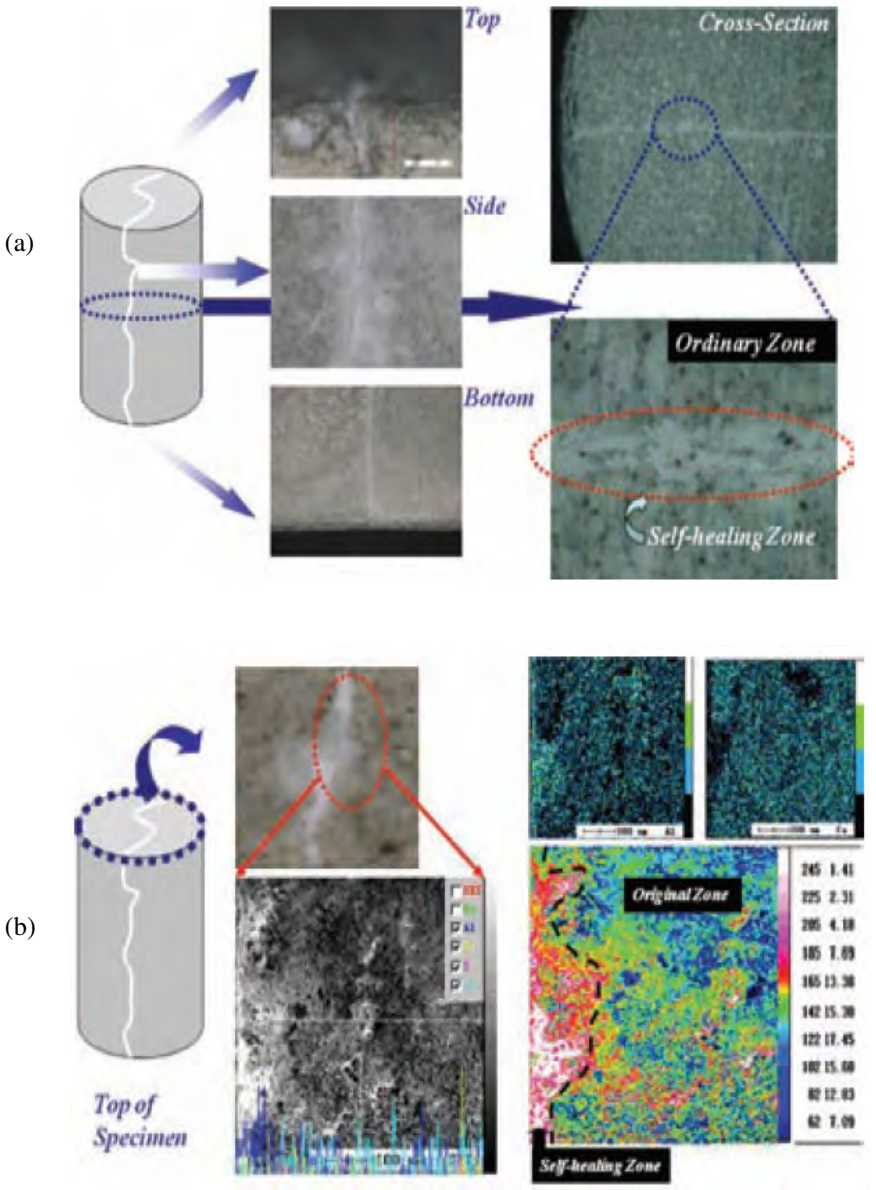

Fig. 4.79 (a) Self-healed shape of cracked pastes according to regions such as top, side, bottom and cross-section; (b) Self-healing phenomenon of crack by crystallization of aluminosilicate phases on the cementitious pastes incorporating CSA and geo-materials (surface analysis of specimen) [4.88].

Fig. 4.79a shows the rehydration products on the surface of the specimen between the original and self-healing zone. Fig. 4.79b shows the X-ray map and spectra taken from rehydration products. It was found that re-hydration products were mainly composed of high alumina silicate materials as shown in the X-ray mapping results. This self-healing phenomenon seems to be related to the crystallization of aluminosilicate with calcium ion.

When tests were done onto concrete with the same mix composition, self-healing was noticed after 33 days of curing in water. This healing mechanism was also caused by the swelling effect, expansion effect and re-crystallization of the cementitious matrix. However, it was also noticed that cracks along aggregates were not completely sealed. Some recrystallization products were deposited from the cementitious paste onto the aggregate surface as shown in Fig. 4.80. The authors concluded that self-healing of these cracks would take more time.

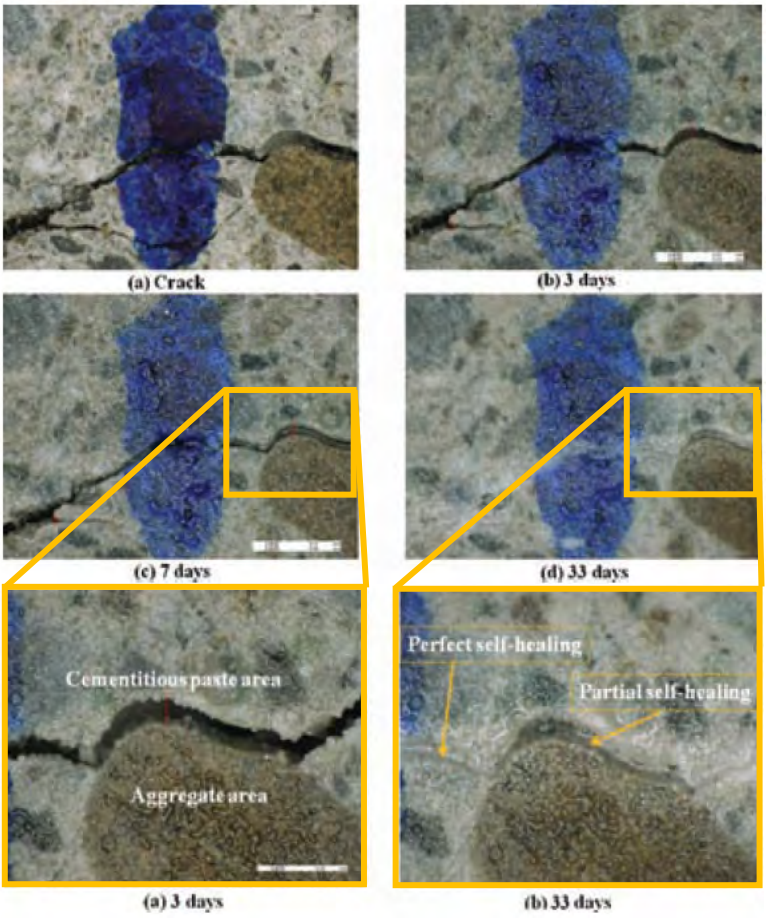

Fig. 4.80 Process of self-healing on self-healing concrete at water to binder ratio of 0.47 [4.88]

Sisomphon and Copuroglu [4.91] mixed in calcium sulfo aluminate (CSA) based agents and crystalline admixtures (CA) in order to obtain autonomous crack healing. It was meant that, upon the ingress of water into a crack, ettringite crystals would form, which would fill the crack. Investigation of the crack width reduction with respect to the wetting period of the samples led to the conclusion that mortar containing CSA and CA showed superior self-healing ability. It was noticed that small cracks (< 200 µ) could heal completely even without the addition of CSA or CA, however, it takes some more time (Fig. 4.81A). For larger cracks (> 300 µm), the addition of CSA or CA and certainly the addition of both components significantly improves the reduction in crack width (Fig. 4.81B).

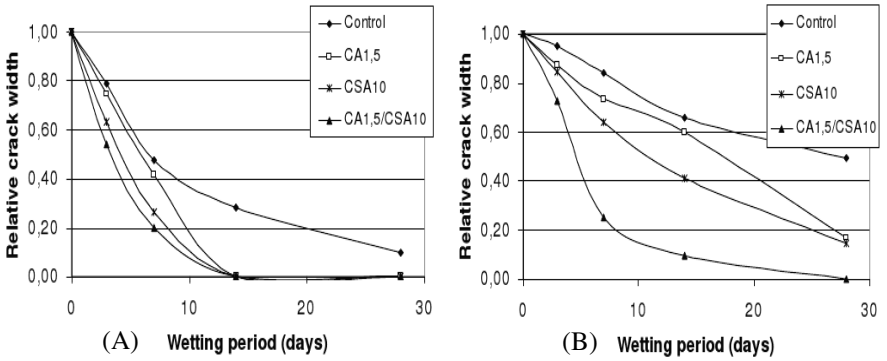

Fig. 4.81 Crack width reduction in function of the wetting period for samples with small cracks (< 200 µm) (A) and larger cracks (> 300 µm) (B) [4.91]

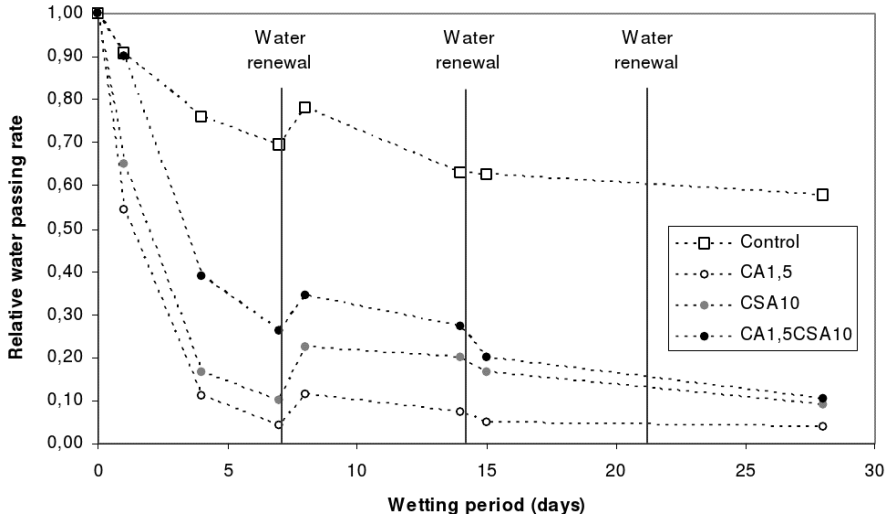

Fig. 4.82 Relative water passing rate of pre-cracked mortars [4.91]

Observation of the amount of water passing through a cracked sample led to similar conclusions (Fig. 4.82). While for the control mortar a slight reduction in water passing rate was observed in the early period, mortars with CA or CSA showed rapid reduction of water passing ability at the first 5 days. Currently, Sisomphon *et al.* [4.92] incorporate CSA's with different chemical compositions in an effort to further enhance the self-healing potential.

In another study, Copuroglu *et al.* [4.93] mentioned that using ettringite formation as mechanism to cause autogenous crack healing might pose certain risk regarding uncontrolled expansion and cracking. Therefore, they proposed to encapsulate the ettringite producing agents to find out whether or not it could provide technical advantages. In Fig. 4.83. the encapsulation process is schematically depicted.

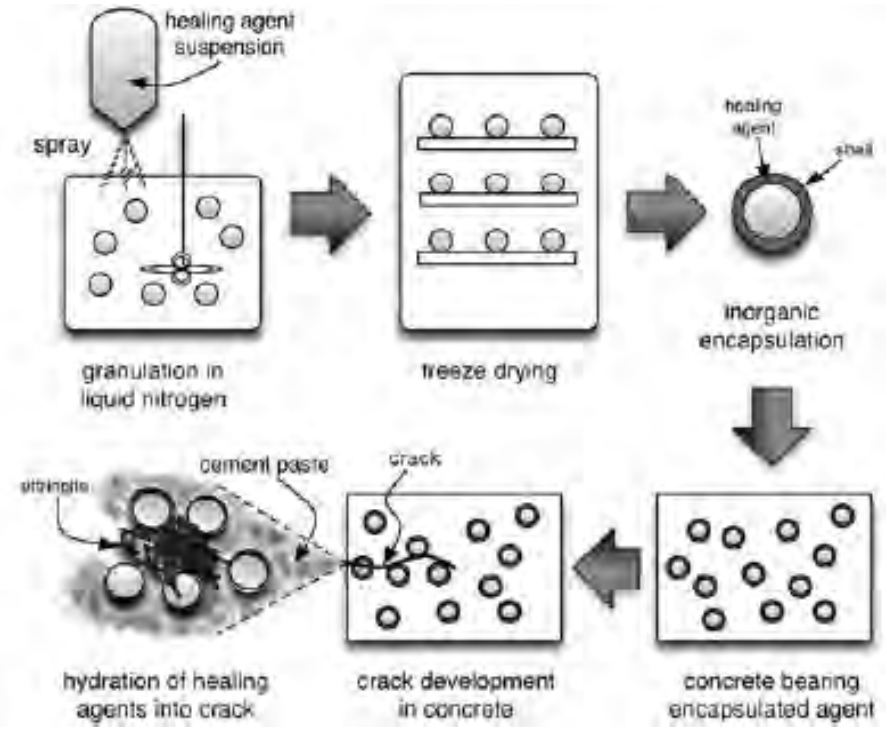

Fig. 4.83 Concept for stages of calcium aluminate based agent encapsulation and its use in concrete [4.93]

Yuan *et al.* [4.94-4.96] proposed the use of ethylene vinyl acetate (EVA) heat-melt adhesive (Fig. 4.84) to heal cracks in concrete. Optical fibers and shape memory alloys (SMA) will be embedded in the concrete matrix together with the solid EVA particles. Once a crack is generated and detected by the optical fibers, the SMA particles will be heated by means of electrifying. When the temperature is raising higher than the martensite start temperature (M_S) [4.33], SMA starts to

impose compressive force onto the concrete matrix and forces the crack to close. In addition, with the increase of temperature, EVA particles will soften and melt, and then penetrate into the cracks through gravity and capillary action.

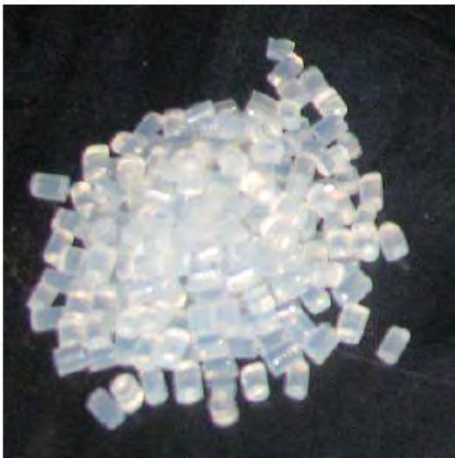

Fig. 4.84 Ethylene vinyl acetate (EVA) particles [4.96]

Up to now the researchers tested the effect of adding EVA particles onto the properties of mortar and they determined the potential of EVA to be used as healing agent. In their experiments [4.94, 4.95] 1%, 3% and 5% of EVA particles with a particle size of ø=3 mm x 2.5 mm were added to the mortar mixture. Specimens were pre-cracked by loading them in three-point bending until 30%, 50% or 70% of their peak load. Afterwards the pre-damaged mortars were placed into a furnace for 2 days at 150°C. In order to evaluate the self-healing efficiency, the strength of EVA specimens before and after repair was compared. The damage repair rate was defined according to Eq. (4.6).

$$R = \frac{P_{strengthafterrepair}}{P_{strengthbeforepre-damage}} \text{ x100\%} \tag{4.6}$$

The strength of the pre-damaged mortar beams before and after repair is shown in Fig. 4.85a. The amount of strength regain in shown in Fig. 4.85b.

The authors concluded from Fig. 4.85 that all pre-damaged specimens were successfully repaired by using EVA particles as the flexural performance exceeded that of control intact specimens. They also concluded that the repair rate in the same pre-damage level increases with the increase in EVA content. It was noticed that due to heating of the samples containing EVA particles, the gaps between EVA particles and concrete matrix are filled improving the properties of the matrix (Fig. 4.86). Besides it was observed visually that the melted particles covered the damaged surface after heating, satisfying the need for repairing.

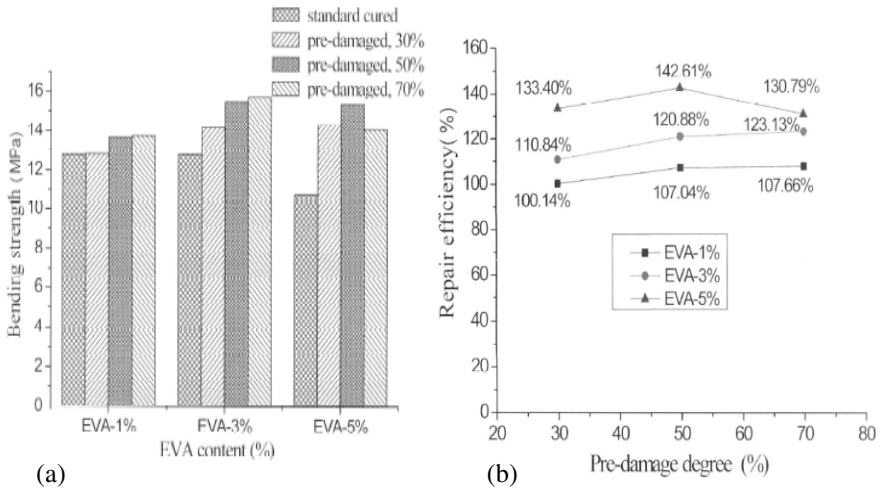

Fig. 4.85 (a) Strength of pre-damaged samples after repair; (b) Repair efficiency of pre-damage in various degrees [4.94]

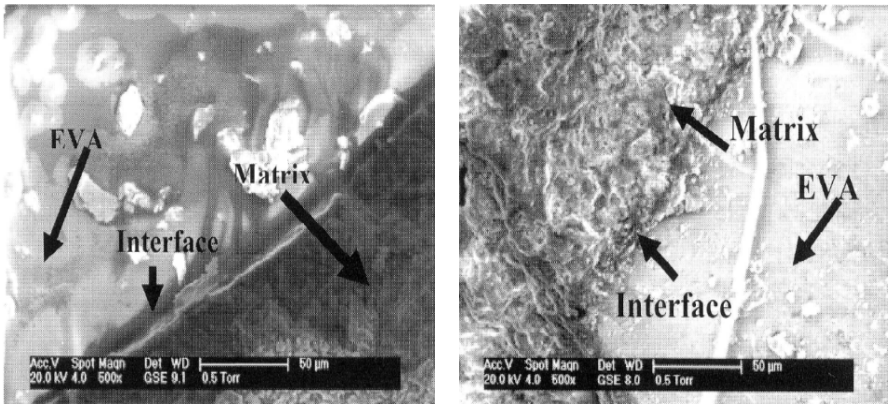

Fig. 4.86 SEM photograph of interface between EVA and matrix of specimen before (A) and after (B) being heated for 2 days [4.94]

4.2.3.3 Super Absorbent Polymers (SAP)

Kim and Schlangen [4.97, 4.98] proposed to combine engineered cementitious composites (ECC) with super absorbent polymers (SAP), which are polymeric materials which can absorb and retain extremely large amounts of liquids relative to their own mass (see Fig. 4.87). As already mentioned before, ECC cracks in narrow hairlines and therefore makes self-healing possible. However, self-healing

of cracks in ECC is only possible when the cracked specimens are stored under water. As this is not realistic for practical application, Kim and Schlangen [4.97, 4.98] proposed to mix in SAP. The water which is stored in SAP will be released during or shortly after the first hydration. When the material cracks at a later stage, no water will be left anymore. But after some rain on the structure, the SAP's located in the cracked zone are again filled and then slowly release the water for the self-healing mechanism. While Dennis Lee *et al.* [4.99, 4.100] used SAP in order to seal cracks in concrete, this research goes one step further and tries to obtain regain in mechanical properties.

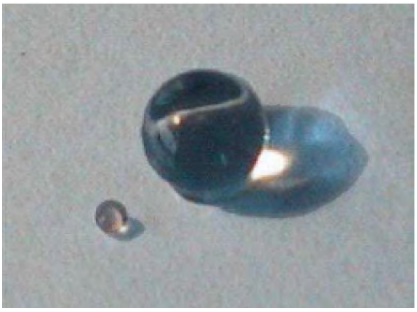

Fig. 4.87 A dry and a swollen SAP [4.101]

Three different mix proportions were made as shown in Table 4.16. Specimens belonging to group 1 were composed according to the standard ECC mix, while specimens belonging to group 2 and 3 contained 0.5% and 1% SAP in proportion to the cement weight. ECC was cast into moulds with dimensions of 240 mm x 60 mm x 10 mm. These coupon specimens were moisture cured for 24 hours and then demoulded. After demoulding, the coupon specimens were evenly sawn into four pieces with dimensions of 120 mm x 30 mm x 10 mm.

Table 4.16 Proportion of fibers and SAP's [4.97]

Group	Proportion
1	PVA 2%
2	PVA 2% and 0.5% of SAP's
3	PVA 2% and 1% of SAP's

Part of the specimens were loaded in four-point bending at the age of 7 days, the other part at 28 days. Half of the specimens were stored in the laboratory (approx. 5% RH and 20°C), the other half of the specimens were subjected to nine cycles of wetting and drying. Each cycle consisted of submersion in water of 20°C for 1 hour and subsequently drying in laboratory air for 3 days. This regime was used to simulate cyclic outdoor environments such as rainy days and unclouded days. Finally, specimens were loaded till failure in four-point bending. Each time

the results were compared with those of virgin specimens which were loaded till failure at the age of 7 days or 28 days. The overall testing program is depicted in Fig. 4.88.

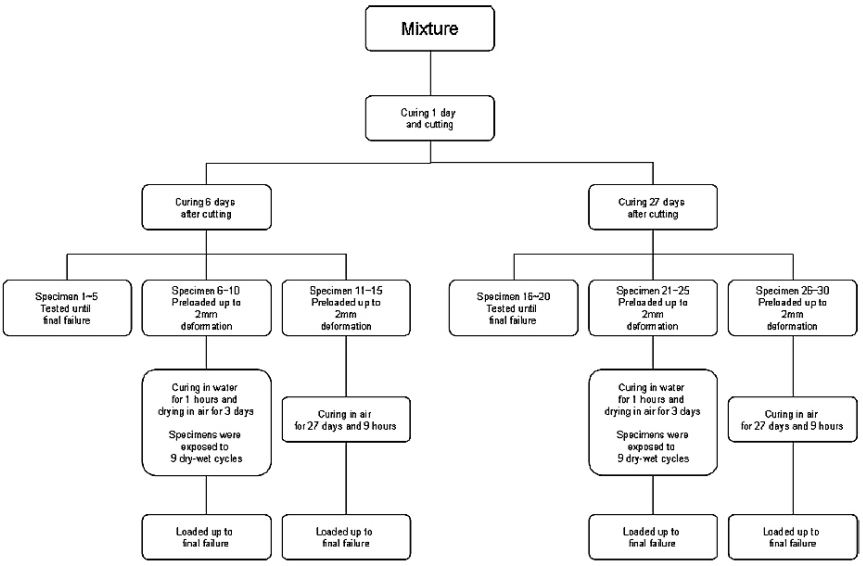

Fig. 4.88 Loading and curing scheme [4.97]

It is seen from Fig. 4.89 that all specimens that were air cured, have a flexural stress-strain curve which has a smooth and even shape. The authors explained this by the fact that when the preloaded specimens are reloaded, there were no new cracks formed but the pre-existing cracks re-opened and extended, proving that no crack healing occurred. In contrast, the stress-strain curves obtained from the specimens that went through the wet-dry cycles of group 2 and 3 had a significant roughness and unevenness. The principle of multiple cracking in ECC-like materials lies on the assumption that, after the first crack has formed, the energy needed to let this crack grow is larger than the energy needed to form a new crack. So, the experimental results obtained in these tests could be explained by the fact that new cracks occurred because of the strength of the self-healed part was higher than the strength of the existing matrix. The specimens of group 1 (without SAP) that followed also the wet-dry cycles have again a smooth and even shape. In that case the material could not hold enough water during the wetting cycle to create any significant self-healing in the sample.

As it is shown in Table 4.17, the strength of cyclic wet-dry cured specimens exceeds the strength of the virgins in all mixtures for both cases of 35 and 56 days old. Particularly, strength recovery ratio of group 2 and 3 is higher than for the specimens of group 1. Apparently, this is also an evidence that SAP's kept the water in the cracked zone and helped the self-healing. It can be seen that the

influence of SAP is limited for air cured specimens. In case of 35 days curing the SAP still contributed because they probably helped to store a small amount of water that can be used for self-healing. However at 56 days air curing, the contribution of SAP has a negative effect.

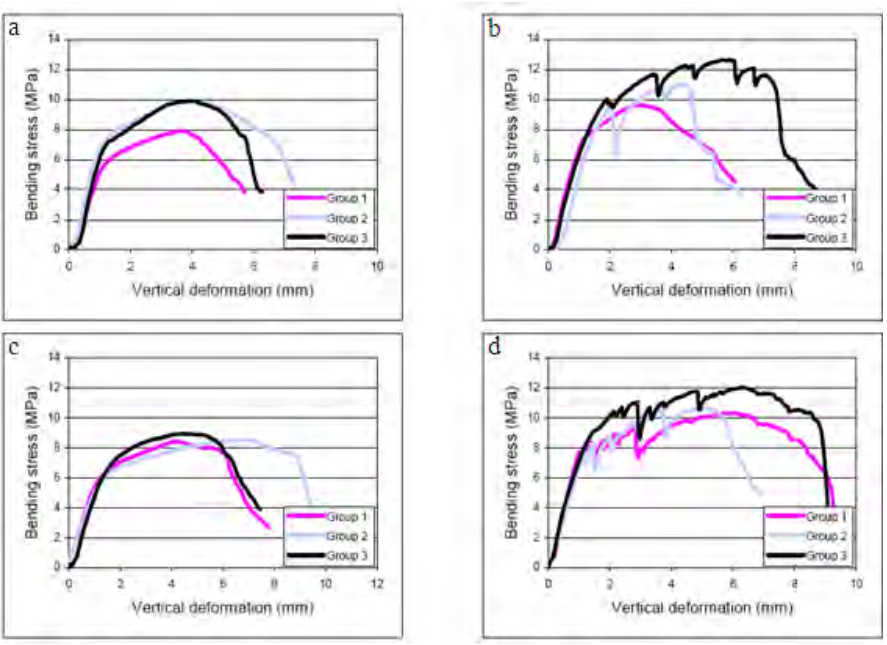

Fig. 4.89 Reloading after 28 days in laboratory air (a and c) or 9 wet-dry cycles (b and d) of 7 days (a and b) or 28 days (c and d) cured ECC specimens [4.97]

Table 4.17 Ultimate flexural stress and strength recovery ratio for cyclic wet-dry cured specimens and air cured specimens

	Group 1		Group 2		Group 3	
	Stress [MPa]	Recovery [%]	Stress [MPa]	Recovery [%]	Stress [MPa]	Recovery [%]
7 days	8.25	-	7.14	-	8.84	-
35 days_water cured	9.96	17.17	9.84	27.44	11.33	21.98
35 days_air cured	8.51	12.72	7.55	15.72	9.63	13.44
28 days	8.37	-	8.63	-	10.24	-
56 days_water cured	9.59	3.06	10.24	5.43	11.83	8.2
56 days_air cured	8.4	0.36	8.55	-0.94	8.96	-14.29

Snoeck *et al.* [4.102, 4.103] performed four-point-bending tests to investigate the regain in mechanical properties upon crack healing. Table 4.18 shows the studied mortar specimens, which contained 2 vol.% of PVA fibres. Table 4.19 gives the main properties of the two types of superabsorbent polymers (SAPs) used.

Table 4.18 Studied mortar samples with their code (n=3), m% of SAP and curing conditions [4.102]

Specimen-Code	m% SAP	Curing
REF	0	Wet/dry cycles
P90	0	RH > 90%
P60	0	RH = 60%
A1	1 (SAP A)	Wet/dry cycles
B1	1 (SAP B)	Wet/dry cycles
B90	1 (SAP B)	RH > 90%
B60	1 (SAP B)	RH = 60%
B2	2 (SAP B)	Wet/dry cycles
B4	4 (SAP B)	Wet/dry cycles

Table 4.19 Mean diameter of SAP A and SAP B particles [µm] (n=50), absorption capacity of SAP [g fluid/g SAP] (n=3) in de-ionised water; tap water and cement slurry with standard deviations, and absorption determined in a dynamic vapour sorption test (DVS) in air of 100% RH [g moisture/g SAP]. [4.102-4.104]

Method	SAP A	SAP B
Diameter	100±22	477 ± 53
de-ionised water (pH=6.5)	305.0 ± 3.7	283.2 ± 2.4
tap water (pH= 6.8)	163.9 ± 1.2	148.9 ± 0.9
cement slurry (pH=12.8)	61.0 ± 1.0	58.4 ± 1.7
Water vapour	1.68	1.50

By performing four-point-bending tests at an age of 28 days, eight to nine small healable cracks were formed instead of a single large unhealable crack. The crack width ranged between 6-36 µm. After cracking, the specimens were stored in different curing conditions (Table 4.18). After curing, the specimens were loaded under four-point-bending to compare the mechanical properties.

Fig. 4.90 shows the first-cracking strength and the regain in first-cracking strength of the studied specimens [4.102]. The macro pores left behind by the formerly saturated SAP particles reduce the tensile strength due to a reduced

active cross section of the matrix. Samples with SAP A show a lower first-cracking strength compared to SAP B samples due to a reduced workability and the smaller particle size. A SAP B content of 1 m% relative to the cement weight gives analogous properties of the first-cracking strength compared to the REF samples without SAPs. Curing by means of SAPs has a positive influence on the amount of regain in mechanical properties. SAPs can sustain hydration by yielding their absorbed water and provide water for the precipitation of $CaCO_3$ and for the formation of new C-S-H crystals. As water is steadily provided to the matrix for healing, samples containing SAPs show more regain in mechanical properties. Furthermore, in a relative humidity of more than 90% and 60%, only samples with SAPs show partial healing. The moisture uptake by SAPs (Table 4.19) seems to be enough to promote autogenic healing in a small extent.

Fig. 4.91 shows the visual closure of all cracks after the curing period [4.103]. Results show that cracks up to 30 µm heal completely and up to 150 µm heal partly when specimens without SAP are subjected to wet/dry cycles. Storage in an environment with a relative humidity of more than 90% only showed visual closure of cracks for samples containing SAPs. SAP particles manage to take moisture out of a humid environment and provide it to the cementitious matrix for crack healing. Due to possible suction of the mortar matrix, the water is provided to the cementitious matrix. This causes autogenic healing to occur as further hydration of the unhydrated cement grains. In wet/dry cycles, cracks up to 130 µm are able to close in specimens containing SAP (Fig. 4.92). Deposition of crystals is not only due to further hydration, but mainly due to precipitation of $CaCO_3$ crystals.

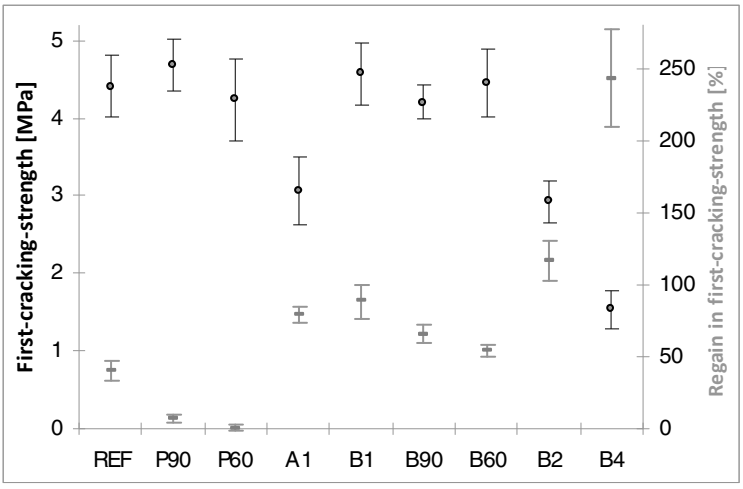

Fig. 4.90 Mean values and standard deviations for first-cracking-strength for virgin (black, left axis) and healed specimens (grey, right axis). REF, A1, B1, B2, B4 = wet/dry cycles; P90, B90 = RH>90%; P60, B60 = RH=60%. REF, P90, P60 containing no SAP; A1 containing 1 m% of cement weight SAP A; B1, B90, B60 containing 1 m% SAP B and B2, B4 containing 2 m%, 4 m% SAP B [4.102]

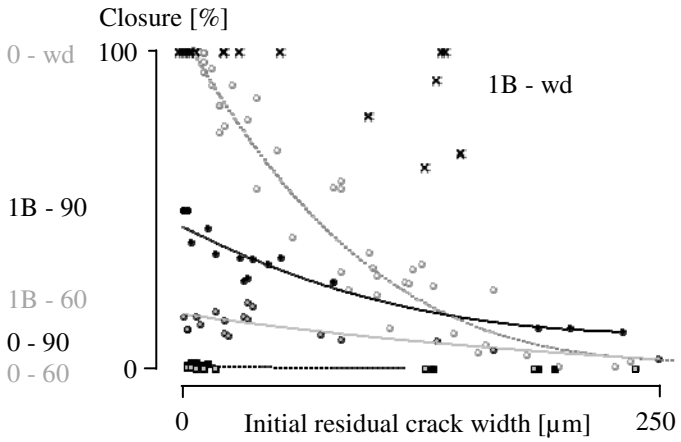

Fig. 4.91 Closure of the cracks [%] after curing as a function of initial crack width [µm] by performing microscopic analysis [4.103]

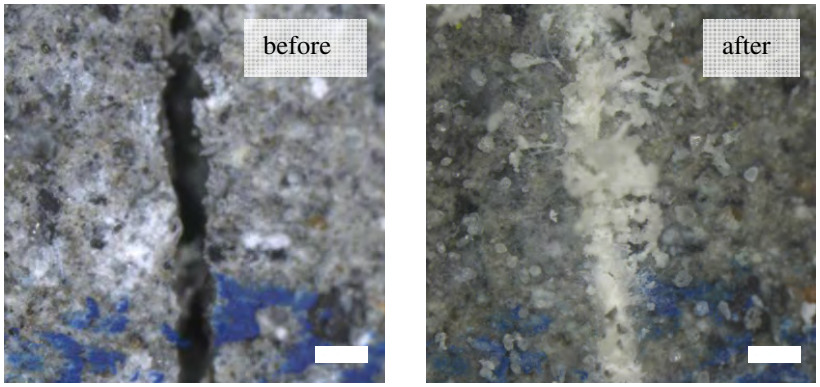

Fig. 4.92 Total healing of a 138 µm crack of a specimen containing 1 m% SAP B after wet/dry cycles. The scale bars have a height of 200 µm [4.102].

The white product formed in the cracks was subjected to thermogravimetric analysis (TGA) [4.102]. TGA showed that the crystals consisted of $CaCO_3$ and washed out hydration products. SAP particles were not found in the TGA analysis, supporting the conclusion that SAPs effectively seal the crack without dissolving or degrading.

The autogenic healing also occurred when flax fibres were used [4.105].

To prevent leaching of the water absorbed by the SAP particles during cement hydration, and hence, to prevent loss of the autogenous healing capacity, Xia [4.102] coated swollen SAP particles with paraffin wax. Before the paraffin could be applied on the SAP core, an extra shell of cement powder was needed.

As the initial swelling of SAP particles during concrete mixing causes the formation of pores and thus a reduction in strength, Lopez-tendero *et al.* [4.107]

tried to modify the polymers so they only swell at reduced pH level (Fig. 4.93). During concrete mixing the pH is around 13, preventing swelling of the SAP.

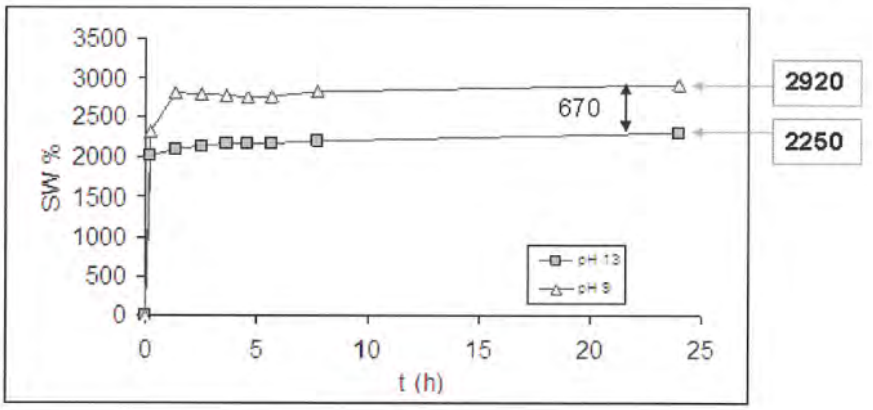

Fig. 4.93 Swelling kinetics for the hydrogel in pH 13 and 9 buffered solutions [4.107]

In their research, Reddy and Liang [4.108] searched for a mechanism to make oil well cements watertight. They mentioned that the sealing efficiency of SAP particles depends on contacting the right type of fluid. Therefore, they preferred to use elastomers with low glass transition temperature, low melting point or low solid to liquid phase transition temperature or those which show cold flow, allowing fractured samples to self-heal without requiring contact with any type of fluid. In their research, elastomeric materials were chemically modified to contain functional groups, particularly carboxylate groups, that are capable of bonding not only to cement surfaces but also to the metal casing used in oil wells. The flow rate through separated cement pieces reduced upon heating showing the efficiency of this technique.

References

4.1. Taylor, H.F.W.: Cement chemistry, p. 475. Academic Press, San Diego (1990)
4.2. Abd-Elmoaty, A.-E.: Self-healing of polymer modified concrete. Alexandria Engineering Journal 50(2), 171–178 (2011)
4.3. Edvardsen, C.: Water permeability and autogenous healing of cracks in concrete. ACI Materials Journal 96(4), 448–454 (1999)
4.4. Jacobsen, S., Marchand, J., Hornain, H.: SEM observations of the microstructure of frost deteriorated and self-healed concretes. Cement and Concrete Research 25(8), 1781–1790 (1995)
4.5. Reinhardt, H.-W., Jooss, M.: Permeability and self-healing of cracked concrete as a function of temperature and crack width. Cement and Concrete Research 33(7), 981–985 (2003)

4.6. Li, V.C., Yang, E.H.: Self-healing in concrete materials. In: van der Zwaag, S. (ed.) Self-healing Materials: An Alternative Approach to 20 Centuries of Materials Science, pp. 161–193. Springer, Dordrecht (2007)
4.7. Li, V.C., Lim, Y.M., Chan, Y.-W.: Feasibility study of a passive smart self-healing cementitious composite. Composites Part B: Engineering 29(6), 819–827 (1998)
4.8. Ying-zi, Y., Lepech, M.D., Li, V.C.: Self-healing of engineered cementitious composites under cyclic wetting and drying. In: International Workshop on Durability of Reinforced Concrete under Combined Mechanical and Climatic Loads (CMCL), Qindao, China, pp. 231–242 (2005)
4.9. Ahmaran, M., Li, V.C.: Durability properties of micro-cracked ECC containing high volumes fly ash. Cement and Concrete Research 39(11), 1033–1043 (2009)
4.10. Yang, Y., Yang, E.-H., Li, V.C.: Autogenous healing of engineered cementitious composites at early age. Cement and Concrete Research 41(2), 176–183 (2011)
4.11. Li, M., Li, V.C.: Cracking and healing of engineered cementitious composites under chloride environment. ACI Materials Journal 108(3), 333–340 (2011)
4.12. Li, M., Sahmaran, M., Li, V.C.: Effect of cracking and healing on durability of engineered cementitious composites under marine environment. In: Reinhardt, H.W., Naaman, A.E. (eds.) Conference on High Performance Fiber Reinforced Cement Composites (HPFRCC 5), Mainz, Germany, pp. 313–322 (2007)
4.13. Li, V.C.: On engineered cementitious composites (ECC): A review of the material and its applications. Journal of Advanced Concrete Technology 1(3), 215–230 (2003)
4.14. Homma, D., Mihashi, H., Nishiwaki, T.: Self-healing capability of fibre reinforced cementitious composites. Journal of Advanced Concrete Technology 7(2), 217–228 (2009)
4.15. Koda, M., et al.: Self-healing capability of fibre reinforced cementitious composites. In: International Conference on Advances in Construction Materials through Science and Engineering, Hong Kong, China (2011)
4.16. Lepech, M.D., Li, V.C.: Water permeability of engineered cementitious composites. Cement and Concrete Composites 31(10), 744–753 (2009)
4.17. Homma, D., et al.: Experimental study on the self-healing capability of fiber reinforced cementitious composites. In: 7th RILEM International Symposium on Fibre Reinforced Concrete: Design and Applications, pp. 769–774. RILEM, Chennai (2008)
4.18. Yang, Y., et al.: Autogenous healing of engineered cementitious composites under wet-dry cycles. Cement and Concrete Research 39(5), 382–390 (2009)
4.19. Yamamoto, A., Kan, L.-L., Li, V.C.: Self-healing behaviour of engineered cementitious composites under different number of wet-dry cycle. In: 11th International Summer Symposium of the Japan Society of Civil Engineers, Tokyo, Japan, pp. 1–4 (2009)
4.20. Kan, L.-L., et al.: Self-healing characterization of engineered cementitious composites (ECC) materials. ACI Materials Journal 107(6), 619–626 (2010)
4.21. Qian, S., et al.: Self-healing behavior of strain hardening cementitious composites incorporating local waste materials. Cement and Concrete Composites 31(9), 613–621 (2009)

4.22. Sahmaran, M., Li, V.C.: Deicing salt scaling resistance of mechanically loaded engineered cementitious composites. Cement and Concrete Research 37(7), 1035–1046 (2007)
4.23. Sahmaran, M., Lachemi, M., Li, V.C.: Assessing the durability of engineered cementitious composites under freezing and thawing cycles. Journal of ASTM International 6(7), 1–13 (2009)
4.24. Bensted, J.: Uses of raman spectroscopy in cement chemistry. Journal of the American Ceramic Society 59(3-4), 140–143 (1976)
4.25. Termkhajornkit, P., et al.: Self-healing ability of fly ash-cement systems. Cement and Concrete Composites 31(3), 195–203 (2009)
4.26. Granger, S., et al.: Mechanical characterization of the self-healing effect of cracks in Ultra High Performance Concrete (UHPC). In: 3rd International Conference of Construction Materials, Performance, Innovations and Structural Implications, Vancouver, Canada (2005)
4.27. Granger, S., et al.: Self-healing of cracks in concrete: from a model material to usual concretes. In: Marchand, J., et al. (eds.) 2nd International RILEM Symposium on Advances in Concrete through Science and Engineering. RILEM Publications SARL, Quebec (2006)
4.28. Morimoto, T., et al.: Self-healing properties of Ultra High Performance Strain Hardening Cementitious Composites (UHP-SHCC). In: 4th International Conference on Construction Materials, Nagoya, Japan, pp. 319–326 (2009)
4.29. Schlangen, E., ter Heide, N., van Breugel, K.: Crack healing of early age cracks in concrete. In: ECF 16, Alexandroupolis, Greece, pp. 1–8 (2006)
4.30. ter Heide, N., Schlangen, E., van Breugel, K.: Experimental study of crack healing of early age cracks. In: Knud Hojgaard Conference on Advanced Cement-based Materials, Denmark, pp. 1–11 (2005)
4.31. ter Heide, N., Schlangen, E.: Self-healing of early age cracks in concrete. In: van der Zwaag, S. (ed.) 1st International Conference on Self-healing Materials, p. 81. Springer, Noordwijk aan Zee (2007)
4.32. Abdel-Jawad, Y., Dehn, F.: Self-healing of self-compacting concrete. In: SCC 2005 Conference, Orlando, Florida, USA, pp. 1023–1029 (2005)
4.33. Sakai, Y., et al.: Experimental study on enhancement of self-restoration of concrete beams using SMA wire. In: Liu, S.-C. (ed.) Conference on Smart Structures and Materials, San Diego, California, pp. 178–186 (2003)
4.34. Kuang, Y., Ou, J.: Self-repairing performance of concrete beams strengthened using superlastic SMA wires in combination with adhesives released from hollow fibers. Smart Materials and Structures 17, 1–7 (2008)
4.35. Kuang, Y., Ou, J.: Passive smart self-repairing concrete beams by using shape memory alloy wires and fibers containing adhesives. Journal of Central South University Technology 15, 411–417 (2008)
4.36. Isaacs, B., et al.: Enhancement of self-healing in cementitious materials, post-tensioned with shrinkable polymers. In: White, S., Bond, I. (eds.) 2nd International Conference on Self-healing Materials, Chicago, USA, p. 102 (2009)

4.37. Isaacs, B., et al.: Enhancement of self-healing in cementitious materials. In: Bond, I., Varley, R. (eds.) 3rd International Conference on Self-healing Materials, Bath, UK, pp. 119–120 (2011)
4.38. Lark, R.J., et al.: Active confinement of cementitious composites with shape memory plastics. In: 2nd International Conference on Self-healing Materials, Chicago, USA, p. 138 (2009)
4.39. Joseph, C., et al.: Experimental investigation of adhesive-based self-healing of cementitious materials. Magazine of Concrete Research 62(11), 831–843 (2010)
4.40. Jefferson, A., et al.: A new system for crack closure of cementitious materials using shrinkable polymers. Cement and Concrete Research 40(5), 795–801 (2010)
4.41. Lark, R.J., Jefferson, A.D., Joseph, C., Dunn, S., Isaacs, B.: Active Confinement of Cementitious Composites with Shape Memory Plastics. In: Proceedings of Seond International Conference on Self- Healing Materials, Chicago (2009)
4.42. Jefferson, A., et al.: A new system for crack closure of cementitious materials using shrinkable polymers. Cement and Concrete Research 40(5), 795–801 (2010)
4.43. Isaacs, B., Lark, R.J., Jefferson, A.D., Joseph, C., Dunn, S.: Autogenous healing in SMP cementitious material system. Magazine of Concrete Research (Sumitted for publication)
4.44. Bornert, M., et al.: Assessment of digital image correlation measurement errors: methodology and results. Experimental Mechanics 49(3), 353–370 (2009)
4.45. Dry, C.: Smart multiphase composite materials that repair themselves by a release of liquids that become solids. In: Symposium on Smart Structures and Materials, Orlando, Florida, pp. 62–70 (1994)
4.46. Dry, C.: Matrix cracking repair and filling using active and passive modes for smart timed release of chemicals from fibers into cement matrices. Smart Materials and Structures 3(2), 118–123 (1994)
4.47. Dry, C.: Smart earthquake resistant materials (using time released adhesives for damping, stiffening, and deflection control). In: 3rd ICIM/ECSSM, Lyon, France, pp. 958–967 (1996)
4.48. Dry, C.: Improvement in reinforcing bond strength in reinforced concrete with self-repairing chemical adhesives. In: SPIE, pp. 44–50 (1997)
4.49. Thao, T.D.P., Johnson, T.J.S., Tong, Q.S., Dai, P.S.: Implementation of selfhealing in concrete - Proof of concept. The IES Journal Part A: Civil & Structural Engineering 2(2), 116–125 (2009)
4.50. Pang, S.D., Tran Diep, P.T., Quek, S.T.: On implementation of self-healing function in concrete - Proof of concept and practical issues. In: White, S., Bond, I. (eds.) 2nd International Conference on Self-healing Materials, Chicago, USA, p. 119 (2009)
4.51. Pang, S.D., Tran Diep, P.T., Quek, S.T.: Self-healing concrete structural elements. In: Bond, I., Varley, R. (eds.) 3rd International Conference on Self-healing Materials, Bath, UK, pp. 322–323 (2011)
4.52. Dry, C., McMillan, W.: Three-part methylmethacrylate adhesive system as an internal delivery system for smart responsive concrete. Smart Materials and Structures 5(3), 297–300 (1996)

4.53. Van Tittelboom, K., De Belie, N.: Self-healing concrete: suitability of different healing agents. International Journal of 3R's 1(1), 12–21 (2010)
4.54. Van Tittelboom, K., De Belie, N.: Self-healing concrete by the internal release of adhesive from hollow glass tubes embedded in the matrix. In: 2nd International Conference on Self-healing Materials, Chicago, USA, p. 101 (2009)
4.55. Van Tittelboom, K., De Belie, N.: Self-healing concrete by means of encapsulated polymers. In: 13th International Conference on Polymers in Concrete, Madeira, pp. 681–688 (2010)
4.56. Van Tittelboom, K., Van Loo, D., De Belie, N., Jacobs, P.: Evaluation of the efficiency of selfhealing in concrete by means of micro-CT. In: 3rd International Workshop on X-ray CT for Geomaterials, New Orleans, pp. 132–139 (2010)
4.57. Dry, C.: Repair and prevention of damage due to transverse shrinkage cracks in bridge decks. In: Liu, S.-C. (ed.) Symposium on Smart Structures and Materials, pp. 253–256 (1999)
4.58. Dry, C.: Three designs for the internal release of sealants, adhesives, and waterproofing chemicals into concrete to reduce permeability. Cement and Concrete Research 30(12), 1969–1977 (2000)
4.59. de Rooij, M.R., et al.: Using natural wood fibers to self heal concrete. In: Alexander, M.G., et al. (eds.) 2nd International Conference on Concrete Repair, Rehabilitation and Retrofitting, Cape Town, South Africa, pp. 229–233 (2008)
4.60. Liu, H., et al.: Self-healing of concrete cracks using hollow plant fibres. In: 2nd International Conference on Self-healing Materials, Chicago, USA, p. 189 (2009)
4.61. Cailleux, E., Pollet, V.: Investigations on the development of self-healing properties in protective coatings for concrete and repair mortars. In: 2nd International Conference on Self-healing Materials, Chicago, USA, p. 120 (2009)
4.62. Huang, H., Ye, G.: Application of sodium silicate solution as self-healing agent in cementitious materials. In: International Conference on Advances in Construction Materials through Science and Engineering, Hong Kong, China (2011)
4.63. Pelletier, M., et al.: Self-healing concrete with a microencapsulated healing agent (2010)
4.64. Mihashi, H., et al.: Fundamental study on development of intelligent concrete characterized by selfhealing capability for strength. Transactions of the Japan Concrete Institute 22, 441–450 (2000)
4.65. Feng, X., et al.: Self-healing mechanism of a novel cementitious composite using microcapsules. In: International Conference on Durability of Concrete Structures, Hangzhou, China, pp. 195–204 (2008)
4.66. Kaltzakorta, I., Erkizia, E.: Silica microcapsules encapsulating epoxy compounds for self-healing cementitious materials. In: 3rd International Conference on Self-healing Materials, Bath, UK, pp. 271–272 (2011)
4.67. Yang, Z., et al.: Laboratory assessment of a self-healing cementitious composite. Journal of the Transportation Research Board (2142), 9–17 (2010)
4.68. Yang, Z., et al.: A self-healing cementitious composite using oil core/silica gel shell microcapsules. Cement and Concrete Composites 33(4), 506–512 (2011)

4.69. Joseph, C., Jefferson, A.D., Canoni, M.B.: Issues relating to the autonomic healing of cementitious materials. In: Van der Zwaag, S. (ed.) 1st International Conference on Self-healing Materials, Noordwijk aan Zee, The Netherlands, p. 53 (2007)
4.70. Joseph, C., Jefferson, A.D., Isaacs, B., Lark, R.J., Gardner, D.R.: Adhesive based self-healing of cementitious materials. In: Proceedings of 2nd International Conference on Self-healing Materials, Chicago (2009)
4.71. Joseph, C., Gardner, D.R., Jefferson, A.D., Lark, R.J., Isaacs, B.: Self-healing Cementitious Materials: A review of recent work. In: Proceedings of the ICE: Construction Materials (2009)
4.72. Mihasi, H., Kaneko, Y., Nishiwaki, T., Otsuka, K.: Fundamental study on development of intelligent concrete characterized by self-healing capability for strength. Transactions of the Japan Concrete Institute 22, 441–450 (2000)
4.73. Dry, C., Corsaw, M.: A comparison of bending strength between adhesive and steel reinforced concrete with steel only reinforced concrete. Cement and Concrete Research 33(11), 1723–1727 (2003)
4.74. Dry, C.: Use of embedded self-repair adhesives in certain areas of concrete bridge members to prevent failure from severe dynamic loading. In: Conference on Smart Materials Technologies, Newport Beach, California, pp. 126–130 (1999)
4.75. Dry, C.: Release of smart chemicals for the in-service repair of bridges and roadways. In: Aatre, V.K., Varadan, V.K., Varadan, V.V. (eds.) Symposium on Smart Materials, Structures, and MEMS, San Diego, California, pp. 140–144 (1998)
4.76. Dry, C.: Design of self-growing, self-sensing, and self-repairing materials for engineering applications. In: Wilson, A.R., Asanuma, H. (eds.) Smart Materials Conference, pp. 23–29 (2001)
4.77. Pareek, S., Oohira, A.: A fundamental study on regain of flexural strength of mortars by using a self-repair network system. In: 3rd International Conference on Self-healing Materials, Bath, UK, pp. 46–47 (2011)
4.78. Sangadji, S., Schlangen, E.: Feasibility and potential of prefabricated porous concrete as a component to make concrete structures self-healing. In: International Conference on Advances in Construction Materials through Science and Engineering, Hong Kong, China (2011)
4.79. Sangadji, S., Schlangen, E.: Porous network concrete: a new approach to make concrete structures self-healing using prefabricated porous layer. In: Bond, I., Varley, R. (eds.) 3rd International Conference on Self-healing Materials, Bath, UK, pp. 291–292 (2011)
4.80. Ludirdja, D., Berger, R.L., Young, J.F.: Simple method for measuring water permeability of concrete. ACI Materials Journal 86(5), 433–439 (1989)
4.81. Nishiwaki, T., et al.: Development of self-healing system for concrete with selective heating around crack. Journal of Advanced Concrete Technology 4(2), 267–275 (2006)
4.82. Nishiwaki, T., et al.: Development of smart concrete with self-healing system using selective heating device. In: 5th International Conference on Concrete under Severe Conditions Environment and Loading, Tours, France, pp. 665–672 (2007)

4.83. Nishiwaki, T., et al.: Smart concrete system with strain monitoring sensors including conductive particles. In: Marchand, J., et al. (eds.) 2nd International RILEM Symposium on Advances in Concrete through Science and Engineering, Quebec, Canada (2006)
4.84. Nishiwaki, T., Oohira, A., Pareek, S.: An experimental study on the application of self-repairing system to RC structures using selective heating. In: Bond, I., Varley, R. (eds.) 3rd International Conference on Self-healing Materials, Bath, UK, pp. 320–321 (2011)
4.85. Nishiwaki, T., de B. Leite, J.P., Mihashi, H.: Enhancement in durability of concrete structures with use of high-performance fibre reinforced cementitious composites. In: 4th International Conference on Concrete under Severe Conditions: Environment & Loading, pp. 1524–1531 (2004)
4.86. Katsuhata, T., Ohama, Y., Demura, K.: Investigation of microcracks self-repair function of polymermodified mortars using epoxy resins without hardeners
4.87. Ohama, Y., Demura, K., Endo, T.: Strength properties of epoxy-modified mortars without hardener. In: 9th International Congress on the Chemistry of Cement, New Delhi, India, pp. 512–516 (1992)
4.88. Ahn, T.H., Kishi, T.: The effect of geo-materials on the autogneous healing behaviour of cracked concrete. In: Alexander, M.G., Beushausen, H.-D., Dehn, F., Moyo, P. (eds.) Concrete Repair, Rehabilitation and Retrofitting II, London, pp. 235–240 (2009)
4.89. Ahn, T.H., Kishi, T.: Crack healing behaviour of cementitious composite materials incorporating geo-materials. In: White, S., Bond, I. (eds.) 2nd International Conference on Self-healing Materials, Chicago, USA, p. 100 (2009)
4.90. Ahn, T.H., Kishi, T.: Crack self-healing behaviour of cementitious composites incorporating various mineral admixtures. Journal of Advanced Concrete Technology 8(2), 171–186 (2010)
4.91. Sisomphon, K., Copuroglu, O.: Self-healing mortars by using different cementitious materials. In: International Conference on Advances in Construction Materials through Science and Engineering, Hong Kong, China (2011)
4.92. Sisomphon, K., Copuroglu, O., Koenders, E.A.B.: Surface crack self-healing behaviour of mortars with expansive additives. In: Bond, I., Varley, R. (eds.) 3rd International Conference on Self-healing Materials, Bath, UK, pp. 44–45 (2011)
4.93. Copuroglu, O., Sisomphon, K., Komatsu, S.: Self-healing of cement paste by calcium aluminate based agents. In: White, S., Bond, I. (eds.) 2nd International Conference on Self-healing Materials, Chicago, USA (2009)
4.94. Yuan, X.Z., et al.: Experimental research on the crack self-healing properties of cement mortar with EVA heat-melt adhesive. In: International RILEM Conference on Material Science, Aachen, Germany, pp. 433–442 (2010)
4.95. Yuan, X.-Z., et al.: The crack self-healing properties of cement-based material with EVA heat-melt adhesive. Journal of Wuhan University of Technology - Materials Science Edition 26(4), 774–779 (2011)
4.96. Yuan, X.-Z., Sun, W., Zuo, X.-B.: Study of feasibility of heat melt adhesive being used in crack self-healing of cement-based materials. Applied Mechanics and Materials 99-100, 1087–1091 (2011)

4.97. Kim, J.S., Schlangen, E.: Super absorbent polymers to stimulate self-healing in ECC. In: 2nd International Symposium on Service Life Design for Infrastructure, Delft, The Netherlands (2010)
4.98. Kim, J.S., Schlangen, E.: Self-healing in ECC stimulated by SAP under flexural cyclic load. In: Bond, I., Varley, R. (eds.) 3rd International Conference on Self-healing Materials, Bath, UK, pp. 324–325 (2011)
4.99. Dennis Lee, H.X., Wong, H.S., Buenfeld, N.: Self-sealing cement-based materials using superabsorbent polymers. In: Jensen, O.M., Hasholt, M.T., Laustsen, S. (eds.) International RILEM Conference on Use of Superabsorbent Polymers and Other New Additives in Concrete, pp. 171–178. RILEM Publications s.a.r.l, Lyngby (2010)
4.100. Lee, H.X.D., Wong, H.S., Buenfeld, N.R.: Potential of superabsorbent polymer for selfsealing cracks in concrete. Advances in Applied Ceramics 109(5), 296–302 (2010)
4.101. Jensen, O.M., Hansen, P.F.: Water-entrained cement-based materials: I. Principles and Theoretical Background. Cement and Concrete Research 31(4), 647–654 (2001)
4.102. Snoeck, D., et al.: Self-healing cementitious materials by the combination of microfibres and superabsorbent polymers. Journal of Intelligent Material Systems and Structures (2012)
4.103. Snoeck, et al.: The use of superabsorbent polymers as a crack sealing and crack healing mechanism in cementitious materials. In: 3rd International Conference on Concrete Repair, Rehabilitation and Retrofitting, Cape Town, pp. 152–157 (2012)
4.104. Snoeck, D., et al.: Visualization of water penetration in cementitious materials with superabsorbent polymers by means of neutron radiography. Cement and Concrete Research 42, 1113–1121 (2012)
4.105. Snoeck, D., De Belie, N.: Mechanical and self-healing properties of cementitious composites reinforced with flax and cottonised flax, and compared with polyvinyl alcohol fibres. Biosystems Engineering 111, 325–335 (2010)
4.106. Xia, H.: Self-healing of engineered cementitious composites (ECC) in concrete repair system. Delft Univeristy of Technology, Delft (2010)
4.107. Lopez-tendero, M.J., et al.: Optimized hydrogel for application as repairing agents in cement based products. In: Bond, I., Varley, R. (eds.) 3rd International Conference on Self-healing Materials, Bath, UK, p. 160 (2011)
4.108. Reddy, B.R., Liang, F.: Self-healing cement compositions for use in oil field applications. In: White, S., Bond, I. (eds.) 2nd International Conference on Self-healing Materials, Chicago, USA, p. 163 (2009)